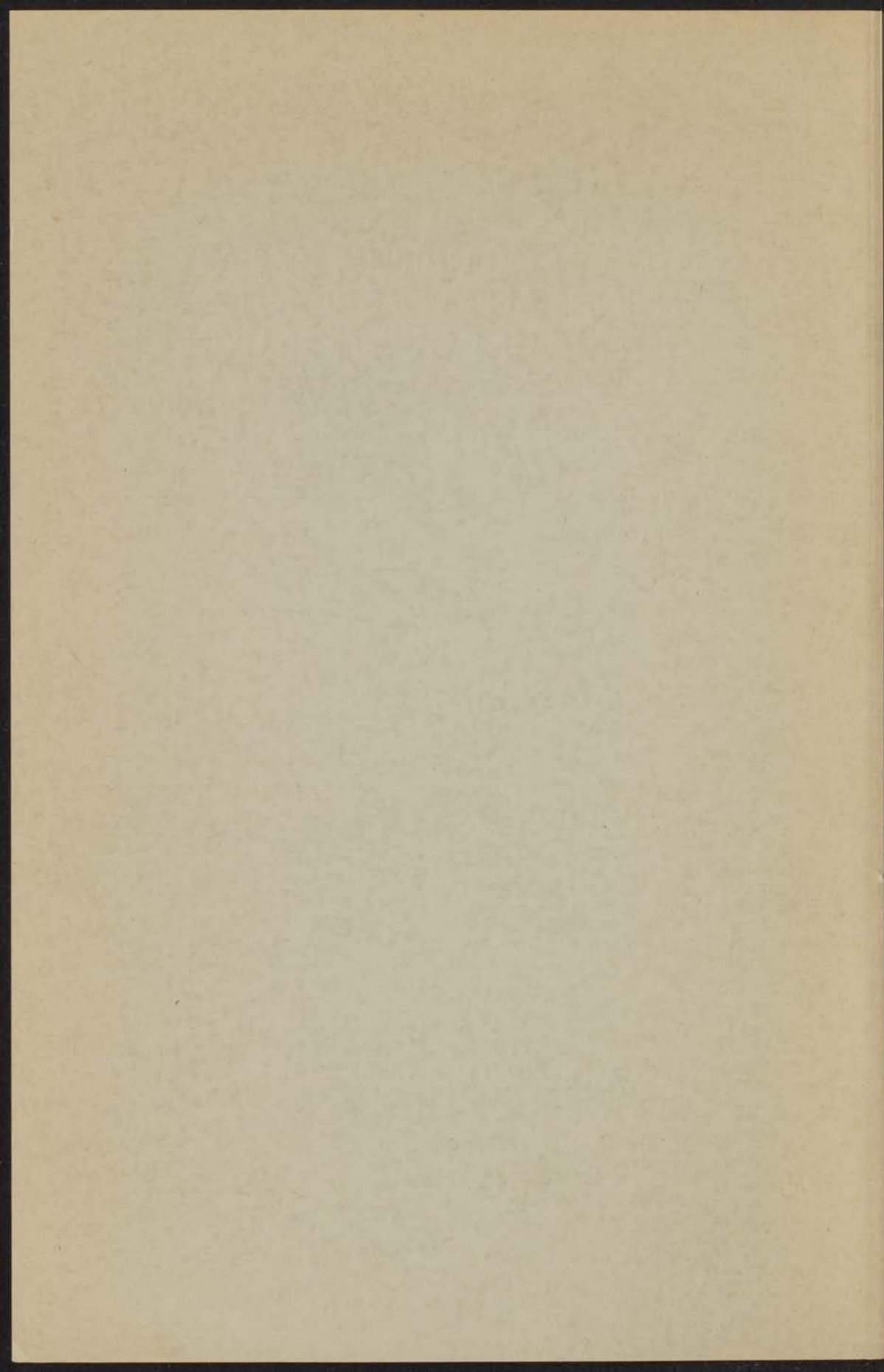# EXCITATION OF HELIUM BY FAST ELECTRONS AND POLARIZATION OF THE RESULTING RADIATION

HAMMAM RASHAD MOUSTAFA MOUSSA

STELLINGEN

I

Het verschil in het energetisch gedrag van He II emissie doorsneden tussen theorie en experiment is waarschijnlijk te wijten aan het gebruik van niet-orthogenale golffuncties in de theoretische berekeningen.

Dit proefschrift, Hoofdstuk 8.
Mittleman, M. H., Phys. Rev. Letters, **16**, 489, (1966).
Mapleton, R. A., Phys. Rev. **109**, 1166, (1957).
Dalgarno, A., and McDowell, M. R. C., The Airglow and the Aurorae, Pergamon Press, New. York, p. 340 (1956).

II

De manier waarop Lee and Lin de emissiedoorsnede van de $4 \rightarrow 3$ overgang (4686 Å) in He II, geïnduceerd door botsingen met electronen, berekenen, is zeer aanvechtbaar.

Lee, E.T.P. and Lin, C. C., Phys. Rev. **138**, A 301 (1965).

III

De verwaarlozing van de interferentie tussen directe aanslag en aanslag met uitwisseling van electronen geeft aanleiding tot te hoge werkzame doorsneden voor de ^1S excitatie van helium door electronen (20-250 eV) in de berekeningen van Fox.

Dit proefschrift, Hoofdstuk 8.
Fox, M. A., Proc. Phys. Soc., **86**, 789, (1965).

IV

Indien men wil beschikken over een intensieve bundel van laag energetische ionen in een botsingsexperiment, is het gewenst de ionen tot een relatief hoge energie vanuit de ionenbron te versnellen en deze pas op korte afstand van de botsingskamer te vertragen tot de gewenste energie.

V

De definitie van de diffusie coëfficienten van een veel-componenten systeem door Hirschfelder, Curtiss and Bird, kan niet worden gebruikt voor systemen met reactieve componenten.

Hirschfelder, J. O., Curtiss, C. F., and Bird, R. B., Molecular Theory of Gases and Liquids, Chap. 7 and 8 (1954).

VI

De vergelijking van de theoretische berekeningen van Dunn en Self betreffende een door een bundel gecreëerd plasma met de experimentele resultaten van Hedvall is onjuist.

Dunn, D. A., and Self, S. A., J. Appl. Phys. **35**, 113 (1964).
Hedvall, P., J. Appl. Phys. **33**, 2426, (1962).

VII

De interpretatie dat de Aston band, afkomstig van de door botsingen geïnduceerde dissociatie van H_2^+-ionen, het gevolg zou zijn van twee verschillende fysische processen, is niet juist.

Gaudano, R., Delfosse, J. M., and Steyaert, J., Ann. de la Soc. Scientifique de Bruxelles, **76**, III, 127 (1963).
McClure, G. W., Phys. Rev. **140**, A 11 (1965).

VIII

Om met behulp van moleculaire bundel-technieken absolute werkzame doorsneden te bepalen verdient het aanbeveling de dichtheid te meten met behulp van een ionisatie manometer, welke aangebracht is in de botsingskamer.

Berkling, K., Helbing, R., Kramer, K., Pauly, H., Schlier, Ch., and Toschek, P., Z. f. Physik **166**, 406, (1962).
Pauly, H., and Toennies, J. P., Advances in Atomic and Molecular Physics, edited by Bates, D. R., and Immanual Eastermann, p. 228, (1965).

IX

Een microgolfholte kan een belangrijk hulpmiddel zijn bij de bepaling van het kwantumrendement van een vacuummonochromator.

De Heer, F. J., Advances in Atomic and Molecular Physics, vol **2**, edited by Bates, D. R., and Immanual Eastermann (1966).
Shreider, E. Ya., Soviet. Tecch. Phys. **9**, 1609, (1965).

X

Evenals gebruikelijk in het buitenland, zou ook voor Nederlandse studenten een gereduceerd treintarief mogelijk moeten zijn.

EXCITATION OF HELIUM BY FAST ELECTRONS AND POLARIZATION OF THE RESULTING RADIATION

EXCITATION OF HELIUM BY FAST ELECTRONS AND POLARIZATION OF THE RESULTING RADIATION

PROEFSCHRIFT

TER VERKRIJGING VAN DE GRAAD VAN DOCTOR IN
DE WISKUNDE EN NATUURWETENSCHAPPEN AAN DE
RIJKSUNIVERSITEIT TE LEIDEN, OP GEZAG VAN DE
RECTOR MAGNIFICUS DR K. A. H. HIDDING, HOOG-
LERAAR IN DE FACULTEIT DER GODGELEERDHEID, TEN
OVERSTAAN VAN EEN COMMISSIE UIT DE SENAAT TE
VERDEDIGEN OP WOENSDAG 17 MEI 1967 TE 16 UUR

DOOR

HAMMAM RASHAD MOUSTAFA MOUSSA
GEBOREN TE MIT-BERA (EGYPTE) IN 1939

kast dissertaties

PROMOTOR: PROF. DR J. KISTEMAKER

Dit werk heeft plaatsgevonden onder leiding van Dr. F. J. DE HEER

To my wife
To Hala and Hany

CURRICULUM VITAE

At the request of the Faculty of Science of the University of Leyden, a short account of my education is given here.

My primary education took place in Mit-Bera, Monofiah, Egypt, where I was born on December, 10, 1939. After finishing my studies at Benha Secondary school at Benha, Kaluobiah, in 1957, I started my study at the Faculty of Science of Ain-Shams University in Cairo. In 1961, I obtained a Bachelor of Science degree in physics with distinction. After that I worked as an assistant in the department of physics at the same University.

In the beginning of 1962 I obtained a scholarship from the National Research Centre in Cairo, U.A.R., to study for the doctors degree in electronics.

In July 1962 I came to Europe. At first I went to Western-Germany. There I joined the Physical Institute of the Technical High School of Aachen for one academic term. I then joined the F.O.M. Institute for Atomic and Molecular Physics in Amsterdam in November 1963, where I studied under the guidance of Prof. J. Kistemaker and Dr. F. J. de Heer. On March, 3, 1965 I obtained the degree of Doctorandus in experimental physics at the University of Leyden.

ACKNOWLEDGEMENTS

CONTENTS

CHAPTER 1

Introduction

CHAPTER 2

Theory

CHAPTER 3

The experimental apparatus

CHAPTER 4

Absolute calibration of the optical equipment

CHAPTER 5

Experimental procedure and evaluation of the results

CHAPTER 6

Dependence of the light emission and the polarization on the gas pressure, the axial magnetic field and the electron beam current

CHAPTER 7

Excictation and polarization results as a function of electron impact energy

CHAPTER 8

Comparison with theory

CHAPTER 9

Comparison between excitation of helium by electrons and protons

CHAPTER 1

INTRODUCTION

1.1. Purpose of this investigation

The excitation functions or cross sections of electrons incident on helium have been studied experimentally over a considerable period of time by different authors, especially in the region below 500 eV impact energy. The experiment consists of measuring the emission of helium spectral lines under welldefined conditions of the electron beam and the gas pressure. Because the intensity of light is often weak in these experiments, a high sensitivity in the detection apparatus is important. The earlier measurements were done with apparatusses which were less sensitive than that available at present. Therefore the investigators were often forced to use relative high gas pressures to increase the yield of light. As we shall see further on this can lead to considerable errors in the excitation cross sections as a result of absorption of resonance radiation or by collisions of the second kind.

The later experiments were generally carried out with lower gas pressures. However, the results are not always in quantitative agreement with the existing theoretical calculations. It is the purpose of this work to try to solve the existing discrepancies. This is done by putting the accent of the experimental work on the region of high electron impact energy of the electrons. The reason for this is that at high impact energy a simpler theory can be applied, namely the Bethe or Born approximation. Therefore a better theoretical analysis of the experimental results can be carried out in this energy region. For instance, we shall see that the collision induced optically allowed transitions in the target atom (1^1S-n^1P transitions for helium), excited by electron impact, can be related to the optical oscillator-strengths of these transitions.

1

The energy range of the electrons in our experiments is from 0.05 to 6 keV. The cross sections are determined from intensity measurements of spectral lines by two different monochromators. One works in the region of 2900 Å to 7300 Å and the other in the vacuum ultraviolet region from 200-2500 Å. Also, measurements are done on the polarization of light between 2900 Å and 7300 Å. In some cases use has been made of interference filters.

1.2. The collision processes

When an electron collides with an atom the collision can be elastic or inelastic. Confining to helium target atoms, we study the following two inelastic processes:

$$e + He \rightarrow e + He^* \qquad \text{(He I spectrum)} \qquad (1.2.1)$$

$$e + He \rightarrow e + He^{+*} + e \text{ (He II spectrum)} \qquad (1.2.2)$$
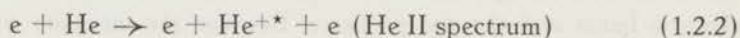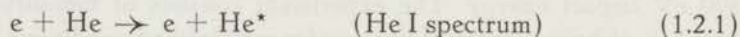
In the first case we look to the excitation of an atomic level. We can form either singlet or triplet excited helium states. In the triplet case the reaction can only occur by exchange of electrons with antiparallel spins. In the singlet case there are two possibilities. The original electron can stay with the helium atom and go to an excited state or exchange of electrons with parallel spins can occur. Non exchange processes dominate at high impact energies. At low impact energies, however, exchange processes become very important.

In the second case the helium atom is ionized, loosing one electron, and simultaneously the other electron is promoted to an excited state. Excitation cross sections are determined by measuring spectral lines from the excited helium ion.

1.3. Definition of the cross sections

Suppose we have a beam of I/e particles per second through a cross section of the collision chamber, filled with a gas with N atoms per cm³. The change per second of the number excited target atoms in state i over a pathlength of 1 cm, as a consequence of collisions

2

with beam particles, is then given by

$$\frac{d\,n_i}{dt} = N\frac{I}{e}\sigma_i + \sum_{k>i} n_k A_{ki} - n_i \sum_{j<i} A_{ij} \qquad (1.3.1)$$

where n_i is the number of atoms excited to state i per cm pathlength and A_{ij} is the transition probability from state i to j. The first term on the right is due to (direct) excitation of the atom from the ground state to the excited state i. The second term represents the population of level i originating from atoms which have been excited to state k. It is called the cascade term. The third term represents the decay of atoms in state i to lower lying levels. Secondary collision processes have been neglected.

When dealing with the excitation of the slow target atoms, the processes of excitation and decay can be considered to take place in the observation region, without flow of excited target particles into or out of it. Then, we can put $dn_i/dt = 0$ and neglecting cascade we get from (1.3.1)

$$\sigma_i = \frac{n_i \sum\limits_{j<i} A_{ij}}{NI/e} \qquad (1.3.2)$$

By definition the emission cross section is given by

$$\sigma_{ij} = \frac{n_i A_{ij}}{N\,I/e} \qquad (1.3.3)$$

where $n_i A_{ij}$ is the number of photons i $\rightarrow$ j emitted per second per cm.

From (1.3.2) and (1.3.3) we find

$$\sigma_i = \sum_{j<i} \sigma_{ij} = \frac{\sigma_{ij}}{A_{ij}} \sum_{j<i} A_{ij} \qquad (1.3.4)$$

Making a first order correction for cascade processes we finally obtain from (1.3.1) and (1.3.3)

$$\sigma_i = \sum_{j<i} \sigma_{ij} - \sum_{k>i} \sigma_{ki} = \frac{\sigma_{ij}}{A_{ij}} \sum_{j<i} A_{ij} - \sum_{k>i} \frac{\sigma_{km}}{A_{km}} A_{ki} \qquad (1.3.5)$$

In order to calculate the excitation cross section σ_i we see from (1.3.4) that, if the transition probabilities of the atom are known

3

it is not necessary to determine all emission cross sections. This is the case for hydrogen and helium.

1.4. Experimental determination of the emission cross section

The photons are observed with a detector, which has a certain efficiency depending on the wavelength λ, determined by the transition $i \rightarrow j$. We assume that the signal measured is S amps, the observation lengths is l cm and the quantum yield of the detector is $k(\lambda)$. The quantum yield is defined as the current of the detector per incoming photon per second. Its dimension is ampere $\times$ second/quanta. Then we have (see also 1.3.3)

$$N \frac{I}{e} \sigma_{ij} \, l = S/k(\lambda) \qquad (1.4.1)$$

Generally the radiation from every emitting particle is only detected over a certain solid angle ω. Assuming isotropic photon emission we finally find the next equation for σ_{ij} :

$$\sigma_{ij} = \frac{4\pi}{\omega} \frac{S(\omega)}{\dfrac{I}{e} N \, l \, k(\lambda)} \qquad (1.4.2)$$

where $S(\omega)$ represents the signal inside angle ω.

1.5. Literature survey on the experiment

1.5.1. *Excitation measurements*

Measurements of the cross section of the transition from the ground state to a given excited state by electron impact have been carried out since 1930 by many experimentators: The measurements of L e e s (1932), T h i e m e (1933) and H a n l e (1929) have been carried out by using photographic techniques. They have worked with such a high gas pressure (T h i e m e 5μ and L e e s 44μ) that second order processes like the absorption of resonance radiation (1^1S-n^1P lines) and secondary collision processes must have occured. For this reason their absolute values are in some cases too high (e.g. for $\lambda = 5016$ Å and $\lambda = 3964$ Å), however, the

4

relative energy dependence of the cross sections seems to be correct. F r o s t and P h e l p s (1957) point out that the excitation functions found by T h i e m e for members of the same series have nearly the same shape. The similarity of excitation shapes is illustrated in Fig. 1.1.
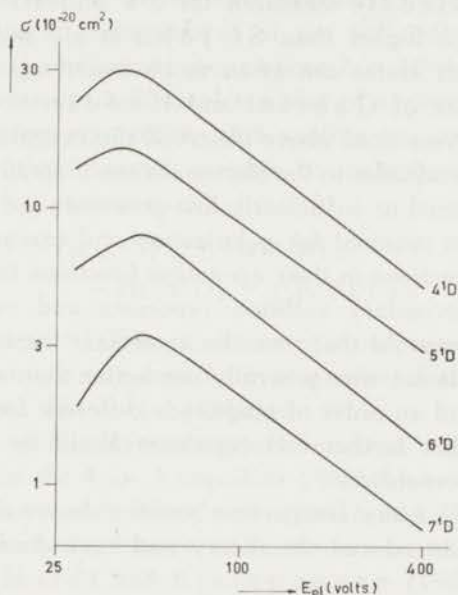
Fig. 1.1 Excitation functions for the 4, 5, 6 and 7^{1}D states determined by T h i e m e (1932). Note that a logarithmic scale is used.

One of the most extensive studies on excitation functions of helium has been made by S t. J o h n et al. (1964), who review at the same time many of the earlier measurements. S t. J o h n has composed two tables on results of different experiments. In the first of these he compares the shape of the apparent experimental excitation cross sections of helium, that is the cross sections uncorrected for polarization, cascade and transfer effects. In the second table the absolute values of the apparent excitation cross sections are given. From his tables we see that generally there is similarity in shape for levels of the same series as is demonstrated in Fig. 1.1. However the same shape is not always found by different investigators. In some cases agreement is present between

5

many experimental excitations functions determined by St. John et al. (1964), Yakhontova (1959), Zapesochnyi and Feltsan (1965) and Gabriel and Heddle (1960) and even with some values of Thieme, though the latter used rather high gas pressures. There are however also unexplained differences: Gabriel and Heddle measured for 3^1P and 4^1P values which were about 50% higher than St. John et al., and St. John's values for triplet states are often much lower, up to about four times, than those of Gabriel and Heddle.

All the observers cited above observed the excitation chamber in a direction perpendicular to the electron beam. Thus all apparent cross sections determined at sufficiently low pressures are subject to the same corrections required for polarization and cascade. St. John et al. made corrections in their excitation functions for polarization, cascade and secondary collision processes and compared their values with theory. At that time the agreement between the theory and their experiment was generally not better than about 50% for singlet states and an order of magnitude different for triplet states. This showed that further investigations should be carried out to solve these discrepancies.

We shall make a new comparison between theory and experiment, after we have introduced the theory and have discussed our own measurements.

Because Yakhontova (1959) used a homogeneous electron beam with an energy resolution of only 0.6 eV, she found premaxima in the excitation cross sections of several helium lines near threshold. Similar premaxima were also found by Smit (1961) who used an energy spread of 0.2 eV. This structure has been investigated in more detail by Chamberlain et al. (1965), in electron energy loss measurements at zero degree scattering in helium. The study of these phenomena is beyond the scope of this work.

Extended measurements on the pressure dependence of the excitation functions, caused by absorption of resonance radiation and collisions of the second kind, have been carried out by Heddle and Lucas (1962), Yakhontova and St. John et al. (1960) in the case of electron impact and by Van Eck et al. (1964a) and Hughes et al. (1961) in the case of ion impact. Resonance radiation and collision processes of the second

6

kind were studied in more detail by Gabriel and Heddle (1960), Reich (1965), Wolf and Maurer (1940), St. John and Fowler (1961), St. John and Tsu-Wei Nee (1965), Pendleton and Hughes (1965) and Teter and Robertson (1966). Absorption of resonance radiation, for instance 3^1P-1^1S, gives rise to a repeated population of the 3^1P level and therefore to an enhancement of the 3^1P-2^1S emission. This process starts to be important above about 2×10^{-4} torr.

At higher pressures collisional transfer of excitation may occur, i.e. an excited atom may collide with another gas atom and change either its azimuthal quantum number or multiplicity or both. An example of such a process is:

$$He(4^1P) + He(1^1S) \rightleftarrows He(1^1S) +$$
$$+ He(4^1D) + \triangle E(0.01 \text{ eV}) \qquad (1.5.1)$$
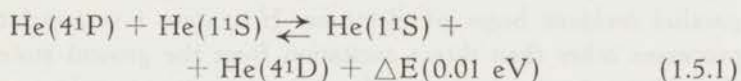
The energy defect $\triangle E$ is small and so such processes can easily occur; cross sections may even be in the order of 10^{-15} cm^2/atom (Gabriel and Heddle (1960)).

In the case of He II excitation by electron impact, only two measurements on the $4 \rightarrow 3$ transition (4686 Å) have been carried out by Hughes and Weaver (1963) and St. John and Lin (1964). Recently, relative measurements on 4686 Å have also been done by Haidt and Kleinpoppen (1966).

Some work on excitation of helium has been performed by non optical methods. Inelastic scattering experiments were, for instance, carried out by Chamberlain et al. (1965), Lassettre et al. (1964), Geiger (1963, 1964), Kuyatt and Simpson (1964) and Kuppermann and Raff (1963). In these experiments differential cross sections with respect to angle were determined for 2^1S, 2^1P, 3^1P and 2^3S levels. In some cases it is possible to derive the optical oscillator strengths or the generalized oscillator strengths of Bethe (1930) from these results.

We also mention other experiments with electron energies in the neighbourhood of the threshold for excitation. These are mainly concerned with the excitation of the metastable states 2^1S and 2^3S of helium. The metastables are detected by secondary emission in the work of Schulz and Fox (1957), Holt and Krotkov (1966) and by the so called Penning effect in the work of

7

Čermák (1966). Fleming and Higginson (1964) used the method of Maier and Leibnitz (1935) for 2^3S excitation, applying a kind of electron trapping method (see also Schulz, 1959). Recently, measurements have been done by Dugan et al. (1967), by observation of a beam of excited atoms in an inhomogeneous magnetic field.

1.5.2. *Polarization measurements of the light induced by electrons*

When helium is excited by a parallel incident beam of electrons, the emitted radiation is in general partially polarized. The impact radiation is polarized because of the anisotropy introduced by the parallel incident beam of electrons. If a state i is populated by processes other than direct excitation from the ground state, then the radiation emitted as a result of the transition to a lower state j will not be referred to the axis of quantization parallel to the electron beam, and so depolarization of the observed radiation results.

For this reason when the pressure is too high, absorption of resonance radiation and collisions of the second kind give rise to depolarization. Measurements of the degree of polarization of light, in the case of helium, excited with electron beams were very rare untill recently. Steiner (1929) was among the first who measured the degree of polarization of some helium lines using photographic techniques. He found very low polarization fractions, probably due to the high gas pressure which was used. The polarization was measured as a function of electron energy by Elenbaas (1929) at fixed pressures of 40 and 100 torr.

Smit (1935) measued the angular distribution of the photons produced by a 60 volt electron beam in helium. He showed that there is a classical relation between the angular distribution of the dipole radiation and the polarization of the light. However, the polarization values obtained by him may be too small because he used high pressures (40 torr).

Heddle and Lucas (1962) studied the polarization of electron impact radiation as a function of helium pressure. The same was done by Van Eck et al. (1964a), using an ion beam instead of the electron beam.

8

It appears that the polarization is more or less constant in the pressure region where the light intensity is proportional with the pressure. More measurements on polarization have been carried out by McFarland and Soltysik (1962), by Hughes et al. (1963), by McFarland (1964), by Heideman (1962), by Fedorov and Golovanevskaya (1966) and by Perel and Fedorov (1966). Some of this work specializes on the behaviour near threshold which is beyond the scope of this work. In general there is agreement between the polarization fractions obtained by different groups, except that the values of Heddle and Lucas (1962) are higher.

CHAPTER 2

THEORY

2.1. Introduction

In order to understand our experimental results, we shall discuss the excitation of atoms by electron impact. Our experiments put the emphasize on the study of the behaviour of excitation cross sections at high impact energies. In this energy region first order approximations are generally used because in this energy region one expects in a wave treatment a small perturbation of the incident wave (representing the moving electron) by the atom.

The known approximations in collision theory are Born approximation and Born-Oppenheimer approximation, the latter taking the indistinguishability between the projectile electron and the atom electrons into account.

We shall give some introductionary explanation obtained from Mott and Massey (1965).

We introduce the scattered amplitude $f_n(\Theta, \varphi)$ for the atom being in the ground state before the collision. Here n is the excited state, Θ is the scattering angle and φ is the azimuthal angle. The cross section for excitation of state n is now given by (see Mott and Massey, 1965a)

$$\sigma_n = \frac{k_n}{k_0} \int_{\Theta=0}^{\pi} \int_{\varphi=0}^{2\pi} |f_n(\Theta, \varphi)|^2 \sin \Theta \, d\Theta \, d\varphi \qquad (2.1.1)$$

where k_0 and k_n are the wave numbers of the incident and scattered electrons.

Generally we have scattering amplitudes corresponding to direct scattering, where no exchange of incident and target electron occurs and scattering amplitudes corresponding to exchange of these

10

electrons. Usually direct scattering is represented by f_n and exchange scattering by g_n. Because of interference of both amplitudes the inelastic cross section is generally represented by:

$$\sigma_n = \frac{k_n}{k_0} \iint \left[\tfrac{1}{4} \mid f_n + g_n \mid^2 + \tfrac{3}{4} \mid f_n - g_n \mid^2 \right] \sin \Theta \, d\Theta \, d\varphi \quad (2.1.2)$$

If the target atom is hydrogen, we have

$$f_n (\Theta, \varphi) =$$

$$= \frac{2\pi \, me^2}{h^2} \iint \left(\frac{1}{r_1} - \frac{1}{r_{12}} \right) \exp \left[i \, (\mathbf{k}_0 - \mathbf{k}_n) \cdot \mathbf{r}_1 \right] \psi_0 \, (\mathbf{r}_2) \, \psi_n^*(\mathbf{r}_2) \, d \, \tau_1 \, d \, \tau_2$$

$$(2.1.3)$$

and

$$\left\langle e^{i\vec{k_n}\cdot\vec{r_1}} \, \psi_n(r_1) \left| \frac{1}{r_1} - \frac{1}{r_{12}} \right| e^{i\vec{k_0}\cdot\vec{r_1}} \, \psi_0 \, (r_2) \right\rangle$$

$$g_n (\Theta, \varphi) =$$

$$= \frac{2\pi \, me^2}{h^2} \iint \left(\frac{1}{r_2} - \frac{1}{r_{12}} \right) \exp \left[i \, (\mathbf{k}_0 \cdot \mathbf{r}_1 - \mathbf{k}_n \cdot \mathbf{r}_2) \right] \psi_0(\mathbf{r}_2) \, \psi_n^*(\mathbf{r}_2) \, d\tau_1 \, d\tau_2$$

$$(2.1.4)$$

Here $\mathbf{r}_1$ and $\mathbf{r}_2$ the position vectors of the projectile and the target electron respectively, ψ_0 and ψ_n are the wave functions of hydrogen in the ground and excited states respectively, m is the mass of the electron, h is Planck's constant, e is the charge of the electron, τ_1 and τ_2 are the volume elements of the electrons, and

$$r_{12} = \mid \mathbf{r}_1 - \mathbf{r}_2 \mid$$

The amplitude of direct scattering, f_n, is equivalent to that used by Born approximation. For high impact velocities and for transitions for which the spacial symmetry of the atomic wave functions does not change (e.g. singlet-singlet transitions in helium) one can use the direct term f_n and neglect g_n.

For excitations for which the symmetry changes (e.g. singlet-triplet transitions in helium) we have an example of the Born-Oppenheimer approximation where the direct term f_n is zero and g_n determines the cross section.

In the following sections we shall give an analysis of both the Born and Born-Oppenheimer approximations.

11

2.2. Born approximation

The cross section σ_n in the Born approximation for atomic hydrogen follows from equation 2.1.1 when we substitute for f_n, the right term of equation 2.1.3.

By working out the expression it is often convenient to change from angular to momentum variables (see M o t t and M a s s e y). We introduce $\hbar\mathbf{K}$, representing the change of momentum of the singlet electron.

$$\mathbf{K} = \mathbf{k}_0 - \mathbf{k}_n \qquad (2.2.1)$$

and

$$K^2 = k_0{}^2 + k_n{}^2 - 2k_0 k_n \cos \Theta \qquad (2.2.2)$$

$$K dK = k_0 k_n \sin \Theta \, d\Theta \qquad (2.2.3)$$

The differential cross section in momentum variables now becomes

$$\sigma_n(K) \, dK = \frac{8\pi^3 m^2}{h^4} \frac{K dK}{k_0^2} \left| \iint \frac{e^2}{\mathbf{r}_1 - \mathbf{r}_2} e^{\mathbf{Ki.r}_1} \psi^\star{}_n(\mathbf{r}_2) \psi_0(\mathbf{r}_2) d\tau_1 \, d\tau_2 \right|^2$$

$$(2.2.4)$$

with $K_{max} = k_0 + k_n$; $K_{min} = k_0 - k_n$; and $k_n^2 = k_0^2 - \dfrac{2m E_n}{\hbar^2}$

B e t h e (1930) simplified this expression by using the next equation:

$$\int \frac{e^{i\mathbf{K.r}_1}}{|\mathbf{r}_1 - \mathbf{r}_2|} \, d\tau_1 = \frac{4\pi}{K^2} e^{i\mathbf{K.r}_2} \qquad (2.2.5)$$

and he obtained the following equation, which is called the Bethe approximation:

$$\sigma_n = \int_{K_{min}}^{K_{max}} \sigma_n (K) \, dK = \frac{128\pi^5 m^2 e^4}{h^4 k_0^2} \int \frac{dK}{K^3} \, | \, \varepsilon_n (K) \, |^2 \qquad (2.2.6)$$

with

$$\varepsilon_n (K) = \int e^{i\mathbf{K.r}_2} \psi_n^\star (\mathbf{r}_2) \psi_0 (\mathbf{r}_2) d\tau_2$$

If we choose the axis of the system of polar coordinates along

12

K, we get

$$\varepsilon_n (K) = \int e^{iKZ_2} \, \psi_n^* (\mathbf{r}_2) \, \psi_0 (\mathbf{r}_2) \, d\tau_2$$

Below we shall leave away the index 2.

In optical spectroscopy transition probabilities are frequently expressed by the oscillator strength. In analogy with this, B e t h e (1930) introduced for collision induced transitions the generalized oscillator strength, defined by:

$$f_n (K) = \frac{E_n}{R} \left| \frac{1}{Ka_0} \right| \varepsilon_n (K) \left|\, \right|^2 \tag{2.2.7}$$

where E_n the excitation energy, R the Rydberg energy and a_0 the first Bohr radius of the hydrogen atom.

In the derivation of (2.2.6) it has been assumed that the incident electrons have high energy and are only slightly deviated from their initial trajectory because of the collision. Then the collisions with small momentum changes will be the most important ones and it is convenient to expand $e^{iK.Z}$ in a power series, so that

$$f_n (K) = \frac{E_n}{R} \left| \frac{1}{Ka_0} \sum_{s=1}^{\infty} \frac{(iK)^s}{s!} \mid Z_n^s \mid \right|^2 \tag{2.2.8}$$

$$\mid Z_n^s \mid = \int \psi_0 (\mathbf{r}) \, (Z)^s \, \psi_n^* (\mathbf{r}) \, d\tau \tag{2.2.9}$$

where the first term in the expansion has vanished due to the orthogonality of the wave functions.

The optical oscillator strength is defined by:

$$f_n = \frac{E_n}{R} \frac{\mid Z_n \mid^2}{a_0^2} = \frac{E_n}{R} \cdot M_n^2 \tag{2.2.10}$$

and it can easily be seen that

$$\lim_{K \to 0} f_n (K) = f_n \tag{2.2.11}$$

By means of (2.2.7) we can finally rewrite (2.2.6) by:

$$\sigma_n = \int_{K_{min}}^{K_{max}} \sigma_n(K) dK = \frac{8 \pi a_0^2 R^2}{E_n E_{el}} \int f_n(K) \frac{dK}{K} \tag{2.2.12}$$

13

where E_{el} is the electron energy.

This relation has been derived for transitions in the hydrogen atom but can be generalized for transitions in other atoms having a nuclear charge $+$ Ne and containing N electrons.

In those cases $f_n(K)$ is defined by:

$$f_n(K) = \frac{E_n}{R} \left| \frac{1}{Ka_0} \int \sum_{i=1}^{N} \psi_0(r_1, r_2, \ldots r_n) e^{iK \cdot r_i} \right.$$

$$\left. \psi_n(r_1, r_2, \ldots r_n) \, d\tau_i \right|^2 \qquad (2.2.13)$$

In our helium excitation experiment we have collision induced transitions with $\triangle l = 1$ (1^1S-n^1P), which correspond to optically allowed transitions and collision induced transitions with $\triangle l \neq 1$ (1^1S-n^1S or 1^1S-n^1D), which correspond to optically forbidden transitions. We shall show with the Bethe approximation that both have a different asymptotic behaviour at high impact energies.

2.2.1. *Optically allowed transitions*

The total coss section associated with the transition $0 \to n$ is obtained by integrating (2.2.12), hence:

$$\sigma_n = \int_{K_{min}}^{K_{max}} \sigma_n(K) \, dK = \frac{4\pi a_0^2 R^2}{E_n E_{el}} \int_{K_{min}}^{K_{max}} f_n(K) \, d \ln (K^2 a_0^2) \qquad (2.2.14)$$

Following Miller and Platzman (1957) we represent in Fig. 2.1 a graph of $f_n(K)$ versus $\ln K^2 a_0^2$. For each excitation process such a graph gives all information on the differential and total cross sections. For $Ka_0 \ll 1$ the ordinate is approaching a constant value (f_n), and declines strongly near $Ka_0 = 1$ and is very small for $Ka_0 \gg 1$, in agreement with the statement made before that the small momentum transfers are the most numerous ones. The shape of this curve is proved by experiment (Lassettre et al., 1964 and Geiger, 1964). The total cross section — σ_n — divided by $4\pi a_0^2 R^2/E_n E_{el}$ is equal to the area

14

under the solid curve between the limits given by K_{min} and K_{max}. It is clear from the graph that this area is equal to that of the dashed
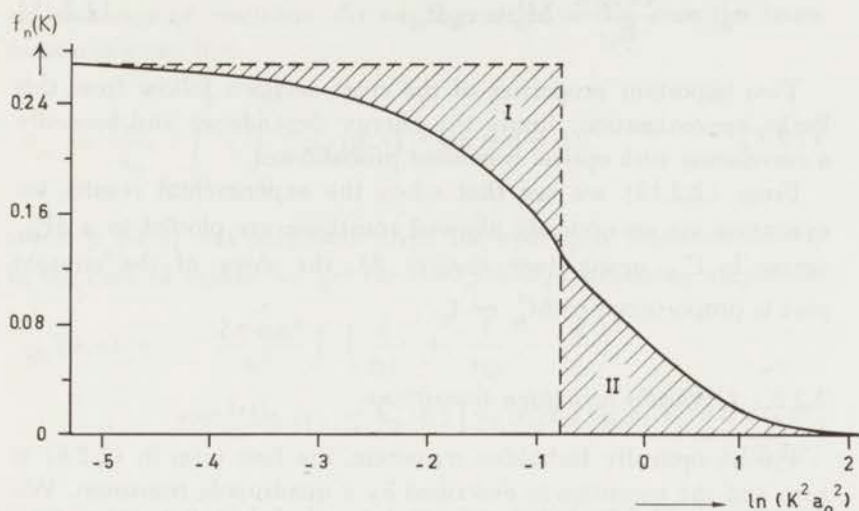
Fig. 2.1 Solid curve: generalized oscillator strength for the 2^1P state of He according to M i l l e r and P l a t z m a n, dashed curve: explained in the text. Area I = area II.

rectangle if area I = area II. The value of K for which I = II is the so called momentum cut off, K_{cd}.

The total cross section is now given by (see S c h r a m and V r i e n s (1965)):

$$\sigma_n = \frac{4\pi a_0^2 R}{E_{el}} \frac{f_n R}{E_n} \ln \frac{K_{cd}^2 a_0^2}{K_{min}^2 a_0^2} = \frac{4\pi a_0^2 R}{E_{el}} \frac{f_n R}{E_{el}} \ln c_n E_{el}$$

with

$$c_n = \frac{R K_{cd}^2 a_0^2}{E_{el}^2 \left\{ 1 - \left(1 - \frac{E_n}{E_{el}} \right)^{\frac{1}{2}} \right\}^2} \qquad (2.2.16)$$

which for high values of E_{el} reduces to:

$$c_n = \frac{4 R K_{cd}^2 a_0^2}{E_n^2} \qquad (2.2.17)$$

15

According to (2.2.10) we can finally rewrite (2.2.15) by:

$$\sigma_n = \frac{4\pi a_0^2 R}{E_{el}} \, M_n^2 \ln c_n E_{el} \qquad (2.2.18)$$

Two important properties of the cross sections follow from this Bethe approximation; firstly the energy dependence and secondly a correlation with optical transition probabilities.

From (2.2.15) we see that when the experimental results for excitation via an optically allowed transition are plotted in a σE_{el} versus $\ln E_{el}$ graph (see chapter 8), the slope of the straight part is proportional to M_n^2 or f_n.

2.2.2. *Optically forbidden transitions*

For an optically forbidden transition, the first term in (2.2.8) is zero and the transition is described by a quadrupole transition. We obtain

$$\lim_{K \to 0} \frac{f_n(K)}{K^2 a_0^2} = \frac{E_n}{R} \frac{|Z_n^2|^2}{a_0^4} \qquad (2.2.19)$$

The total cross section is now given by (see S c h r a m and V r i e n s (1965) or S c h r a m (1966a)).

$$\sigma_n = \frac{\pi a_0^2 R}{E_{el}} \frac{|Z_n^2|^2}{a_0^4} \left[K_{cq}^2 \, a_0^2 - \frac{E_{el}}{R} \left\{ 1 - \left(1 - \frac{E_n}{E_{el}} \right)^{\frac{1}{2}} \right\}^2 \right] \qquad (2.2.20)$$

which for large E_{el} can be simplified to:

$$\sigma = \frac{\pi a_0^2 R}{E_{el}} \frac{|Z_n^2|^2}{a_0^4} \left(K_{cq}^2 \, a_0^2 \right) = \frac{B}{E_{el}} \qquad (2.2.21)$$

i.e. $\sigma \sim E_{el}^{-1}$

The physical meaning of the momentum cut off factor K_{cq} for a quadrupole transition will be clear if $f_n(K)/K^2 a_0^2$ is plotted against $K^2 a_0^2$ which should give similar curves as given in Fig. 2.1 for a dipole transition.

16

2.3. Born-Oppenheimer approximation

We shall consider triplet excitation of helium; corresponding with an exchange of electrons. As we have seen in this case the cross section is given by:

$$\sigma_n = \frac{k_n}{k_0} \int_{\Theta=0}^{\pi} \int_{\varphi=0}^{2\pi} |g_n(\Theta, \varphi)|^2 \sin \Theta \, d\Theta \, d\varphi \qquad (2.3.1)$$

where $g_n(\Theta, \varphi)$ has only been given for hydrogen (equation 2.1.4). In the case of helium we get for the exchange scattering amplitude

$$g_n(\Theta, \varphi) = - \frac{2\pi me^2}{h^2} \int \left(\frac{1}{r_{13}} + \frac{1}{r_{23}} - \frac{2}{r_3} \right)$$

$$\exp\left[i(\mathbf{k}_0 \cdot \mathbf{r}_3 - \mathbf{k}_n \cdot \mathbf{r}_1)\right] \psi_0(\mathbf{r}_1, \mathbf{r}_2) \psi_n(\mathbf{r}_2, \mathbf{r}_3) \, d\tau_1 \, d\tau_2 \, d\tau_3$$

$$(2.3.2)$$

Here $\psi_0(\mathbf{r}_1, \mathbf{r}_2)$ and $\psi_n(\mathbf{r}_2, \mathbf{r}_3)$ are the initial and final states of helium with different symmetries. In the reaction an exchange has taken place between the projectile electron $\mathbf{r}_3$ and the helium electron $\mathbf{r}_1$.

2.3.1. *Ochkur approximation*

This approximation is based principally on the expansion of the exchange scattering amplitude of equation (2.3.2) in a series of inverse powers of k_0.
At high impact energies the term with the lowest power of k_0 determines the scattering amplitude. In order to obtain his result, O c h k u r (1964) broke up g_n into three terms and carried out an integration by parts for each of these terms. The following three terms have been found:

a) $g_n^{(1)} = 2k_0^{-2} \int \psi_n^*(\mathbf{r}_2, \mathbf{r}_1) \psi_0(\mathbf{r}_1, \mathbf{r}_2) \exp(i\mathbf{K} \cdot \mathbf{r}_1) \, d\tau_1 \, d\tau_2$

$$(2.3.4)$$

with $\mathbf{K} = \mathbf{k}_0 - \mathbf{k}_n$

17

b) $g_n^{(2)} =$

$$- \frac{2\pi me^2}{h^2} \int \frac{1}{r_{32}} \exp i\,(\mathbf{k}_0 \cdot \mathbf{r}_3 - \mathbf{k}_n \cdot \mathbf{r}_1)\, \psi_0(\mathbf{r}_1 \cdot \mathbf{r}_2)\, \psi_n^*(\mathbf{r}_2, \mathbf{r}_3)\, d\tau_1\, d\tau_2\, d\tau_3$$

$$= O\ (k_0^{-6}) \tag{2.3.5}$$

c) $g_n^{(3)} =$

$$= \frac{2\pi me^2}{h^2} \int \frac{1}{r^3} \exp.\, i\,(\mathbf{k}_0 \cdot \mathbf{r}_3 - \mathbf{k}_n \cdot \mathbf{r}_1)\, \psi_0\,(\mathbf{r}_1, \mathbf{r}_2)\, \psi_n^*\,(\mathbf{r}_2, \mathbf{r}_3)\, d\tau_1\, d\tau_2\, d\tau_3$$

$$= O\ (k_0^{-6}) \tag{2.3.6}$$

and consequently, there is all the more reason for neglecting the last two terms. Thus we see that the amplitude of the exchange scattering amplitude g_n reduces to expression (2.3.4). Then we get:

$$\sigma_n \text{ (Ochkur)} = 3\frac{k_n}{k_0} \int |g_n(\Theta, \varphi)|^2 \sin\Theta\, d\Theta\, d\varphi$$

$$= \frac{24\pi}{k_0^6} \int_{K_{min}}^{K_{max}} |< n| e^{i\mathbf{K}.\mathbf{r}_1} |0>|^2\, K\,dK \tag{2.3.7}$$

For sufficiently large k_0 the integral over K practically does not depend on k_0 and the cross section turns out to be inversely proportional to the cube of the energy, i.e. $\sigma \sim E_{el}^{-3}$.

This dependence has also been found in the binary-encounter theory (see Vriens (1966). However it differs from that mentioned by Mott and Massey (1949a) who note that in the case of helium the cross section for ³S is proportional to E_{el}^{-2} for ³P to E_{el}^{-3} and for ³D to E_{el}^{-4} at high impact energies.

2.4. Relativistic corrections

Formula (2.2.18) needs a correction for relativistic effects when the electron energy exceeds 1 keV. A complete relativistic treatment leads to (see Mott and Massey, 1949b):

$$\dot{\sigma}_n = \frac{4\pi a_0^2 R}{E'_{el}}\ M_n^2 \left\{ \ln c_n\ E'_{el} - \ln\left(1 - \frac{v^2}{c^2}\right) - \frac{v^2}{c^2} \right\} \tag{2.4.1}$$

18

where v is the electron velocity, c is the velocity of light, $E'_{el} = \frac{1}{2} m_0 v^2$ and m_0 is the rest mass of the electron. Here E'_{el} is related to $E_{el} = eV_{el}$ with V_{el} the applied accelerating voltage, by:

$$E'_{el} = \frac{1}{2} m_0 c^2 \left\{ 1 - \frac{1}{\left(1 + \dfrac{E_{el}}{m_0 c^2}\right)^2} \right\} \qquad (2.4.2)$$

which relation is easily obtained from the definition for the relativistic

kinetic energy $\left(= \dfrac{m_0 c^2}{\sqrt{1 - \dfrac{v^2}{c^2}}} - m_0 c^2 \right)$

In the energy range of this work (2.2.18) may be reduced to:

$$\sigma_n = \frac{4 \pi a_0^2 R}{E'_{el}} M_n^2 \ln c_n E'_{el} \qquad (2.4.3)$$

or

$$\sigma_n = \frac{A}{E'_{el}} \ln c_n E'_{el} \qquad (2.4.4)$$

Analogously formula (2.2.21) becomes

$$\sigma_n = \frac{B}{E'_{el}} \qquad (2.4.5)$$

and formula (2.3.6) becomes

$$\sigma_n = \frac{24 \pi}{E'_{el}{}^3} \int_{K_{min}}^{K_{max}} |<n| e^{iK.r_1} |0>|^2 K \, dK \qquad (2.4.6)$$

For the sake of simplicity of notation we shall omit the prime of E_{el} in the following chapters when the relativistic correction of E_{el} has been applied.

2.5. Polarization of the resulting photons of excited levels

In order to get a qualitative insight into the high energy behaviour

19

of the polarization of radiation from excited levels we extend the Bethe approximation for sublevels with magnetic quantum number m (see also Van Eck et al. (1964a). Let us start the problem for excitation of atomic hydrogen, neglecting effects of hyperfine structure (see Percival and Seaton (1958)).

First we consider the polarization from P-S photons, produced as a consequence of the collision which leads via a dipole transition from the ground state to the P state of hydrogen.

For excitation of a level n we can make use of equation 2.2.6. We now look to the expression of ε_n (K) in that equation:

$$\varepsilon_n (K) = \int_{K_{min}}^{K_{max}} e^{i K . r_2} \, \psi_n^* (r_2) \, \psi_0 (r_2) \, d\tau_2$$

In order to find excitation of substates of a P level with magnetic quantum numbers m = 0 and m = ± 1, orientated with respect to the initial velocity direction of the colliding electrons, one has to take the polar axis along velocity v instead of K as is done in the Bethe approximation. In the latter case one only gets excitation of substate m = 0 with respect to K. Carrying out a procedure like in (2.2.8) and (2.2.9), we find from (2.2.6) for excitation of nP states (collision induced dipole transition):

$$\sigma_n \text{ (dipole)} \cong \frac{8 \pi m^2 e^4}{h^4 k_0^2} \int_{K_{min}}^{K_0} \frac{dK}{K} \left| \int \psi_n^* (r) \, r \cos(K . r) \, \psi_0 (r) \, dr \right|^2$$

(2.5.1)

The symbols have the same meaning as before; K_0 is a cut off of the momentum transfer, taken equal to $1/a_0$. In the usual Bethe theory cos ($K.r$) was taken equal to cos ϑ, now we get :

$$\cos(K.r) = \cos \xi \cos \vartheta + \sin \xi \sin \vartheta \cos (\zeta - \Phi) \quad (2.5.2)$$

where ϑ = angle between r and v, Φ = azimuthal angle of the plane (r. v), ξ = azimuthal angle between K and v and ζ = angle of the plane (K, v), the latter being taken equal to zero:

Substituting the wavefunctions for ψ_n^* (r) and $\psi_0 (r)$ of nP

20

and ^1S of atomic hydrogen in equation (2.5.1), we find after some mathematical operations

$$\left.\begin{aligned}
\sigma_n \text{ (dipole, m} = 0) \equiv \sigma(0) &\cong \frac{C}{E_{el}} \int_{K_{min}}^{K_0} \cos^2\xi \frac{dK}{K} \\[2em]
\sigma_n \text{ (dipole, m} = \pm 1) \equiv \sigma(\pm 1) &\cong \frac{C}{E_{el}} \int_{K_{min}}^{K_0} \sin^2\xi \frac{dK}{K}
\end{aligned}\right\} \qquad (2.5.3)$$

where C is a constant and $\sigma(0)$ and $\sigma(\pm 1)$ correspond to $nP_{m=0}$ and $nP_{m=\pm 1}$ states.

For the polarization of the resulting P-S photons, neglecting hyperfinestructure effects, one has

$$\frac{I_\perp}{I_{//}} = \frac{\sigma(\pm 1)}{\sigma(0)} \cong \frac{\displaystyle\int_{K_{min}}^{K_0} \sin^2\xi \frac{dK}{K}}{\displaystyle\int_{K_{min}}^{K_0} \cos^2\xi \frac{dK}{K}} \qquad (2.5.4)$$

where $I_{//}$ and $I_\perp$ are the intensities of the light with electric vectors respectively parallel and perpendicular to the direction of the impacting beam. We see from (2.5.3) that the polarization is about the same for photons from all nP levels, a small difference arising from a different K_{min} because of change in the excitation energy with n.

We want to use expressions (2.5.2) and (2.5.3) to investigate the high energy behaviour of the polarization. We write for $\cos\xi$ the following expression (see Fig. 2.2) by using the cosine rule

$$\cos\xi = \frac{k_0^2 - k_n^2 + K^2}{2Kk_0} = \frac{\dfrac{2m E_n}{\hbar^2} + K^2}{2Kk_0} =$$

$$= \frac{1}{2k_0}\left(\frac{\tau^2}{K} + K\right) \qquad (2.5.5)$$

21
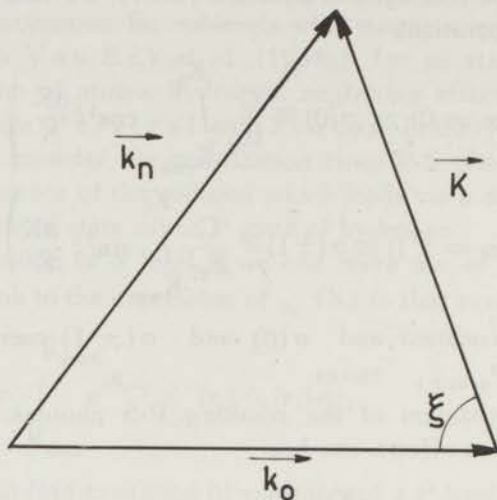
Fig. 2.2   Relation between k_0, k_n, K, and ξ

where we have replaced $\dfrac{2m\,E_n}{\hbar^2}$ by τ,

Further we shall use

$$K_{min} \cong \frac{E_n}{\hbar\,v} \tag{2.5.6}$$

Then we find

$$\int_{K_{min}}^{K_0} \cos^2\xi\, \frac{dK}{K} =$$

$$= \frac{1}{4\,k_0^2}\left[2\,k_0^2 - \tfrac{1}{2}\frac{\tau^4}{K_0^2} + \tfrac{1}{2}K_0^2 - \tfrac{1}{2}\,K_{min}^2 + 2\,\tau^2\ln K_0/K_{min}\right] \tag{2.5.7}$$

In the high energy limit, the term $2\,k_0^2$ between the brackets will dominate, so that

$$\int_{K_{min}}^{K_0} \cos^2\xi\, \frac{dK}{K} \xrightarrow[E_{el}\,\to\,\infty]{} \frac{1}{2} \tag{2.5.8}$$

22

For the $\sigma\,(\pm 1)$ integral of (2.5.3) we write

$$\int_{K_{min}}^{K_0} \sin^2\xi \,\frac{dK}{K} =$$

$$= \int_{K_{min}}^{K_0} (1 - \cos^2\xi)\,\frac{dK}{K} \quad\xrightarrow[E_{el}\to\infty]{}\quad \ln K_0/K_{min} - \tfrac{1}{2} \qquad (2.5.9)$$

From (2.5.3), (2.5.4), (2.5.8) and (2.5.9) we find at last for $E_{el}\to\infty$

$$\frac{\sigma(\pm 1)}{\sigma(0)} = \frac{I_\perp}{I_{//}} = \frac{\ln(K_0/K_{min}) - \tfrac{1}{2}}{\tfrac{1}{2}} = \ln c E_{el} \qquad (2.5.10)$$

where c is a constant. From the calculation it follows that $\sigma(\pm 1)$ or $I_\perp$ is dominating. Also we see from (2.5.3), (2.5.8) and (2.5.9) that $\sigma\,(\pm 1)$ is proportional with $E_{el}^{-1}\ln E_{el}$ and $\sigma(0)$ is proportional with E_{el}^{-1}. This asymptotic behaviour can also be derived from analytical expressions in the Born wave or impact parameter treatment, as given by C r o t h e r s and H o l t (1966) and V a n d e n B o s and D e H e e r (1967) for electrons and protons on atomic hydrogen.

Secondly we consider the polarization of D-P photons, arising as a consequence of the collision which goes via a quadrupole transition (optical forbidden) from the ground state to a D state of hydrogen.

In a similar manner as for σ_n (dipole), we now get

$$\sigma_n(\text{quadrupole}) \cong \frac{8\pi m^2 e^4}{\hbar^4 k_0^2}\,\frac{1}{4}\int_{K_{min}}^{K_0} K\,dK\,|\,\psi_n^*(\mathbf{r})r^2[\cos(\mathbf{K}\cdot\mathbf{r})]^2\psi_0(\mathbf{r})d\mathbf{r}\,|^2$$

$$(2.5.11)$$

where the symbols are the same as before: only $\psi_n(\mathbf{r})$ is now the electron wavefunction for the excited D state of hydrogen, with

23

magnetic quantum number m = 0, ± 1, or ± 2. Proceeding in the some way as for σ_n (dipole) in (2.5.1) by making use of (2.5.2) we find from (2.5.11)

$$\left.\begin{aligned}
\sigma_n \text{ (quadrupole m = 0)} &\equiv \sigma(0) \cong \frac{C}{E_{el}} \int_{K_{min}}^{K_0} (3\cos^2\xi - 1)^2 \, KdK \\[2em]
\sigma_n \text{ (quadrupole m = ± 1)} &\equiv \sigma(\pm 1) \cong \frac{12\,C}{E_{el}} \int_{K_{min}}^{K_0} \sin^2\xi \cos^2\xi \, KdK \\[2em]
\sigma_n \text{ (quadrupole m = ± 2)} &\equiv \sigma(\pm 2) \cong \frac{3C}{E_{el}} \int_{K_{min}}^{K_0} \sin^4\xi \, KdK
\end{aligned}\right\}$$

(2.5.12)

For the polarization of the resulting D-P photons, one can derive, (see McFarland and Soltysik (1962a) neglecting hyperfinestructure effects

$$\frac{I_{//}}{I_\perp} = \frac{4\sigma(o) + 6\sigma(\pm 1)}{\sigma(0) + 3\sigma(\pm 1) + 6\sigma(\pm 2)}$$

(2.5.13)

We now proceed with equations (2.5.12), substituting the expression for $\cos\xi$ of equation (2.5.5). One gets rather lengthy expressions which simplify in the high energy limit to

$$\left.\begin{aligned}
\sigma(0) &= \frac{C}{E_{el}} \, K_0^2 \\[1.5em]
\sigma(\pm 1) &= \frac{3\,C}{E_{el}^2} \, E_n \, \tau^2 \ln c \, E_{el} \\[1.5em]
\sigma(\pm 2) &= \frac{3\,C}{E_{el}} \, K_0^2
\end{aligned}\right\}$$

(2.5.14)

Combining these results with equations (2.5.13) we get in the high energy limit for D-P photons

$$\frac{I_{//}}{I_\perp} = \frac{4}{19}$$

(2.5.15)

24

We see that in the high energy limit the polarization of D-P photons is energy independent.

The asymptotic behaviour found in equations (2.5.14) and (2.5.15) has also been found with the analytical expressions of the Born impact parameter treatment carried out by Van den Bos and De Heer (1967) for protons on atomic hydrogen.

In the case of helium excitation by making use of the Bethe approximation and of hydrogeneous wave functions (see for instance Mott and Massey (1949, p. 227), results can be found with the same energy dependence of the polarization of ^1P-^1S photons and ^1D-^1P photons in the high energy limit.

For helium the expression for $\varepsilon_n(K)$ (see eq. 2.2.6) becomes:

$$\varepsilon_n(K) = \int_{K_{min}}^{K_{max}} \psi_n^*(\mathbf{r}_1, \mathbf{r}_2) \left\{ e^{i\mathbf{K}.\mathbf{r}_1} + e^{i\mathbf{K}.\mathbf{r}_2} \right\} \psi_0(\mathbf{r}_1, \mathbf{r}_2) \, d\tau_1 \, d\tau_2 \quad (2.5.16)$$

Now we write for $\psi_0(\mathbf{r}_1, \mathbf{r}_2)$ the function $\psi_0(Z, \mathbf{r}_1) \psi_0(Z, \mathbf{r}_2)$ and for $\psi_n(\mathbf{r}_1, \mathbf{r}_2)$ the function $\left\{ \psi_0(2, \mathbf{r}_1) \psi_n(1, \mathbf{r}_2) + \psi_n(1, \mathbf{r}_1) \psi_0(2, \mathbf{r}_2) \right\} / \sqrt{2}$ where $\psi_n(Z, \mathbf{r})$ is a hydrogeneous wavefunction of state n in the field of charge Ze. Then we can derive from (2.5.16)

$$\varepsilon_n(K) \cong \int_{K_{min}}^{K_{max}} \psi_0(Z, \mathbf{r}) e^{i\mathbf{K}.\mathbf{r}} \psi_n^*(1, \mathbf{r}) \, d\tau \quad (2.5.17)$$

One can easily see that this expression is almost the same as for $\varepsilon_n(K)$ in the case of atomic hydrogen and leads to the same energy dependence for the polarization.

CHAPTER 3

THE EXPERIMENTAL APPARATUS

3.1. General

A diagram of the apparatus is given in Fig. 3.1. It is the same setup as used for measuring gross ionization cross sections for high energy electrons incident on gases (see S c h r a m et al., 1965 and 1966b). However, some modifications were necessary in order to allow observation of photons by means of a monochromator.

The apparatus consists of a stainless steel cylindrical vessel, divided in two parts: the vacuum chamber and the collision chamber.
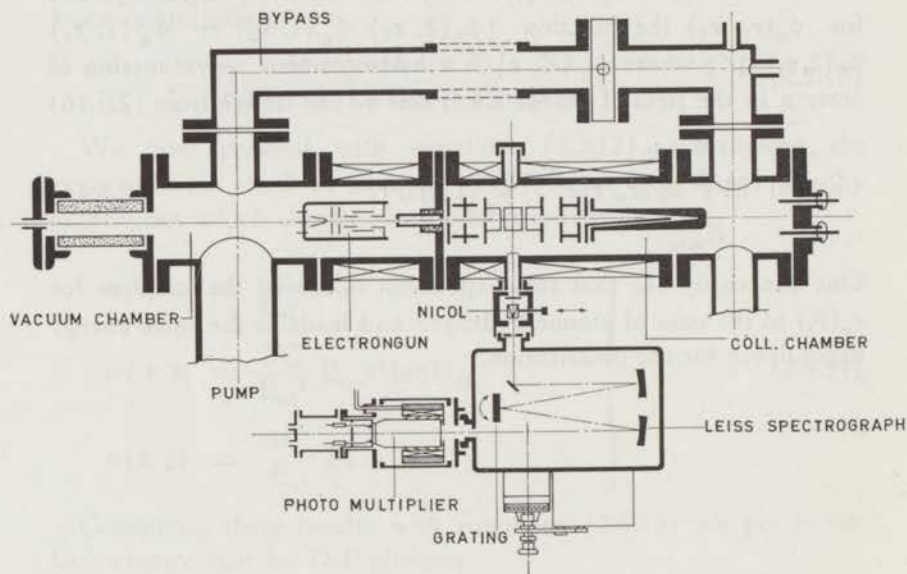
Fig. 3.1 Schematic view of the apparatus used for the excitation and polarization measurements.

The first one contains the electron source and the second one contains the electrode system and a quartz window to the monochromator to allow observation of the light. Both chambers are connected via the collimator and a bypass. An electron beam, generated by the electron source, is shot into the collision chamber and the current is measured in a Faraday cage. Light produced along a well defined pathlength is detected by the monochromator.

Target gas can be introduced into the collision chamber via a needle valve and its pressure is determined with a McLeod gauge.

An axial magnetic field is produced by magnetic coils around both chambers.

3.2. Vacuum

The vacuum chamber is connected to a 650 1/s oil diffusion pump. This pump has a specially designed water cooled chevron baffle (G. Zinsmeister, 1958), which needs no extra freon or liquid air cooling. During the measurements the bypass is closed and, when using the cold trap, the final pressure in the collision chamber is 5×10^{-6} torr. Differential pumping through the collimator (conductance 0.3 1/s for air) enables us to operate the electron source at a pressure of 10^{-6} torr, while maintaining a much higher target gas pressure, 10^{-4}-10^{-3} torr, in the collision chamber.

The absolute pressure of the gas is measured with a McLeod gauge, constructed in the laboratory; its capillary has a diameter of 0.7 mm, constant within $1^0/_{00}$ over the whole length, and a bulb volume of 577 cm^3

Recent experiments (Ishii and Nakayama (1961), Meinke and Reich (1963), and De Vries and Rol (1965)) showed, that a McLeod often gives incorrect results, the error being dependent on gas, temperature and dimensions of the instrument .This effect is a consequence of the steady stream of mercury vapour from the mercury reservoir to the cold trap between the McLeod and the collision chamber. The target gas has to diffuse against this mercury stream, which gives rise to a difference between the pressure in the glass bulb and in the collision chamber. To eliminate this effect, the McLeod was designed following the

27

idea of M e i n k e and R e i c h (1963), see Fig. 3.2. Here the flow of mercury is decreased by mounting a capillary (length 15 cm; diameter 2 mm) between the reservoir and the rest of the McLeod gauge. Any possible effects that might occur in the time it takes the mercury to pass the opening of the side tube, were eliminated by closing off the cold trap with a magnetic valve during that time

TO APPARATUS

MAGNETIC VALVE

COLD TRAP

CAPILLARY
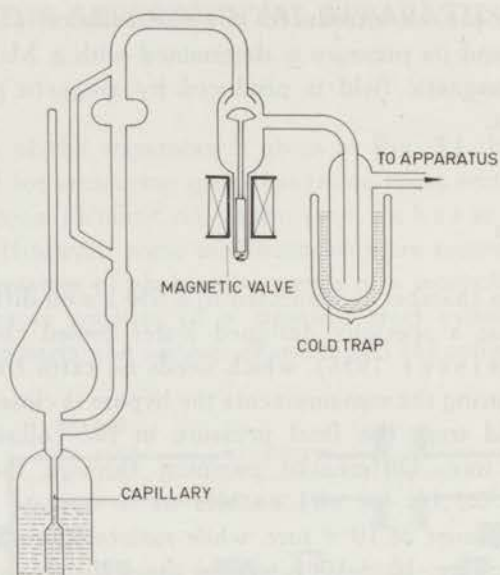
Fig. 3.2 The McLeod gauge, modified to prevent diffusion effects.

(about ½ minute). It has been found (see also D e V r i e s and R o l, 1965) that in the case of light gases such as helium, the diffusion effect is small (~ 1.5%).

As pressure monitor a thermocouple and a Veeco ionization gauge have been used.

3.3. The electron source

The electron source is a Philips 6-AW-59 electron gun from a television tube. The normal operating voltage is 17 kV, but by applying the axial magnetic field, we could use it over the whole energy range of 0.05-6 keV.

28

In order to increase the current output, the original indirectly heated oxide cathode has been replaced by a directly heated tungsten filament of $28\,\mu$ thickness. Currents of up to 1 mA were obtained.

The diameter of the beam was limited by the collimator opening (3 mm) located between the vacuum and collision chambers.

A John Fluke High Voltage Power supply (Model 408 B) was used for the energy range of 0.05 to 6 keV. It has been calibrated by a compensation method.

3.4. Magnetic field

An axial magnetic field was applied for the focusing of the electron beam.

The external magnetic coil around the collision chamber used by S c h r a m et al. has been replaced by two other magnetic coils connected in series with a gap in between. This was necessary to make space for a hole in the collision chamber for observation of the light. The homogeneity of the magnetic field has been achieved in the measuring region within 5% (see Fig. 3.3). We have checked this field by a Gauss meter, taking the best ratio of currents through the coils of the collision chamber.
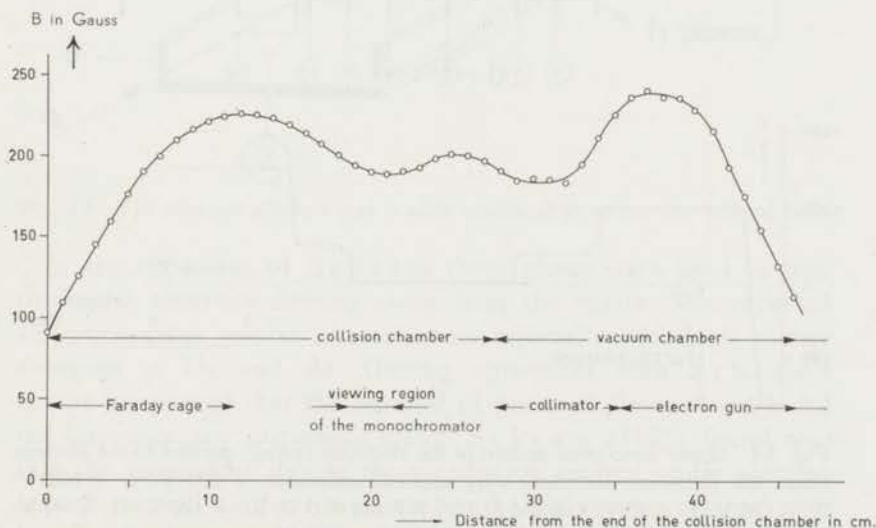
Fig. 3.3 The homogeneity of the axial magnetic field along the axis of the apparatus.

29

In order to prevent asymmetric disturbances in the axial field, caused by the iron frame on which the whole apparatus is mounted or by stray magnetic fields of other apparatusses in the neighbourhood, both chambers with their magnetic coils have been surrounded by a cylindrical iron shield.

3.5. The electrode system

Though the electrode system has not a direct purpose in our optical experiment as it had in the ionization experiment of S c h r a m et al. (1965), we maintained most of the system. The reason was that in this system disturbing effects were avoided with much care. But we had to make however an opening in the closed electrode system in order to see the produced light. The electrode system consists of a number of gold plated stainless steel plates, separated by glass spacers. Fig. 3.4 shows the electrode system
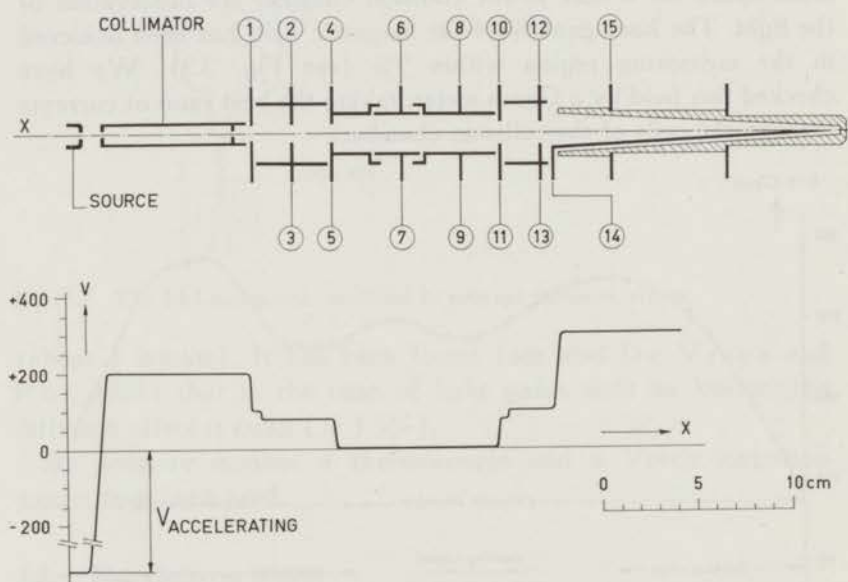
Fig. 3.4 Upper part: cross section of the electrode system, parallel to the electron beam; the following potentials were applied: collimator: + 200 V; 1: + 100 V; 2: + 120 V; 3: + 40 V; 4, 6 and 8: 0 V; 5, 7 and 9: 0 V; 10: + 120 V; 11: + 40 V; 12: + 150 V; 13: + 100 V; 14: + 400 V; 15 + 200 V.
Lower part: potential distribution along the axis of the electrode system.

30

together with the potential configuration along the axis. S c h r a m et al. (1965) showed that by having the measuring region at a lower potential than the collimator and Faraday cage, the disturbances by secondary electrons emitted by these can be avoided. For observation of the radiation we were obliged to remove part of the flat plates a and b at the position of the observation room over a hight of 8 mm (which is about three times the diameter of the electron beam), see Fig. 3.5.
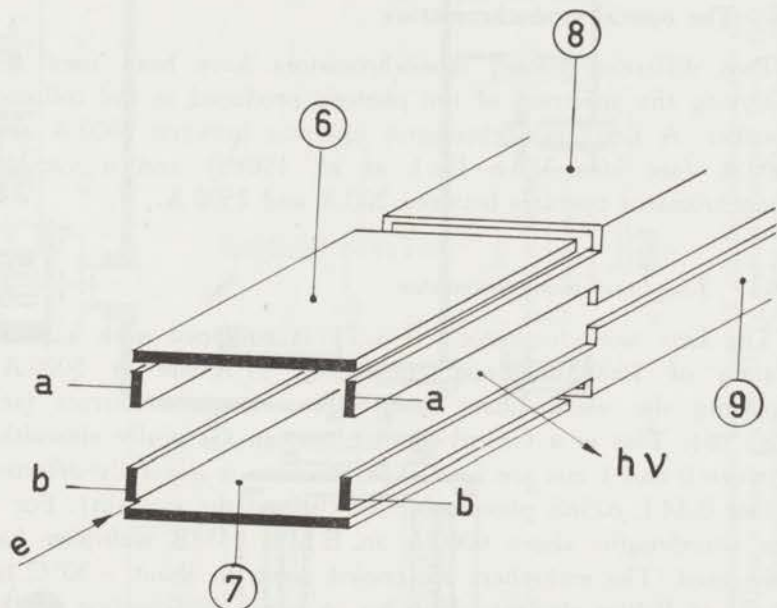
Fig. 3.5   The two flat plates a and b after modification to see the induced light.

In the apparatus of S c h r a m these plates were used to trap trochoidal electrons drifting away from the centre. We repeated ionization cross section measurements especially with high energy electrons in He and Ar. Getting agreement with S c h r a m's results we proved that the removal of parts of plates a and b did not introduce any disturbing effect. S c h r a m (1965) found also that the corrections due to the x-radiation emitted under electron impact, as well as the correction for the increase in relative path length of electrons due to the cycloidal motion can be fully neglected.

31

Mostly we put electrode 4, 6 and 8 at zero potential (see Fig. 3.4) instead of 80 V as used in S c h r a m's setup. At high electron impact energies this seems to have no influence on our excitation measurements. At low electron impact energies the zero setting is better for the energy determination of our electron beam in the observation room and the trochoidal motion of secondary electrons is also avoided.

3.6. The optical monochromators

Two different grating monochromators have been used for analyzing the spectrum of the photons produced in the collision chamber. A Leiss monochromator operates between 2900 Å and 7300 Å (see also Van E c k et al. 1964b) and a vacuum monochromator operates between 200 Å and 2500 Å.

3.6.1. *The Leiss monochromator*

The Leis monochromator ($f \approx 7$) is equipped with a plane grating of 1800 lines/mm (dispersion 17 Å/mm at 5000 Å) replacing the usual prism and of two concave mirrors (see Fig. 3.6). This is a Czerny-Turner system. Generally slitwidths between 0 and 1 mm are used. The radiation is generally detected by an E.M.I. 6256S photomultiplier (behind the exit slit). For a few wavelengths above 6000 Å an E.M.I. 9558B multiplier has been used. The multipliers are cooled down to about $-30°C$ by means of Peltier elements. In order to avoid condensation on the quartz window of the photomultiplier, a case with silicagel is put inside the monochromator and the cooling is not continued during the night. The gain of the multiplier is about 5×10^8 at an overall voltage of 1500 Volt. A dark current of 5×10^{-11} Amp. is usually obtained. The gain is regularly checked with a radioactive sample and luminescent substance ($ZnS + RaCl_3$), which is mounted in the monochromator box just in front of the exit slit. The resulting d.c. signal of the photomultiplier is measured with a Solatron Digital Voltmeter. The exit slit of the original apparatus has been replaced by a movable slit which can be moved by a synchronous motor. When measuring a spectral line, the exit slit can be shifted out of
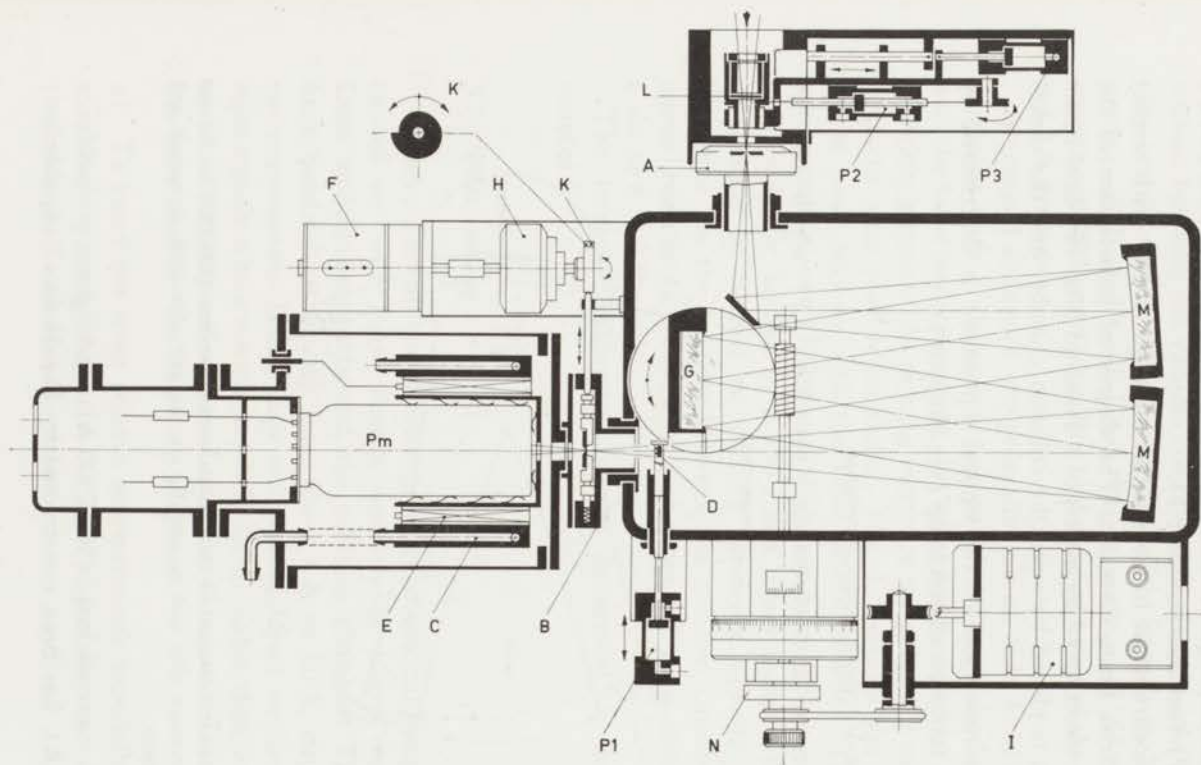
Fig. 3.6 Schematic diagram of the Leiss monochromator. Light from the collision processes enters slit A and is reflected on a plane mirror, on a concave mirror (M), on a plane grating (G), on a second concave mirror (M) and then focused on exit slit (B). The desired wavelength is selected by rotating (G). The light beam can be interrupted by D, containing a mixture of radioactive and luminescent material, acting as monitor. The exit slit can be moved in the focusing plane by motor. On the shaft of this motor potentiometer H with a spiral shaped disc K is mounted. In this way part of the the spectrum (about 15 Å) can be scanned. Photomultiplier Pm is cooled down to $-25°C$ by four Peltier elements E. The polarizer (L) may be rotated over 90° by the pneumatic cylinder P_2 and moved out of the light path by cylinder P_3.

the peak position to measure the continuous background on the line (the span of slit positioning system is about 15 Å). More modifications on the instrument in connection with a future automatization program have been described by S c h u t t e n et al. (1967) (see also section 5.1).

The monochromator is mounted at an angle of 90° with respect to the electron beam direction. The degree of polarization of the radiation is determined by means of a Polaroid filter or Nicol Prism (L), which is placed between the collision chamber and the mono-chromator.

The quantum yield of the optical equipment is determined by means of a tungsten ribbon lamp (see chapter 4).

3.6.2. *The Vacuum monochromator*

The vacuum monochromator (see Fig. 3.7) which can be
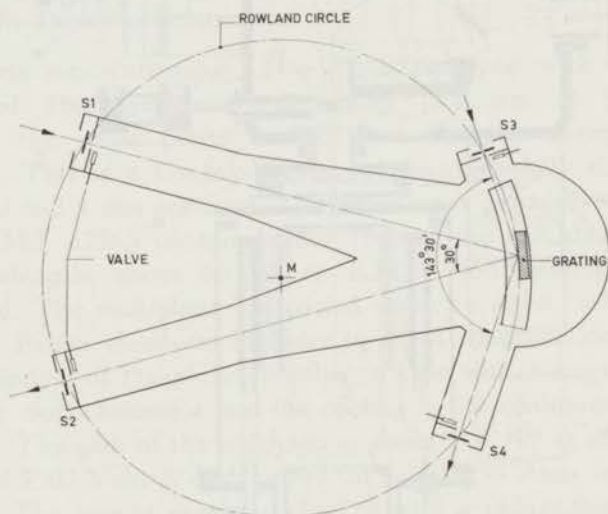
Fig. 3.7 Schematic diagram of the vacuum monochromator (200-2500 Å). S₁ and S₃ are the entrance slits and S₂ and S₄ are the exit slits used at normal and grazing incidence.

used both at normal (500-2500 Å) and grazing incidence (200-1250 Å), has been constructed by D e H a a s (unpublished)

following a design of T o u s e y et al. (1951). The four slits are fixed, while the grating is moving along the Rowland circle with a diameter of about one meter. Also in every slitbody we have built a vacuum lock, so that light sources and detectors can be exchanged without breaking the vacuum conditions in the monochromator. The slits can be varied continuously in width from 0 to 2 mm. The grating of Bausch and Lomb has a surface of 54×96 mm², containing 1200 grooves per mm and the dispersion of the instrument is 8.3 Å per mm.

At normal incidence we generally use an E.M.I. 6256S photomultiplier with a fluorescent screen of sodium salicylate. Just as with the Leiss monochromator, this multiplier is cooled by application of Peltier elements. At grazing incidence we generally use a Bendix magnetic strip particle multiplier. The d.c. signals are registrated in the same way as with the Leiss monochromator. The vacuum system consists of a 650 l/sec oil diffusion pump with a water cooled chevron baffle, backed by a 150 l/min rotary pump. The entrance slits either at normal or grazing incidence operate also as a resistance for the gasflow between the collision chamber and the monochromator (a pressure ratio of about 160 is accomplished with a slit of 8×0.5 mm²).

The intensity calibration of the instrument is described in chapter 4.

3.7. Filter set-up

Relative intensity measurements of some spectral lines have been carried out with Baird Atomic interference filters replacing the Leiss monochromator behind the collision chamber. These filters have bandwidths varying from about 6 Å to 60 Å, dependent on our requirements. Using these interference filters we have obtained light signals which were a factor 30 to 40 higher than for the same spectral line measured with the Leiss monochromator. This advantage has been used for the following purposes:

a) To carry out some relative measurements especially at higher electron energies where the light signal becomes very weak with the Leiss monochromator

b) To carry out the measurements at very low pressures in order to study the influence of collisions of the second kind and of the absorption of resonance radiation more carefully (see chapter 6)

c) To do some control measurements on the results of the polarization degree measured with the monochromator.

Fig. 3.8 represents the filter setup constructed in the laboratory. It consists mainly of a disc holding 12 filters. The disc rotates in a vertical plane behind the collision chamber and is turned by a motor.

In the case of polarization measurements the polarizer (P) can be rotated over 90° by the pneumatic cylinder P_1 and moved out of the light beam by cylinder P_2.

The position of the polarizer is also remotely controlled, as the pneumatic cylinders are operated by solenoid valves.
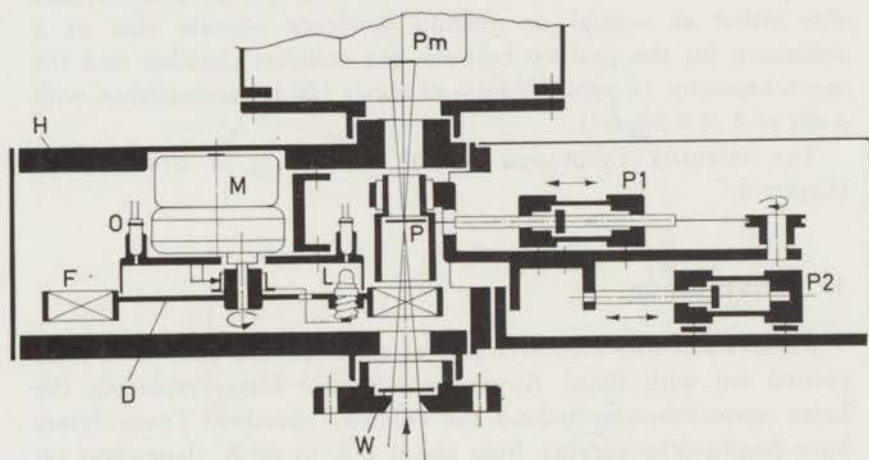
Fig. 3.8 Schematic drawing of the filter setup. The disc (D) serves as a holder of 12 filters (F) and lamp (L). This disc (D) rotates in a vertical plane behind the collision chamber with the motor (M).
Corresponding to the twelve different wavelengths there are twelve photocells (O) (type ORP 60). During the rotation of the disc, when the light of the lamp (L) falls on the selected photocell (corresponding to the required wavelength) the motor stops and the interference filter is positioned exactly opposite the hole of the tube to the collision chamber. The light was detected with the photomultiplier (Pm). W is a quartz window.

36

CHAPTER 4

ABSOLUTE CALIBRATION
OF THE OPTICAL EQUIPMENT

4.1. Leiss monochromator

To find out the emission cross section (eq. 1.4.2), it is necessary to determine the quantum yield $k(\lambda)$ of the optical equipment.

The method of this absolute calibration has been described in details by Van Eck (1964b) and Sluyters (1959). We shall repeat some details. The calibration is performed with a gas ribbon filled lamp with a quartz window. The lamp is provided with a vertical tungsten ribbon of area 10×2 mm² and an index line in the centre to indicate the part where the temperature calibration was performed. In the calibration procedure the standard can be put in a holder, attached to the collision chamber on the opposite side of the monochromator. The light of the standard is geometrically limited by a diaphragm located rather close to the standard and by the entrance slit to the monochromator. A disadvantage of this method is that only a small part of the grating is filled with light, but control measurements have been carried out about the homogeneity of response of the grating surface. The energy radiated from a tungsten ribbon E_w — in a direction perpendicular to the ribbon as a function of the wavelength λ and the absolute temperature T — was taken from the tables of De Vos (1953). The temperature of the ribbon as a function of the current was calibrated by the producer of the lamp. The current through the ribbon was measured by comparing the voltage drop over a $0.6000 \, \Omega$ resistance with the voltage of a normal element (1.018 V) in a Wheatstone bridge circuit. In this way 0.1% accuracy in the current measurement is obtained. The quantum yield $k(\lambda)$, the current signal per incoming photon per second, is given by:

$$k(\lambda) = \frac{S(\lambda)}{E_w(\lambda, T) \cdot \lambda \cdot t_\lambda \cdot \overline{\Delta \lambda}} \times \frac{hc}{\omega \, 0} \qquad (4.1.1)$$

where

S = the measured signal in Amp.;

h = the Plank's constant;

c = the velocity of light;

ω = used solid angle;

0 = surface area of tungsten ribbon which was used;

E_w = emissivity in ergs cm^{-2} $ster^{-1}$ λ^{-1} sec^{-1};

t_λ = the transmission of the quartz window of the lamp;

$\overline{\Delta \lambda}$ = wavelength range used in Å which is determined by the slit width in front of the multiplier.

It appeared necessary to make corrections for straylight at the lower wavelength (< 4000 Å). At these wavelengths we did the calibration both with and without a glass window, which absorbs the radiation below 3300 Å and which transmits about 85% of the radiation above 4000 Å. The signal $S(\lambda)$ we should measure, is now for $\lambda < 3300$ Å:

$$S(\lambda) = S \text{ (total)} - \frac{1}{0.85} S \text{ (glass)} \qquad (4.1.2)$$

From 3300 Å downwards the straylight appeared to be constant. As the straylight signal above 3300 Å could not be measured separately, we assumed it would remain the same from there up to 4000 Å from where this correction becomes unimportant .

In order to control the amplification of the multiplier, both the calibration and excitation measurements are normalized on the signal of a radioactive-fluorescent sample (see section 3.6.1).

The random error in our calibration was about 3%, determined from different calibrations in the time of these measurements. The standard deviation is about 6%.

At the lowest (< 3500 Å) and highest (> 5800 Å) wavelengths these errors may be somewhat larger. For more details on the absolute calibration one can refer to V a n d e n B o s (1967).

38

Separate experiments were taken to check the homogeneity of the grating. This is necessary because in the calibration procedure and in the excitation measurements (see chapter 5), different parts of the grating are illuminated. In the calibration we use only a small width (~ 2 mm) of the grating while in the beam experiment almost the whole width (53 mm) is used. Also the heights of the grating illuminated in both cases are not equal.

We first varied the height of the entrance slit of the Leiss monochromator with an E.M.I. 6256S photomultiplier both in a helium emission measurement and in the quantum yield determination. In this case we found a constant ratio between the intensity of the light from excited helium (measured for 4^1S-2^1P) and the quantum yield of the monochromator (measured at the corresponding wavelength) varying the height of the entrance slit between 8 mm and 1 mm (normally 8 mm is used).

We then varied the observation length in a beam experiment by an extra collimator between the electron beam and the entrance slit of the monochromator in such a way, that in the width direction only 2 mm of the grating was used, comparable with the width in the calibration procedure. In the electron beam experiment we normally have an effective width of about 47 mm. The emission in this experiment was taken for 4^1S-2^1P, 3^1P-2^1S and 4^1D-2^1P. It was found that the emission cross sections (see chapter 5 and equation 5.1.1) obtained with the extra collimator were only 3% larger than those obtained without the collimator in our usual procedure. A correction has been made for this effect in the evaluation of the excitation cross section.

Similar control experiments have been started with the Leiss monochromator equipped with the E.M.I. 9558B photomultiplier, which has been used for a few lines in the near infrared region. Varying the height of the entrance slit of the monochromator between 8 mm and 1 mm, we did not find a constant ratio between the intensity of the light of the excited helium and the quantum yield of the monochromator. The cause of this effect has not yet been found.

The radiation produced in the electron beam experiments may be polarized. It is, therefore, important to achieve the intensity calibration by determining the sensitivity of the optical equipment to polarized light.

The tungsten standard emits unpolarized light and $k(\lambda)$ can then be represented by

$$2k(\lambda) = k_{//}(\lambda) + k_{\perp}(\lambda) \qquad (4.1.2)$$

where $//$ and $\perp$ correspond to light with electric vectors respectively parallel and perpendicular to the electron beam direction in the setup of Fig. 3.1, or with electric vectors respectively perpendicular and parallel to the entrance slit of the Leiss monochromator in the setup of Fig. 3.6. It is therefore sufficient to determine the ratio of $k_{//}(\lambda)$ and $k_{\perp}(\lambda)$, which can be easily done by means of a polaroid filter used as a polarizer behind the light source.
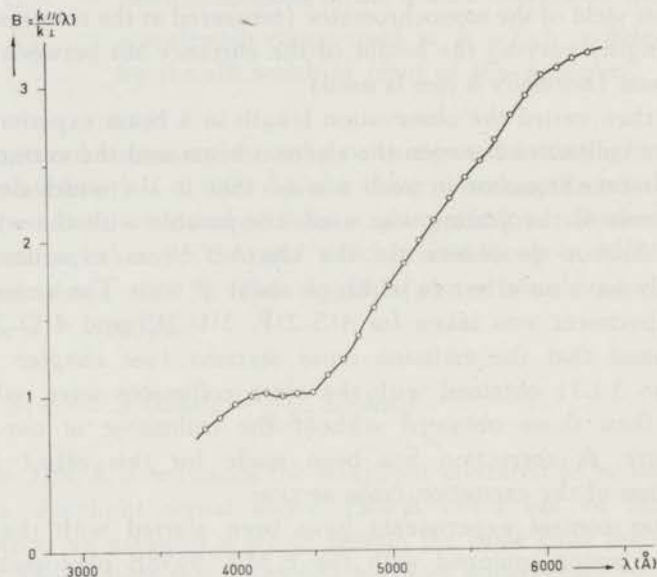
Fig. 4.1 Sensitivity of the Leiss monochromator for polarized light.

In Fig. 4.1 we show the polarization action of the Leiss monochromator.

4.2. Vacuum monochromator

In the vacuum ultraviolet region no simple light standard is available for the intensity calibration and other methods have to be

40

used. These methods are reviewed by De Heer (1966) and Shreider (1965).

In the vacuum ultraviolet, excitation measurements have been done (see chapter 7) on He II lines at 1640 Å, 1215 Å, 303 Å and 256 Å and on the He I line at 584 Å. However, with our available equipment, we had to confine the intensity calibration to two wavelengths, namely 1215 Å and 537 Å. Measurements were done both with the Bendix multiplier and E.M.I. photomultiplier covered with sodium salicylate. We obtained $k(\lambda)$ at the other mentioned wavelengths by inter- and extrapolation of data obtained with the photomultiplier, because this detector has a rather uniform response (see Johnson et al. (1951), and Watanabe and Edward (1953)).

For absolute normalization of our results at 1215 Å we used the cross section results on Lyman-α radiation of Fite and Brackmann (1958) in the case of electron impact (from threshold to 500 eV) on molecular hydrogen as standard cross sections. By comparing the output of the optical instrument at 1215 Å in the case of electron impact on helium and in the case of electron impact on molecular hydrogen (1216 Å), it was then possible to obtain the abolute value of the cross sections for He II emission at 1215 Å. From the measurements with H_2 it is also possible to calculate the quantum yield $k(\lambda)$ of the vacuum monochromator by means of the equation for the emission cross section (see section 1.4), where $k(\lambda)$ is the only unknown.

As far as 1640 Å is concerned, we assumed that when working with near normal incidence, the quantum yield $k(\lambda)$ is about the same as at 1215 Å. This is correct if the reflected fraction of light at the grating does not change much between 1215 Å and 1640 Å, and if the response of the photomultiplier is independent on the wavelength. In this case we used a fluorescent layer of sodium salicylate in front of the multiplier, which has an uniform response over a large wavelength region (see Johnson et al., 1951). Measurements from Hass and Tousey (1959) indicate that the reflection of light is not changing much from 1640 Å to 1215 Å if the grating is coated with MgF_2 as in our case.

At 537 Å, we used the method of Van Eck and De Heer

41

(1963). It is based on measuring the intensities of two spectral lines having the same upper level in an atom for which the atomic transition probabilities are known. If one of the lines is in the visible region, where its intensity can be measured by an absolutely calibrated spectrograph and the other one in the vacuum ultraviolet region, the intensity of the ultraviolet line can be calculated. Van Eck and De Heer (1963) have used the helium lines 3^1P-2^1S ($\lambda = 5016$ Å) in the visible region and 3^1P-1^1S ($\lambda = 537$ Å) in the far ultraviolet. The spectral lines originate from excited neutral atoms which are formed in a beam of fast He^+ ions (30 keV) passing through a collision chamber filled with hydrogen or neon gas. A He^+ ion can capture an electron from a target atom into the He I 3^1P state. Decay of this state gives rise to the emission of the desired radiation.

In order to have an absolute normalization of our data at 303 Å and 256 Å, measured at grazing incidence, we made a linear extrapolation of our $k(\lambda)$ values at 1215 Å and 537 Å, which were also measured at grazing incidence.

For 584 Å we took the quantum yield equal to that of 537 Å when both lines were measured at grazing incidence.

Generally, the calibration in the vacuum ultraviolet is not so accurate as in the higher wavelength region, because the calibration measurements have been carried out at only a few wavelengths and inter and extrapolations have been made to other wavelengths. Also the effect of polarization of radiation has been neglected. Therefore the values of $k(\lambda)$ may often be as inaccurate as about 100%.

42

CHAPTER 5

EXPERIMENTAL PROCEDURE AND
EVALUATION OF THE RESULTS

5.1. The experimental procedure

If one measures the light produced by the electron beam in helium, the emission cross section for a spectral line is calculated (apart from corrections to be discussed later on) from the next equation (see also eq. (1.4.2.)):

$$\sigma_{ij} = \frac{4\pi}{\omega} \times \frac{S(\omega)}{l\,\dfrac{I}{e}Nk(\lambda)} \qquad (5.1.1)$$

This formula shows us what quantities have to be determined in a cross section experiment: The current I of the electron beam is measured in the Faraday cage (see Fig. 5.1). Disturbing
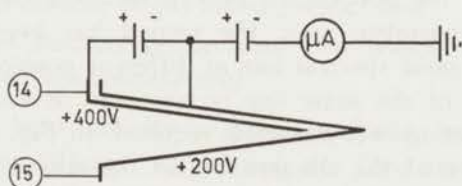
Fig. 5.1   Schematic view of the measurement of the electron beam current.

effects influencing this measurement have been avoided, as has been described by S c h r a m et al. (1965). A Solatron Digital Voltmeter is used for measuring the electron current. The photomultiplier detects the induced radiation and its current is measued by the same Digital Voltmeter. The output of the multiplier as well as the Faraday cage are connected with three different channels of the Digital Voltmeter in series. For every energy of the primary electrons

we get, therefore, three values of the light signal and also three values of the electron beam intensity. At every energy the measurement is repeated twice and the average of the six values for both intensities is determined.

The real intensity of the line has been determined by measuring the signal at two slightly different positions of the exit slit: at "peak" corresponding to the intensity of the spectral line and background together, and at "valley" (i.e. at a wavelength region where only the continuous background is present) corresponding to the background signal only. The valley signal gives the background and has to be subtracted from the peak to give the correct signal value.

In the Leiss monochromator (see section 3.6.1) the two positions are obtained by moving the exit slit in the focusing plane by a motor, which depends on the setting of switches on the control panel: one is fixed and gives the calibrated wavelength of the spectral line by the position of the grating, the second can be chosen by a potentiometer on the control panel, and is determined by the physical conditions, i.e. the continuous background. This way of determining the intensity of a spectral line is allowed only when the two following conditions are fullfilled: the background signal must not change abruptly with wavelength and the sensitivity of the multiplier must not depend on the position of the exit slit. The first condition is checked in a complete scan, the second has been checked by measuring the same spectral line at different positions of the exit slit. The peak of the same line is measured in each position by rotating the grating over the angle required. In Fig. 5.2 the results of the influence of the slit position on the output of the photo-multiplier are indicated. It is clear that the influence of the position of the exit slit is small, so that our method appears correct.

The operation mechanism and the electronic circuits are explained in more details by S c h u t t e n et al. (1967).

In the vacuum monochromator the peak and valley can only be obtained by moving the grating because the exit slit is not movable in the focusing plane as in the Leiss monochromator.

The procedure of intensity measurements is carried out at a known pressure and at vacuum conditions. In many cases the intensity at

vacuum can be neglected, but as we shall see in chapter 6 this is not always the case.
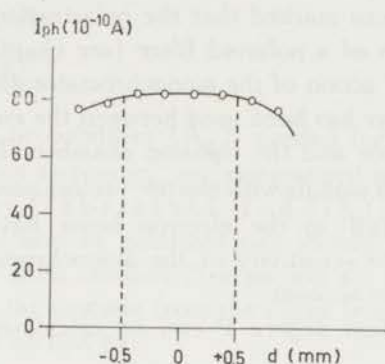
Fig. 5.2 Influence of change of slit position d on photomultiplier output I_{ph} at constant light input. (The grating G was rotated to compensate for the slit movement).

The quantity N in equation (5.1.1) follows from the pressure measured by the McLeod gauge (see section 3.2). The relation is:

$$P = N k T$$

k = Boltzman's constant

N = the number of gas atoms per c.c., and

T = the absolute temperature (for which we have taken the room temperature).

An extensive light intensity — pressure relation was determined for every line at different impact energies (see next chapter), in order to verify that the intensity measurements were carried out in the linear proportional region. $k(\lambda)$ follows from the intensity calibration (see chapter 4).

Each light intensity measurement is normalized by means of the current output of the radioactive luminescent sample, as is also done in the intensity calibration (see also chapters 3 and 4).

ω, is the solid angle of the optical system determined by the dimensions of the entrance slit of the monochromator (equal to that of the exit slit) and the distance of the electron beam to the entrance slit.

45

l is the length of the beam region from which the light is seen by the monochromator, in our case about 2.5 cm, depending on the wavelength as a consequence of rotation of the grating.

It has already been marked that the polarization of light can be measured by means of a polaroid filter (see chapter 4), correcting for the polarization action of the monochromator (see next section).

The polaroid filter has been used between the entrance slit of the Leiss monochromator and the collision chamber. This filter can be rotated and the light signals with electric vectors parallel $(S_{//}(\omega))$ and perpendicular $(S_{\perp}(\omega))$ to the electron beam have been measured separately. Also the sensitivity of the monochromator to polarized light was taken into account.

So the polarization degree P can be calculated from the next equations:

$$
\left.
\begin{aligned}
I_{//} &= \frac{S_{//}}{K_{//}} \\[2mm]
I_{\perp} &= \frac{S_{\perp}}{K_{\perp}}
\end{aligned}
\right\}
\tag{5.1.2}
$$

$$
P = \frac{I_{//} - I_{\perp}}{I_{//} + I_{\perp}} \times 100\% = \Pi \times 100\% \tag{5.1.3}
$$

Π is the polarization fraction.

$I_{//}$ and $I_{\perp}$ are the radiation intensities observed at an angle $90°$ to the direction of the electron beam, with electric vectors parallel and perpendicular to the electron beam respectively.

In the next section the correction on equation (5.1.1) as a consequence of the polarization is discussed.

No polarization measurements were carried out in the vacuum ultraviolet region.

5.2. Evaluation of the excitation cross section

From the calculated values of the emission cross sections by equation 1.4.2 of chapter 1, one can derive the excitation cross section σ_i with the help of equation (1.3.5) of chapter 1, neglecting

the second term of the right hand side of this formula (which is due to the cascade cross section) one can write:

$$\sigma_i = \sigma_{ij} \frac{\sum\limits_{j < i} A_{ij}}{A_{ij}}$$

(5.2.1)

The transition probabilities (A_{ij}), needed for the calculation of the excitation cross section σ_i, are summarized in Table 5.1, which has been given by G a b r i e l and H e d d l e (1960). Because the induced radiation may be polarized one should apply a correction on the excitation cross sections (see section a). Moreover, another correction due to the cascade from the upper levels should be taken into account (see section b).

a. *Correction due to the polarization degree of the induced radiation*

In the collision of a beam of electrons with helium atoms, the induced radiation often appears to be partially polarized. This is because of the anisotropy introduced by the parallel incident beam of electrons. It is known that the angular distribution of the radiation is proportional to $(1 - \Pi \cos^2 \Theta)$ in the case of dipole radiation; this means that,

$$\frac{I(\Theta)}{I(90)} = 1 - \Pi \cos^2 \Theta$$

(5.2.2)

$\Theta =$ the angle between the observational and the electron beam direction

$I(\Theta) =$ the measured intensity under an angle Θ

We define the cross section per unit solid angle for photon emission to be $\sigma(\Theta)$ where

$$\sigma(\Theta) = C (1 - \Pi \cos^2 \Theta)$$

(5.2.3)

The total cross section σ_{ij} is calculated by integration of the differential cross section over the whole sphere

47

TABLE 5.1
Radiative transition probabilities (units of 10^6 sec $^{-1}$)

	2¹P	3¹P	4¹P	5¹P	6¹P	7¹P	8¹P
1¹S	1780	571	246	127	74.0	46.6	31.0
2¹S	1.97	13.4	6.81	3.85	2.56	1.60	1.07
3¹S	18.8	0.25	1.47	0.94	0.57	0.43	0.26
4¹S	6.60	4.54	0.06	0.30	0.25	0.19	0.14
5¹S	3.12	2.01	1.49	0.02	0.08	0.07	0.07
6¹S	1.76	1.07	0.72	0.61	0.01	0.03	0.05
7¹S	1.21	0.62	0.42	0.30	0.26	0	0.04
8¹S	0.74	0.41	0.27	0.21	0.15	0.14	0
3¹D	65.1	0	0.29	0.13	0.09	0.08	0.07
4¹D	19.3	7.14	0	0.16	0.08	0.05	0.03
5¹D	8.89	3.28	1.52	0	0.08	0.04	0.03
6¹D	4.94	1.80	0.84	0.47	0	0.04	0.02
7¹D	2.63	1.17	0.52	0.29	0.18	0	0.02
8¹D	1.82	0.66	0.38	0.22	0.15	0.14	0

	2³P	3³P	4³P	5³P	6³P	7³P	8³P
2³S	10.2	9.28	5.67	3.08	1.87	1.15	0.79
3³S	27.5	1.07	0.71	0.60	0.41	0.29	0.21
4³S	9.26	6.42	0.22	0.12	0.14	0.17	0.18
5³S	4.33	2.68	2.05	0.06	0.03	0.05	0.07
6³S	2.40	1.40	0.90	0.76	0.03	0.01	0.02
7³S	1.75	0.86	0.51	0.37	0.36	0.01	0.01
8³S	1.18	0.60	0.34	0.25	0.17	0.15	0.01
3³D	71.7	0	0.65	0.27	0.06	0.01	0
4³D	24.4	6.65	0	0.32	0.16	0.03	0.01
5³D	11.9	3.38	1.26	0	0.16	0.09	0.02
6³D	5.87	1.99	1.05	0.35	0	0.09	0.05
7³D	4.53	1.33	0.60	0.26	0.13	0	0.03
8³D	3.03	0.98	0.43	0.22	0.10	0.06	0

$$\sigma_{ij} = \int\limits_0^\pi \int\limits_0^{2\pi} C(1 - \Pi \cos^2 \Theta) \sin \Theta \, d\Theta \, d\varphi$$

$$= \frac{4\pi}{3} \cdot C \cdot (3 - \Pi) \rightarrow C = \frac{3\sigma_{ij}}{4\pi(3-\Pi)} \tag{5.2.4}$$

So we find that:

$$\sigma(\Theta) = \frac{3\sigma_{ij}}{4\pi(3-\Pi)} \times (1 - \cos^2 \Theta) \tag{5.2.5}$$

In our case where $\Theta = 90°$, eq. (5.2.5) becomes

$$\sigma_{ij} = \sigma_{ij}(90°) \cdot \frac{4\pi(3-\Pi)}{3} \tag{5.2.6}$$

Since the monochromator has different sensitivity for light polarized parallel and perpendicular to the grating rulings, we have to make a correction according to the sensitivity of the monochromator (see section 4.1). This has been done as follows:

We have seen that the emission cross section is given by eq. (1.4.2) if the influence of the polarization is not taken into account.

We now introduce the quantity $I_\lambda (\Theta)$:

$$I_\lambda(\Theta) = \frac{S_\lambda(\Theta)}{k(\lambda)} \tag{5.2.7}$$

For convenience we omit the subscripts λ and the space angle ω.

$S(\Theta)$ is the measured signal at an angle Θ and given by the sum of the signals with parallel and perpendicular electric vectors:

$$S(\Theta) = S_{//}(\Theta) + S_\perp(\Theta) \tag{5.2.8}$$

where parallel corresponds to the electric vector in the plane through the electron beam and the direction of observation of light and perpendicular corresponds to the electric vector perpendicular to this plane.

Taking into account polarization, $I(\Theta)$ in (5.2.7) has to be replaced by:

$$I(\Theta) = I_{//}(\Theta) + I_\perp(\Theta) = \left(\frac{S_{//}(\Theta)}{k_{//}} + \frac{S_\perp(\Theta)}{k_\perp} \right) \tag{5.2.9}$$

49

Making use of equations (5.2.8) and (4.1.2), eq. (5.2.7) becomes after correction:

$$I(\Theta) = \frac{S(\Theta)}{k} \cdot \frac{(B+1)(C(\Theta)+1)}{2(BC(\Theta)+1)} \tag{5.2.10}$$

where

$$B = \frac{k_{//}}{k_\perp} \quad \text{and} \quad C(\Theta) = \frac{I_{//}(\Theta)}{I_\perp(\Theta)} \tag{5.2.11}$$

B follows from the polarization of the apparatus and $C(\Theta)$ from the polarization measured at an angle (Θ).

Our measurements have been taken at 90°. Combining equations (5.1.1), (5.2.6) and (5.2.10), we find the emission cross section:

$$\sigma_{ij} = \frac{4\pi}{\omega} \times \frac{S(90°)}{l\frac{I}{e}Nk(\lambda)} \left[\frac{(1+B)(C_{90°}+2)}{3(BC_{90°}+1)} \right] \tag{5.2.12}$$

where the term between brackets at the right hand is the correction term due to polarization.

b. *Cascade correction*

The state i may be populated by normal radiative transitions from atoms in higher states k. For the calculation of the absolute excitation cross section such a contribution should be taken into account.

Corrections for cascade effects are calculated using the second term of the right hand side of equation 1.3.5 and this correction can be applied if $\sum_{k>i} \sigma_{ki}$ is known.

The correction procedure was carried out as follows: σ_i values were calculated for different i's from equation 1.3.4 with neglection of the cascade. Then the cascade contribution was calculated by putting

50

$$\sigma_{ki} = \sigma_k \frac{A_{ki}}{\sum\limits_{i}^{k-1} A_{ki}} = \sigma_k A_{ki} \tau_k$$

where $\tau_k = 1/\sum\limits_{i}^{k-1} A_{ki}$ is the life time.

For the higher k values, σ_k was estimated by extrapolation of the uncorrected excitation cross sections with an n^{-x} dependence. The exponent x and the cascade contributions from levels up to $n = 8$ for each measured energy were calculated by means of a simple computer program.

In this calculation, when determining the cascade contribution to ^1S and ^1D levels, we had to use the apparent excitation cross sections of the ^1P levels at the same pressure at which uncorrected ^1S and ^1D cross sections were determined ($\sim 10^{-3}$ torr).

Table 5.2 shows the corrections due to cascade relative to the uncorrected excitation cross sections. Cascade from F levels has been neglected for both singlet and triplet levels.

TABLE 5.2

First order cascade correction in percentage relative to the uncorrected excitation

E_{el} in keV	3^1S	4^1S	5^1S	6^1S	3^1P	4^1P	5^1P	3^1D	4^1D	5^1D	6^1D	3^3S	4^3S	5^3S	3^3P	4^3P	5^3P	3^3D	4^3D
0.06	12.4	5.4	1.8	1.2	5.5	3.1	2.1	1.0	1.0	0.9	0.7	28.4	11.4	9.7	18.5	8.7	4.1	20.5	22.7
0.08	15.2	6.0	2.1	1.4	5.1	2.7	1.7	1.3	1.2	1.1	0.9	28.2	12.0	10.2	18.0	8.4	3.6	18.8	23.7
0.10	16.2	6.6	2.2	1.6	4.1	3.4	1.5	1.5	1.6	1.3	1.0	26.0	10.6	8.5	18.6	10.8	3.9	13.4	19.5
0.20	19.2	7.6	2.5	1.5	3.3	2.0	1.3	2.2	2.5	2.1	2.0	17.0	7.9	6.4	27.0	15.5	6.3	6.5	11.4
0.30	19.5	6.6	2.6	1.8	3.0	1.9	1.3	2.8	3.3	2.3	1.6	15.2	7.4	6.1	34.7	15.9	7.6	5.9	9.0
0.40	21.3	6.9	2.5	1.8	2.9	2.1	1.3	3.1	3.6	3.0	2.0	15.8	7.6	6.6	38.0	15.2	7.5	5.2	9.4
0.50	21.0	7.4	2.6	1.8	2.8	1.8	1.2	3.3	3.8	2.5	2.4	14.9	6.4	5.0	35.4	15.1	7.2	6.2	7.3
0.60	21.0	7.3	2.5	1.8	2.7	1.8	1.2	3.4	3.8	3.0	2.5	15.9	7.9	5.2	35.4	18.9	9.9	3.6	7.9
0.80	22.1	7.1	1.6	1.8	2.6	1.8	1.2	3.6	3.8	3.0	2.6	14.5	5.4	2.9	38.1	20.4	11.4	5.7	6.2
1.00	22.4	8.0	2.7	1.9	2.5	1.6	1.1	4.1	4.6	3.4	2.8	14.0	5.8	3.3	40.0	21.6	11.5	5.7	5.7
1.50	23.7	8.7	2.9	2.1	2.2	1.6	1.1	4.8	4.5	3.6	3.4	15.8	6.4	4.0	40.1	23.0	13.7	7.5	6.2
2.00	24.5	8.2	3.1	2.3	2.3	1.5	1.1	5.4	5.7	3.9	3.6	14.6	5.5	2.5	40.0	21.5	12.5	7.7	5.7
2.50	26.5	8.6	3.1	1.8	2.1	1.5	1.0	5.2	5.3	3.7	3.1								
3.00	27.5	9.3	3.0	2.2	2.3	1.3	0.9	5.2	5.6	3.7	3.5								
4.00	29.8	10.0	3.4	2.0	2.3	1.4	1.0	6.6	6.3	3.8	3.3								
5.00	30.1	10.3	3.4	2.7	2.3	1.3	1.0	6.9	6.7	4.2	2.5								

CHAPTER 6

DEPENDENCE OF THE LIGHT EMISSION AND THE POLARIZATION ON THE GAS PRESSURE, THE AXIAL MAGNETIC FIELD AND THE ELECTRON BEAM CURRENT

6.1. The emission and polarization of the light as a function of gas pressure

6.1.1. Introduction

As has been explained before (see section 1.5), some of the discrepancies in the cross section magnitudes were due to too high pressures used during the measurements. One should always carry out the cross section measurement in the pressure region where a linear relationship between the pressure and the light intensity exists. The deviation from the linearity is due to different processes, such as:

a) The absorption of resonance radiation, which has a very short free pathlength in its own gas and this absorption gives rise to a repeated occupation of the n^1P levels and therefore an enhancement of the n^1P-m^1S ($m > 1$) transitions

b) Second order collision processes (sec eq. 1.5.1) or collisions of the second kind.

These processes cause also a depolarization of the light (see also H e d d l e and L u c a s, 1962). For, if a state is populated by these processes instead of by a direct collision, the resulting radiation will have no prefered direction. This means that it will be emitted isotropically which is observed as depolarization of the primary impact radiation.

The secondary effects are different from one transition to an-

53
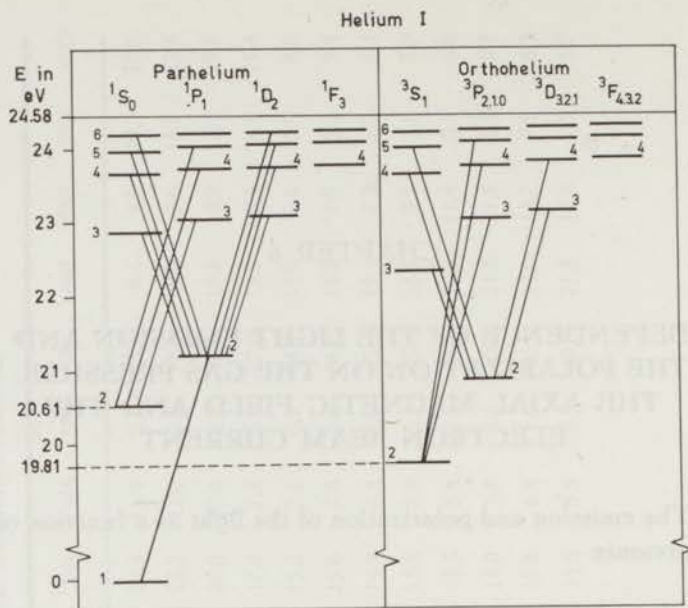
Fig. 6.1 Level scheme of He I. For the indicated transitions the light intensity is measured as a function of energy.
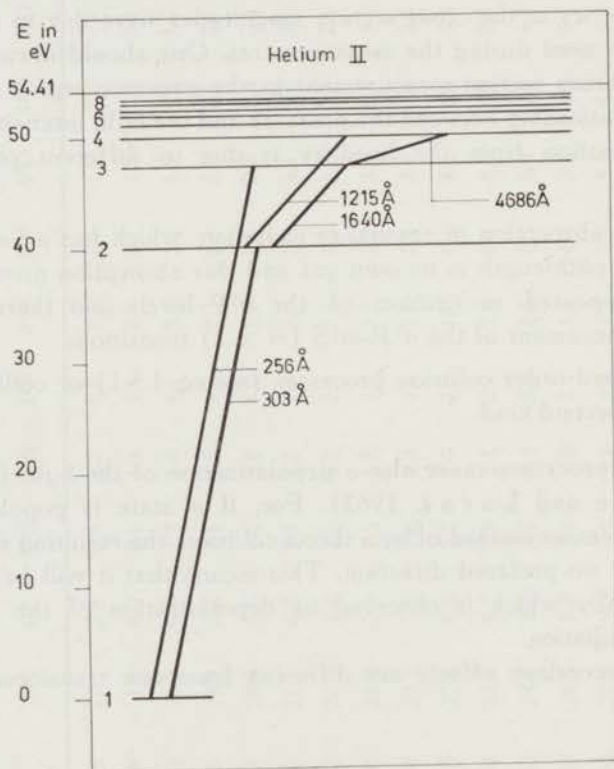
Fig. 6.2 Level scheme of He II. For the indicated transitions the light intensity is measured as a function of energy.

other, and sometimes depend on the energy of the impacting electron. Therefore, the pressure-light intensity dependence has been done (generally between 10^{-4} and 10^{-2} torr) in this experiment for all transitions which have been measured using different electron impact energies.

Fig. 6.1 and 6.2 represent the He I and He II spectra and the measured spectral lines (see also Table 6.1).

6.1.2. Singlet transitions

a) The n^1S-2^1P ($n = 3, 4, 5$ and 6) transitions

Fig. 6.3 shows that the light intensity of the 4^1S-2^1P transition (5047 Å) is proportional with the pressure up to $> 3 \times 10^{-3}$ torr. The intensity as a function of electron impact energy has been determined at about 2×10^{-3} torr. For the other members of the same series (4437 Å and 4169 Å) similar results have been obtained.
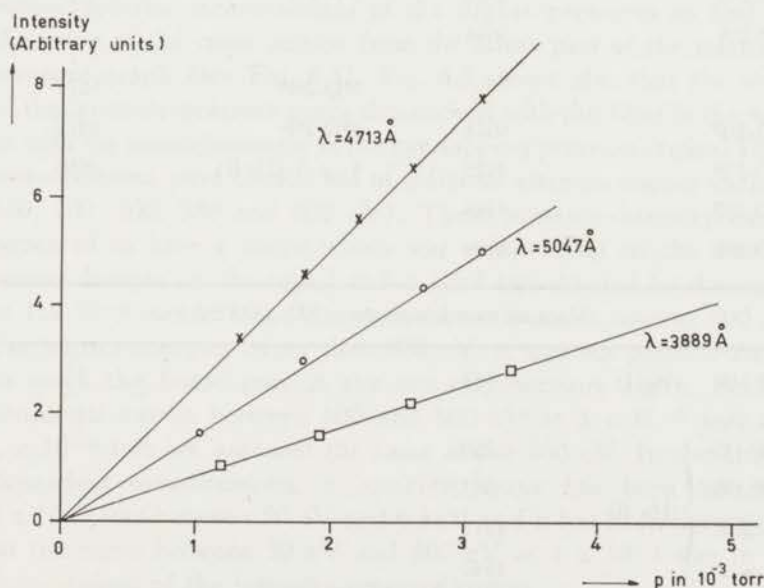
Fig. 6.3 Light intensity versus helium gas pressure at 200 eV for the transitions 4^1S-2^1P ($\lambda = 5047$ Å); 4^3S-2^3P ($\lambda = 4713$ Å); 3^3P-2^3S ($\lambda = 3889$ Å).

TABLE 6.1

Spectrum measured between 200 and 7300 Å at an angle of 90° with respect to the beam direction

Leiss monochromator (2900→7300 Å)			
Transition	(Å)	Transition	(Å)
3^1S-2^1P	7281	3^3S-2^3P	7065
4^1S-2^1P	5047	4^3S-2^3P	4713
5^1S-2^1P	4437	5^3S-2^3P	4121
6^1S-2^1P	4169		
		3^3P-2^3S	3889
3^1P-2^1S	5016	4^3P-2^3S	3188
4^1P-2^1S	3965	5^3P-2^3S	2945
5^1P-2^1S	3614		
		3^3D-2^3P	5875
3^1D-2^1P	6678	4^3D-2^3P	4472
4^1D-2^1P	4922	$4 \rightarrow 3$ (He II)	4686
5^1D-2^1P	4388		
6^1D-2^1P	4144		

Vacuum monochromator (200→2000 Å)		
2^1P-1^1S	(He I)	584
3^2P-1^2S		256
2^2P-1^2S	(He II)	303
$4 \rightarrow 2$		1215
$3 \rightarrow 2$		1640

b) *The n^1P-2^1S (n = 3, 4 and 5) transitions*

For the 3^1P-2^1S transition a linear relationship is found for gas pressures up to 1.2×10^{-4} torr. The deviation is caused by absorption of resonance radiation. The larger the product of pressure and radius of the collision chamber, the larger the enhancement of the 3^1P-2^1S light signal (P h e l p s, 1958).

Because of the weak light signal at such low pressures as 1×10^{-4} torr, the accuracy of the measurements was poor. Therefore, we have used an interference filter (Baird Atomic, B12, 6 Å band-with) instead of the Leiss monochromator (see section 3.7) to carry out the measurements at lower pressures. Using this narrow filter we could separate 3^1P-2^1S (5016 Å) from 4^1S-2^1P (5047 Å), see Fig. 6.4. Using the Leiss monochromator we have measured the light intensity as a function of the pressure from 5×10^{-4} torr up to 3×10^{-3} torr. Then, we continued the measurements with the inter-ference filter from the vacuum pressure ($\approx 5 \times 10^{-6}$ torr) up to 2.5×10^{-3} torr. The filter measurements have been normalized to the monochromator measurements at the higher pressures to find out the value of the cross section from the linear part of the intensity-pressure graph (see Fig. 6.5). Fig. 6.5 shows also that the shape of the intensity-pressure curve determined with the filter is the same as with the monochromator in the overlapping pressure region. These measurements were carried out at different electron impact energies (60, 100, 300, 500 and 800 eV). These pressure-intensity curves appeared to have a shape which was independent on the electron impact energy; i.e. the signal at 3×10^{-3} torr divided by the signal at 1×10^{-4} torr at 100 eV was equal to the same ratio at 800 eV. For impact energies larger than 800 eV, it was not possible for us to reach the linear part in the intensity-pressure curve. Finding conformal curves between 100 and 800 eV at 3×10^{-3} torr and 1×10^{-4} torr we assumed the same above 800 eV. In the energy dependent measurements, a complete curve has been taken at 5×10^{-4} torr between 50 eV and 6 keV and it has been normalized on the curve between 50 eV and 800 eV at 1×10^{-4} torr in the linear region of the intensity-pressure curves.

This normalization method has also been applied for the higher members of this series (4^1P-2^1S and 5^1P-2^1S). In the case of
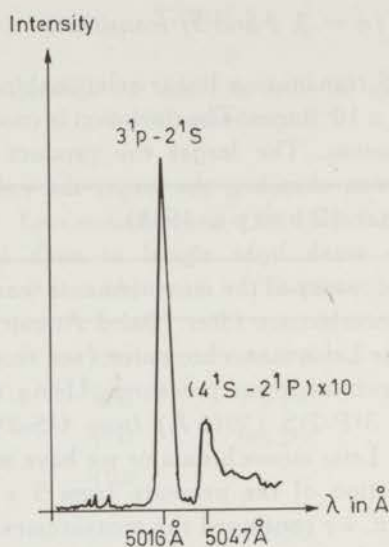
Fig. 6.4 Separation of 3¹P-2¹S ($\lambda = 5016$ Å) from 4¹S-2¹P ($\lambda = 5047$ Å) using an interference filter.

4¹P excitation a linear behaviour with pressure was found up to 2.5×10^{-4} torr while for 5¹P the linearity extended up to 4.5×10^{-4} torr (see Fig. 6.6). The increase of the "critical" pressure is explained from the fact that the higher the principal quantum number, the smaller the effect of the absorption of resonance radiation.

The polarization is also shown in Fig. 6.5 as a function of the target gas pressure at 100 eV incident electron energy. One can see that the polarization degree decreases by increasing the pressure. This is due to the depolarization of the light caused by resonance absorption of the radiation. This measurement has also been performed by using an interference filter because of the weak signal at lower pressures. Below 4×10^{-4} torr the polarization degree becomes independent on the pressure. This is also in agreement with H e d d l e and L u c a s (1962).

c) *The n¹D-2¹P (n = 3, 4, 5 and 6) transitions*

Fig. 6.7 shows the light intensity and the polarization degree of 4¹D-2¹P (4922 Å) as a function of the target gas pressure at

58

Intensity
(Arbitrary units)

π

o Leiss monochrometer
Δ Interference filter

→ p in 10⁻³ torr

Intensity
(Arbitrary units)

→ p in 10⁻⁴ torr
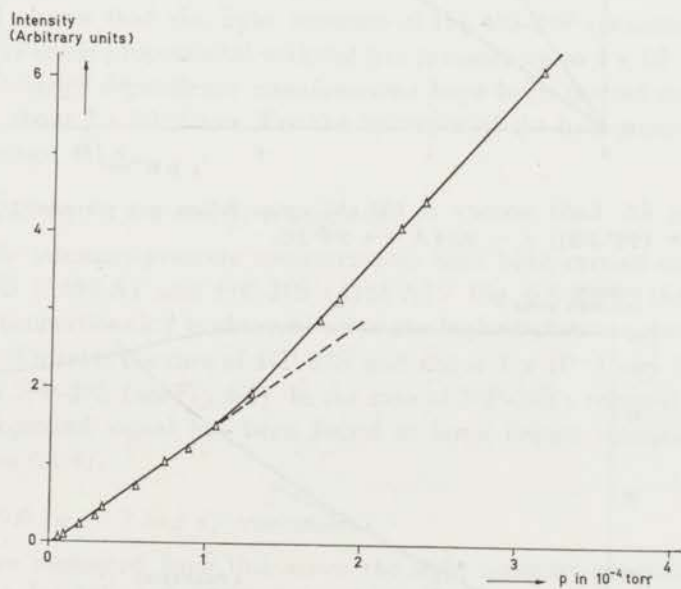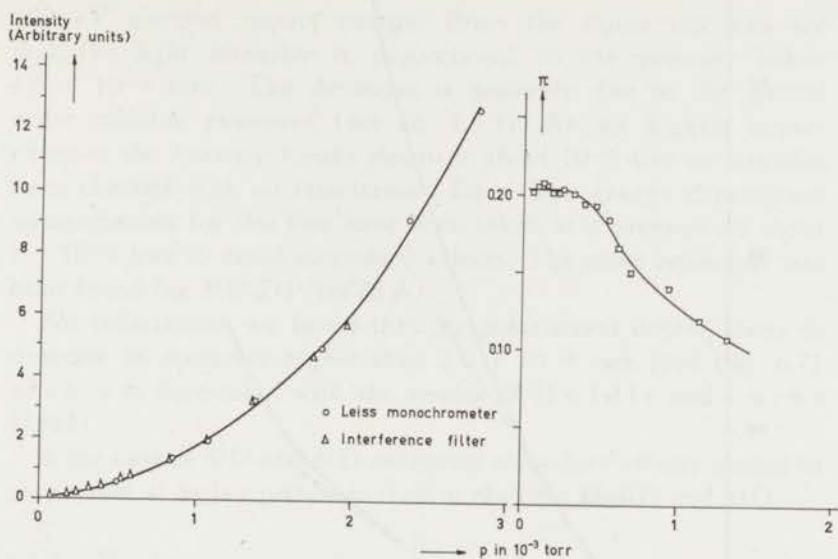
Fig. 6.5 Light intensity and polarization fraction at 100 eV versus helium gas pressure of the 3^1P-2^1S line ($\lambda = 5016$ Å).

Fig. 6.6 Light intensity at 100 eV versus helium gas pressure $\lambda = 3965\,\text{Å}$ $\leftrightarrow$ $(4^1P\text{-}2^1S)$; $\lambda = 3614\,\text{Å}$ $\leftrightarrow$ $5^1P\text{-}2^1S$.
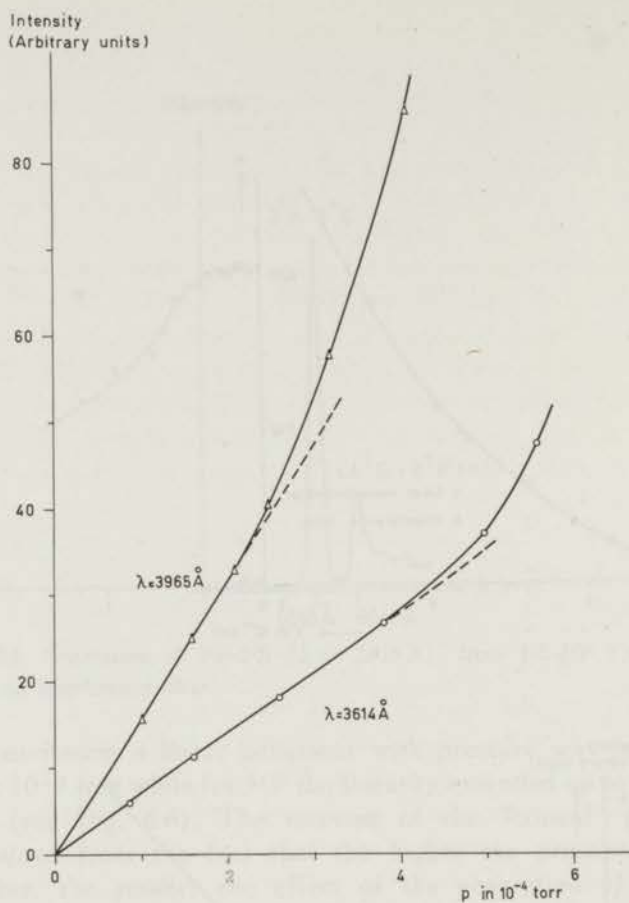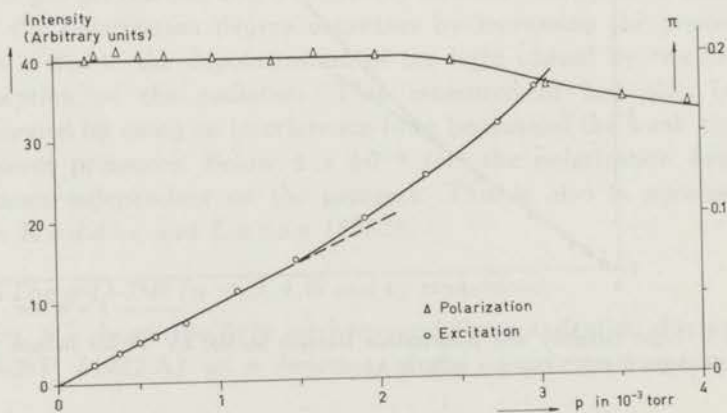

Fig. 6.7 Light intensity and polarization fraction versus helium gas pressure at 100 eV of the $4^1D\text{-}2^1P$ line ($\lambda = 4922\,\text{Å}$).

100 eV electron impact energy. From the figure one can see
that the light intensity is proportional to the pressure below
1.6×10^{-3} torr. The deviation is probably due to the second
order collision processes (see eq. 1.5.1). At our highest impact
energies the linearity breaks down at about 10^{-3} torr as has also
been checked with an interference filter. The energy dependence
measurements for this line have been taken at a pressure of about
1×10^{-3} torr to avoid secondary effects. The same behaviour has
been found for 3^1D-2^1P (6678 Å).

For polarization we found that the polarization degree starts to
decrease at pressures higher than 2.0×10^{-3} torr (see Fig. 6.7)
which is in agreement with the results of H e d d l e and L u c a s
(1962).

In the case of 5^1D and 6^1D excitation secondary effects started to
play a role at higher pressures than in the case of 3^1D and 4^1D.

6.1.3. Triplet transitions

a) n^3S-2^3P (n = 4 and 5) transitions

Fig 6.3 shows that the light intensity of the 4^3S-2^3P transition
(4713 Å) is linear proportional with the gas pressure up to 4×10^{-3}
torr. The energy dependence measurements have been carried out
usually at about 2×10^{-3} torr. For the influence of the background
gas see section 6.1.4.

b) n^3P-2^3S (n = 3, 4 and 5) transitions

The light intensity-pressure measurements have been carried out
on 3^3P-2^3S (3889 Å) and 4^3P-2^3S (3188 Å). Fig. 6.8 shows that
the linear proportionality is obtained up to the highest pressure used
($\sim 2 \times 10^{-3}$ torr) in the case of 4^3P-2^3S and about 4×10^{-3} torr in
the case of 3^3P-2^3S (see Fig. 6.3). In the case of 3^3P-2^3S a relatively
large background signal has been found at large impact energies
(see section 6.1.4).

c) n^3D-2^3P (n = 3 and 4) transitions

We have measured from this series the light intensity-pressure
dependence for 4^3D-4^3P (4472 Å) with the Leiss monochromator.
Fig. 6.8 shows the light intensity-pressure dependence of 4^3D-2^3P.

61
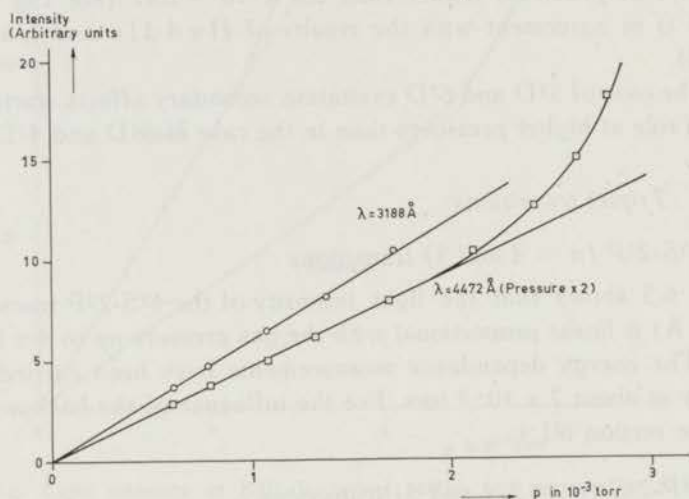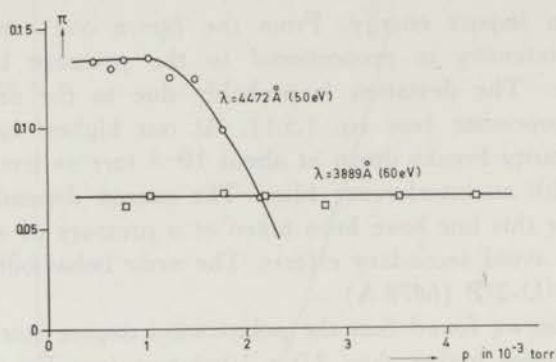
Fig. 6.8 Light intensity (100 eV) and polarization fraction (50 and 60eV) of the 4^3D-2^3P (4472 Å) and 4^3P-2^3S (3188 Å) lines versus helium gas pressure.

One can see that the deviation in the curve started at pressures higher than 1×10^{-3} torr. This may be due to the excitation transfer processes as in the case of 4^1D-2^1P. The same behaviour has been found also in case of 3^3D-2^3P (5876 Å) transition as has been checked with an interference filter.

6.1.4. Vacuum background

In the case of 4^3S-2^3P (4713 Å) and 3^3P-2^3S (3889 Å) transitions

62

we observed a considerable signal due to the background gas especially at high impact energies. We, therefore, wanted to do an extra check on the effect of the background signal on all helium transitions which we have measured (see Table 6.1). For that reason we did a scanning of the molecular oxygen and molecular nitrogen spectrum (the components of the restgas) by electron impact at three different energies (100, 500 and 1000 eV). The scanning was carried out at a pressure of 8×10^{-4} torr. We found two very strong lines both of O_2 and N_2 having the same wavelength as He I 4^3P-2^3S and also two extremely strong bands both of O_2 and N_2 very close to the wavelength of He I 3^3P-2^3S.

Fig. 6.9 and 6.10 show the magnitude of the vacuum signal with respect to the signal of He I at the wavelengths of 4^3S-2^3P (4713 Å) and of 3^3P-2^3S (3889 Å). One can see that the effect of the background gas increases relatively with increasing electron energy. This is due to the difference in the cross section-energy behaviour for the background and the triplet excitation. This shows that one has to be extremely careful in assuming that if the vacuum signal is negligible with respect to the He I signal at low electron energy, that this would also be the case at high electron energies.

At the wavelengths of other helium lines, which we have measured we found that the vacuum signals were negligibly small at all electron impact energies with respect to the He I signals.

6.1.5. *He II lines*

In case of He II excitation a direct proportionality with the gas pressure has been found (see Fig. 6.11) in all cases up to the highest pressures used (7×10^{-3} torr).

6.2. **Variation of the intensity and the polarization fraction with the axial magnetic field**

For some singlet and triplet transitions the dependence of the light signal on the axial magnetic field has been determined, see Fig. 6.12. The ordinate represents the photomultiplier signal divided by the beam current at constant pressure, while the abscissa represents the axial magnetic field. We found that the cross section is independent on the axial magnetic field up to the maximum magnetic field as shown in the figure.
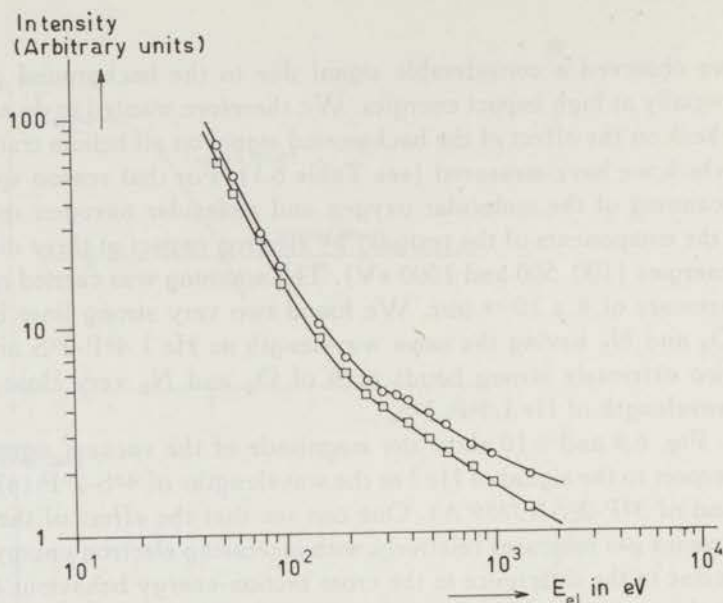
Fig. 6.9 The light intensity of the 4^3S-2^3P line ($\lambda = 4713$ Å) as a function of electron energy. The circles are the uncorrected light intensities for the background signal, while the rectangles are the corrected light intensities for the background signal.
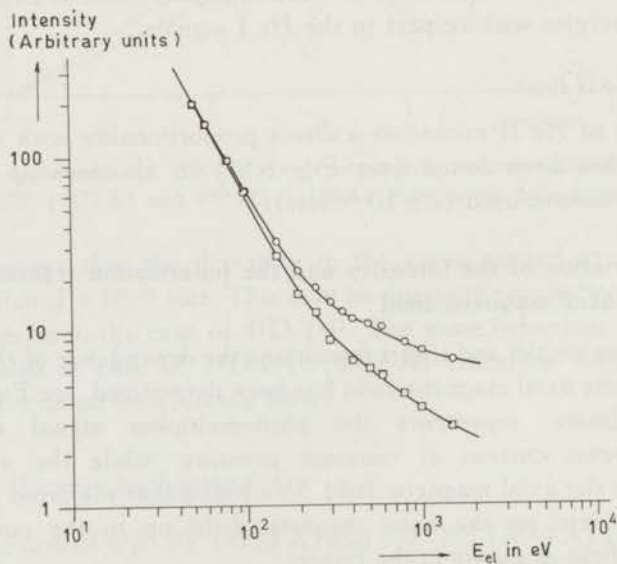
Fig. 6.10 The light intensity of the 3^3P-2^3S line ($\lambda = 3889$ Å) as a function of electron energy. The circles are the uncorrected light intensities for the background signal, while the rectangles are the corrected light intensities for the background signal.
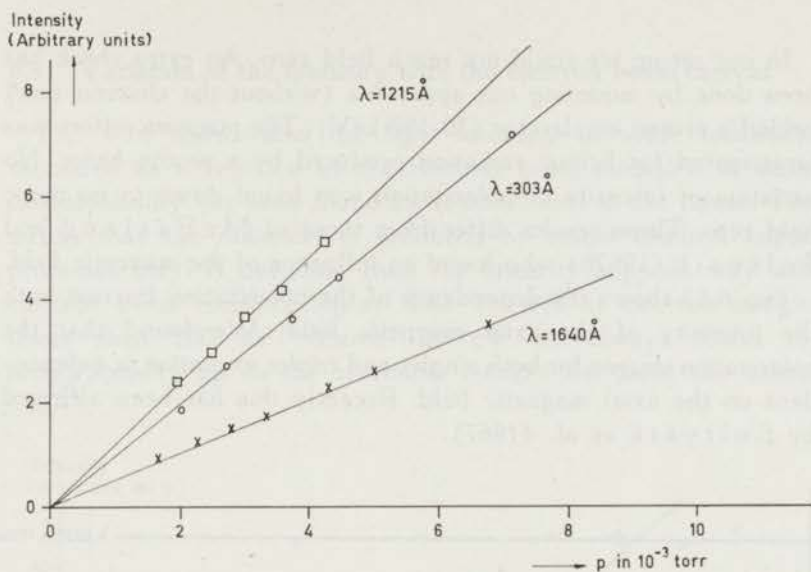
Fig. 6.11 Light intensity at 200 eV versus helium gas pressure of He II lines.
2^2P-1^2S ($\lambda = 303$ Å); $4 \rightarrow 2$ ($\lambda = 1215$ Å); $3 \rightarrow 2$ ($\lambda = 1640$ Å).
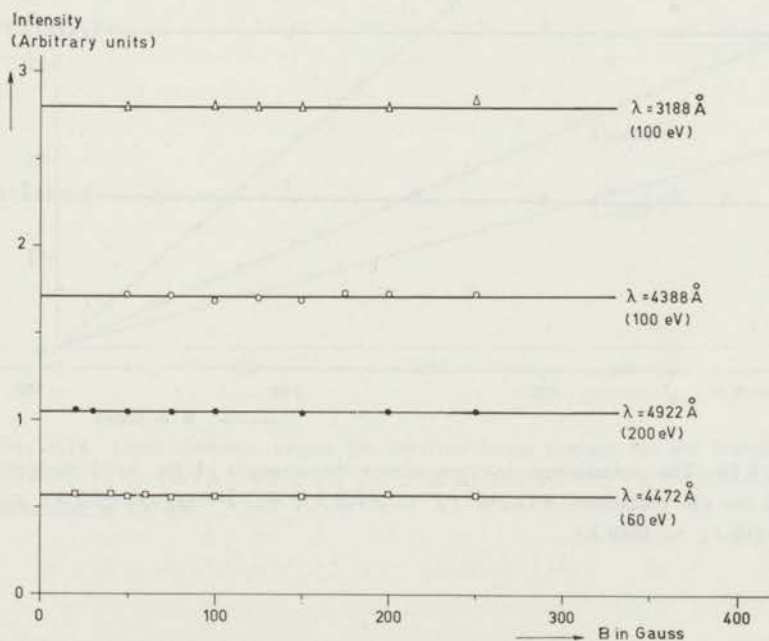
Fig. 6.12 Light intensity versus the strength of the axial magnetic field
for the transitions 4^1D-2^1P ($\lambda = 4922$ Å), 5^1D-2^1P ($\lambda = 4388$ Å), 4^3P-2^3S
($\lambda = 3188$ Å) and 4^3D-2^3P ($\lambda = 4472$ Å).

In our set-up we could not reach field zero. An extra check has been done by mounting our apparatus (without the electron gun) behind a proton accelerator (30-150 keV). The magnetic effect was investigated for helium radiation produced by a proton beam. No variation of intensity or polarization was found down to magnetic field zero. These results differ from those of Mc F a r l a n d and S o l t y s i k (1962b) who found an influence of the magnetic field.

Fig. 6.13 shows the dependence of the polarization fraction with the intensity of the axial magnetic field. We found that the polarization degree for both singlet and triplet excitation is independent on the axial magnetic field. Recently this has been affirmed by S o l t y s i k et al. (1967).
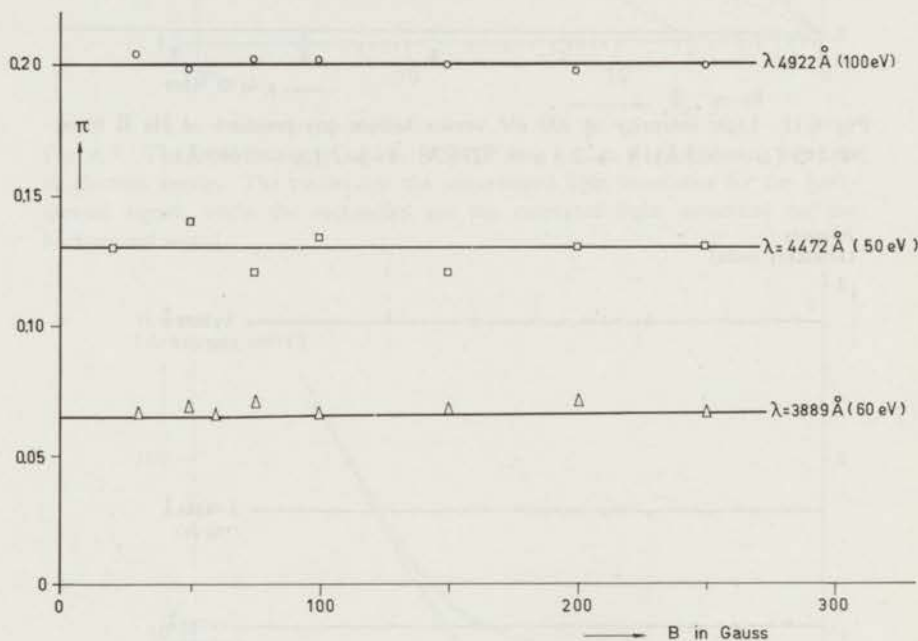
Fig. 6.13 The polarization fraction versus the strength of the axial magnetic field for the transitions 4^1D-2^1P ($\lambda = 4922\,\text{Å}$), 4^3D-2^3P ($\lambda = 4472\,\text{Å}$) and 3^3P-2^3S ($\lambda = 3889\,\text{Å}$).

6.3. Variation of the intensity with the electron beam current

Fig. 6.14 shows also the light intensity of some transitions measured as a function of the electron beam intensity. A direct proportionality has been found as demonstrated in the figure. This means that the radiation is produced by single electron impact processes only. A deviation from the linearity happens only with electron beam currents higher than $150\ \mu A$ at electron energies lower than 100 eV. Above 100 eV we always found the proportionality up to the maximum current we could get (about 1 mA).
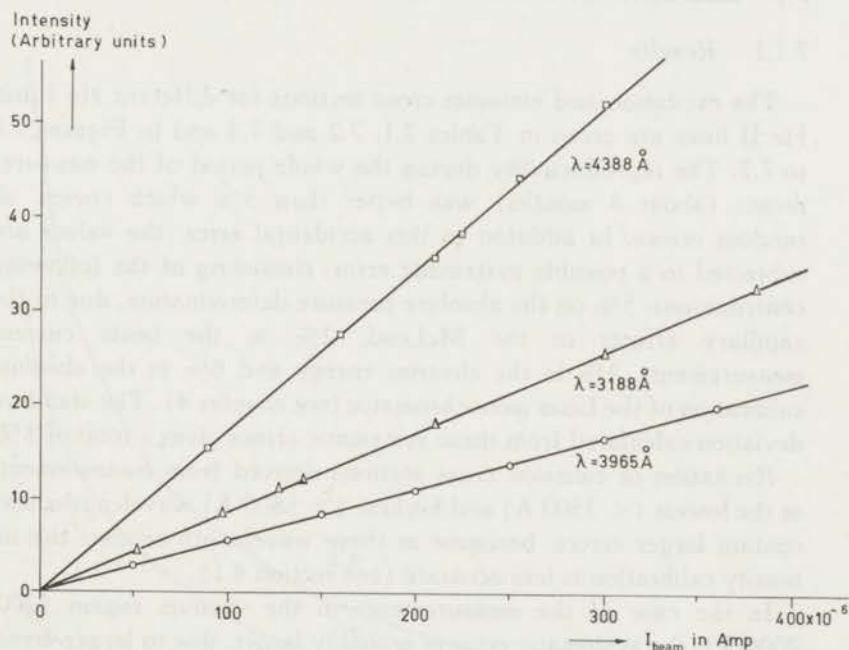
Fig. 6.14 Light intensity versus the electron beam current for the transitions $5^1D\text{-}2^1P$ ($\lambda = 4388$ Å), $4^1P\text{-}2^1S$ ($\lambda = 3965$ Å) and $4^3P\text{-}2^3S$ ($\lambda = 3188$ Å) and measured at 100 eV.

CHAPTER 7

EXCITATION AND POLARIZATION RESULTS AS A FUNCTION OF ELECTRON IMPACT ENERGY

7.1. Excitation cross sections

7.1.1. *Results*

The excitation and emission cross sections for different He I and He II lines are given in Tables 7.1, 7.2 and 7.3 and in Figures 7.1 to 7.7. The reproducibility during the whole period of the measurements (about 8 months) was better than 5% which covers all random errors. In addition to this accidental error, the values are subjected to a possible systematic error, consisting of the following contributions: 5% on the absolute pressure determination, due to the capillary effects in the McLeod, 2% in the beam current measurements, 1% in the electron energy and 6% in the absolute calibration of the Leiss monochromator (see chapter 4). The standard deviation calculated from these systematic errors gives a total of 8%.

Excitation or emission cross sections derived from measurements at the lowest (< 3500 Å) and highest (> 5800 Å) wavelengths may contain larger errors, beccause in these wavelength regions the intensity calibration is less accurate (see section 4.1).

In the case of the measurements in the vacuum region (200-2000 Å), the systematic error is probably larger, due to larger errors in the absolute calibration (see chapter 4). In the case of $\lambda = 1215$ Å, this depends on the accuracy of the cross sections of F i t e and B r a c k m a n n (1958) for Lyman α production in the case of electron impact on H_2. The accuracy of the calibration at 537 Å by the method of V a n E c k and D e H e e r (1963) is about 20%. At other wavelengths extrapolation procedures had to be applied so that we estimate that for corresponding wavelengths

68

the systematic errors in the cross section may increase to at least 100%.

Excitation cross sections of the 2^1P level have been obtained by fitting the experimental results to the optical oscillatir strength calculated by S c h i f f and P e k e r i s (1965) (see section 2.2 and 8.1). An absolute value could not be obtained as a consequence of the absorption of resonance radiation. Inaccuracies may be introduced by this method, also because no correction is made for effects of polarization of the radiation.

Fig. 7.1   Absolute excitation cross sections for n^1S levels.

69
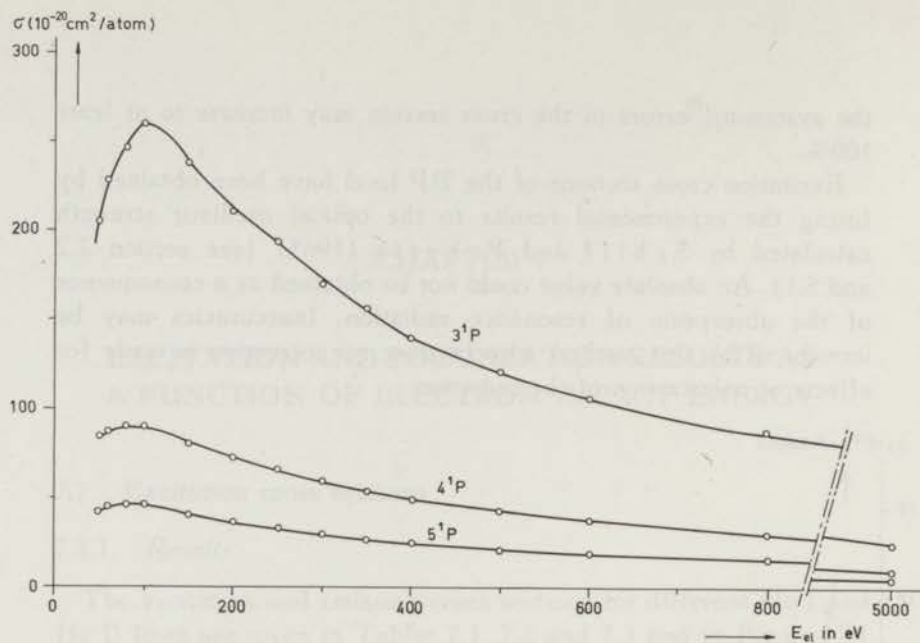
Fig. 7.2 Absolute excitation cross sections for n^1P levels.
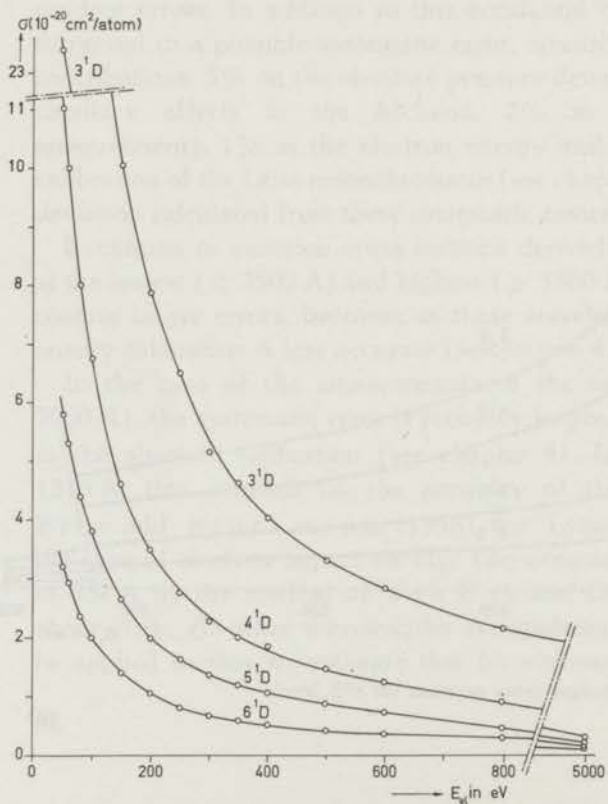
Fig. 7.3 Absolute excitation cross sections for n^1D levels.
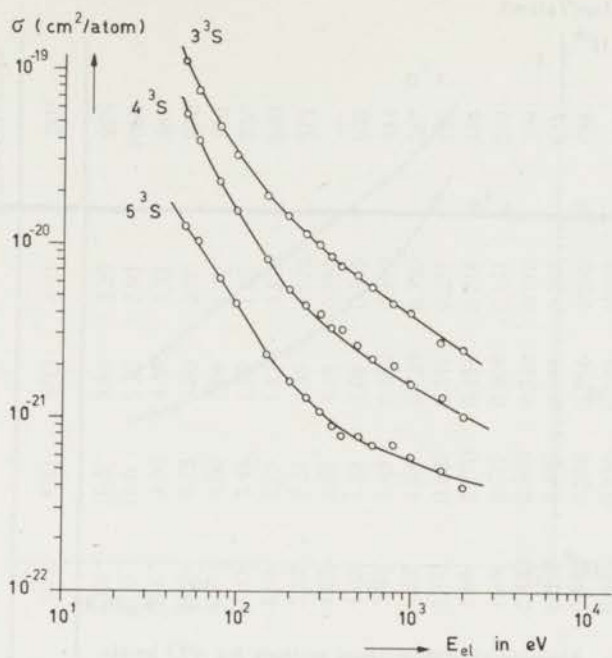
Fig. 7.4 Absolute excitation cross sections for n^3S levels.
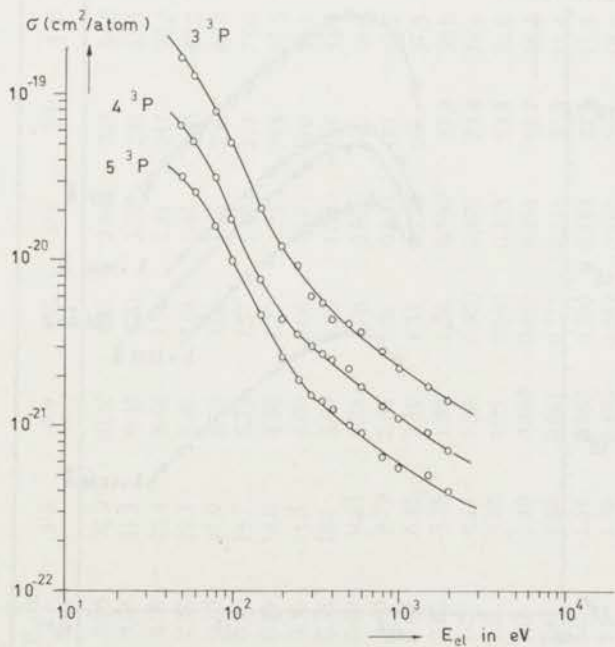
Fig. 7.5 Absolute excitation cross sections for n^3P levels.

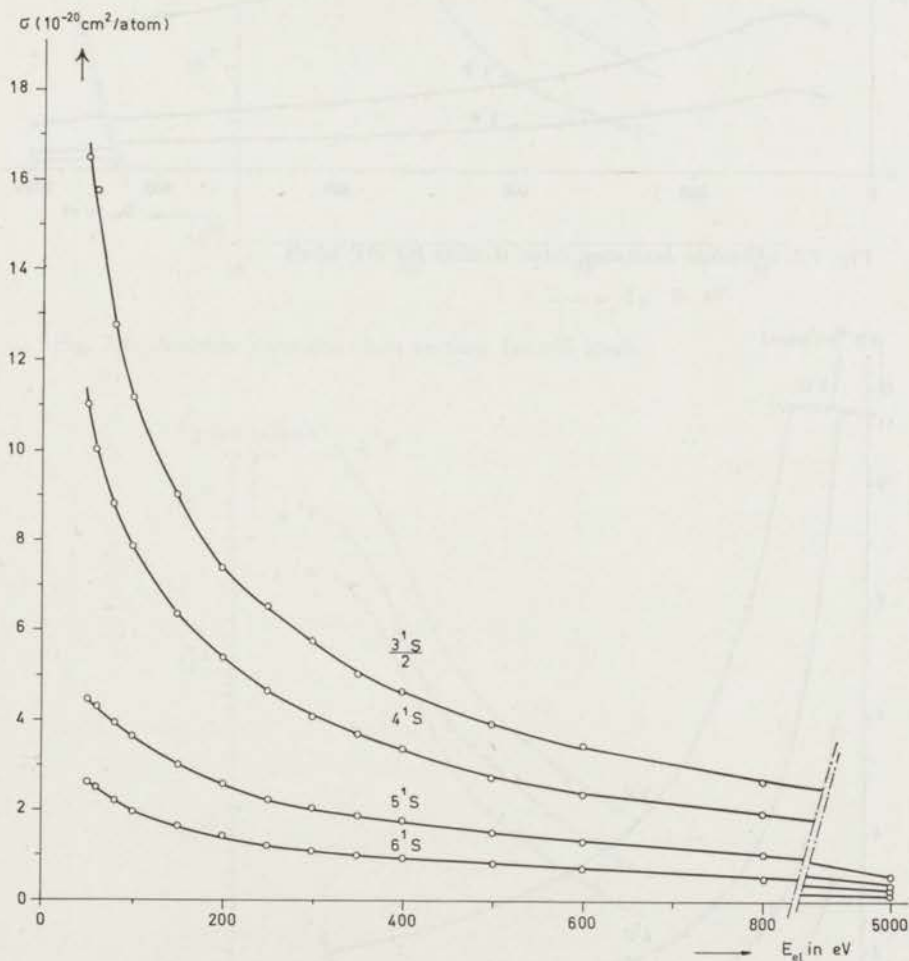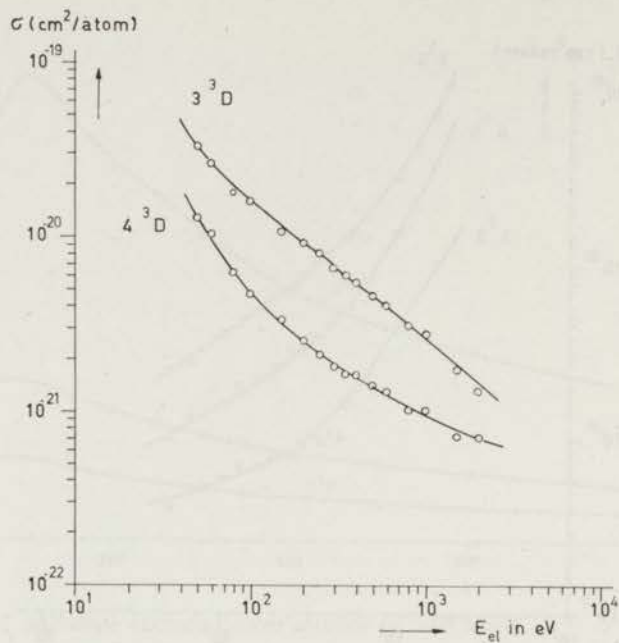Fig. 7.6   Absolute excitation cross sections for n^3D levels.
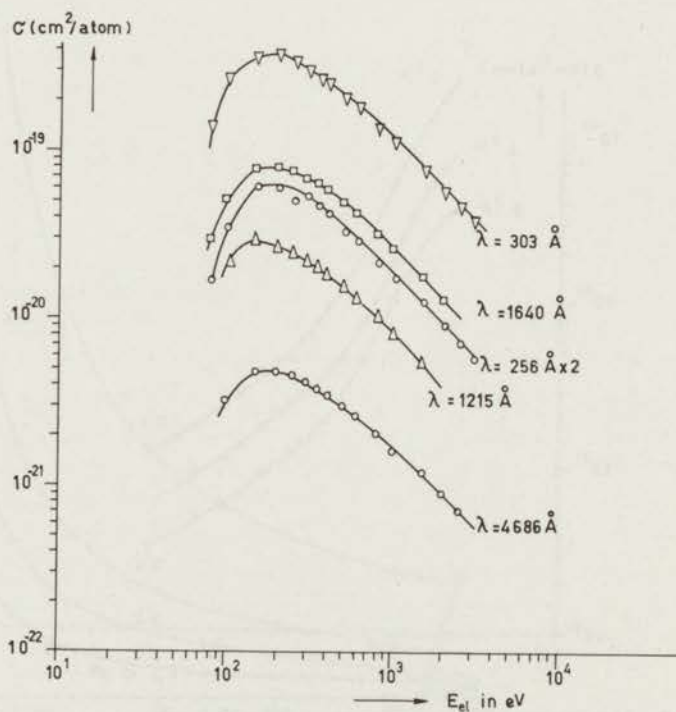
Fig. 7.7   Emission cross sections of He II lines.

TABLE 7.1

The absolute excitation cross sections corrected for polarization and cascade in units of 10^{-20} cm^2/atom.

	He I											Vacuum monochromator
	Leiss monochromator											
E_{el} in keV	3^1S	4^1S	5^1S	6^1S	3^1P	4^1P	5^1P	3^1D	4^1D	5^1D	6^1D	2^1P
0.05	32.9	10.40	4.47	2.64	205	84.0	42.0	23.4	10.8	5.80	3.20	975
0.06	31.5	9.85	4.30	2.50	228	87.5	45.0	21.0	10.0	5.30	2.93	1080
0.08	25.4	8.60	3.96	2.21	247	90.0	46.2	16.8	8.00	4.40	2.35	987
0.10	22.3	7.67	3.64	1.98	260	89.2	45.2	14.2	6.75	3.80	2.00	870
0.15	17.9	6.26	3.00	1.64	238	80.0	40.0	10.0	4.60	2.64	1.40	810
0.20	14.7	5.23	2.57	1.40	211	72.0	36.0	7.85	3.48	1.97	1.05	710
0.25	13.0	4.50	2.23	1.22	194	65.5	32.5	6.48	2.75	1.62	0.810	640
0.30	11.5	4.00	2.06	1.10	170	59.1	29.3	5.15	2.27	1.36	0.672	579
0.35	10.1	3.63	1.90	1.02	157	53.5	26.4	4.63	2.00	1.18	0.580	—
0.40	9.03	3.28	1.76	0.95	140	49.0	24.2	4.03	1.83	1.06	0.512	504
0.50	7.79	2.64	1.50	0.831	121	42.5	21.0	3.30	1.45	0.880	0.422	444
0.60	6.85	2.31	1.33	0.732	106	37.5	18.8	2.84	1.23	0.720	0.350	387
0.80	5.28	1.96	1.06	0.550	87.0	30.0	15.2	2.17	0.890	0.541	0.271	337
1.0	4.28	1.50	0.900	0.470	73.4	26.4	12.8	1.68	0.770	0.434	0.216	289
1.5	3.07	1.05	0.641	0.335	53.4	20.6	9.92	1.08	0.512	0.305	0.151	210
2.0	2.40	0.840	0.482	0.251	43.2	16.3	8.11	0.830	0.403	0.230	0.110	169
2.5	1.86	0.681	0.375	0.214	37.3	13.4	6.80	0.659	0.320	0.185	0.097	131
3.0	1.64	0.562	0.320	0.182	32.5	11.3	5.85	0.565	0.264	0.151	0.080	128
3.5	1.39	0.470	0.282	0.160	28.4	10.1	5.25	0.485	0.230	0.132	0.060	—
4.0	1.08	0.431	0.260	0.140	27.3	9.40	4.80	0.415	0.201	0.125	0.060	—
4.5	0.99	0.391	0.230	0.122	26.0	8.61	4.41	0.370	0.176	0.101	0.058	—
5.0	0.88	0.350	0.202	0.120	23.4	8.40	4.15	0.330	0.162	0.111	0.048	—
6.0	—	0.274	—	—	19.2	7.10	3.82	—	0.130	—	—	—

TABLE 7.2

The absolute excitation cross sections corrected for polarization and cascade in units of 10^{-20} cm²/atom

E_{el} in keV	3^3S	4^3S	5^3S	3^3P	4^3P	5^3P	3^3D	4^3D
0.05	11.0	5.38	1.24	16.3	6.30	3.17	3.42	1.24
0.06	7.52	3.88	1.02	12.5	5.02	2.57	2.72	1.02
0.08	4.68	2.27	0.626	7.75	3.15	1.60	1.86	0.610
0.10	3.24	1.51	0.451	5.01	1.74	0.987	1.61	0.471
0.15	1.89	0.769	0.223	2.02	0.747	0.471	1.07	0.317
0.20	1.46	0.550	0.161	1.17	0.431	0.254	0.944	0.250
0.25	1.14	0.433	0.129	0.920	0.341	0.187	0.804	0.207
0.30	0.992	0.387	0.108	0.580	0.290	0.146	0.682	0.182
0.35	0.840	0.332	0.094	0.532	0.262	0.135	0.601	0.161
0.40	0.747	0.314	0.085	0.412	0.246	0.124	0.550	0.154
0.50	0.667	0.264	0.076	0.391	0.219	0.103	0.471	0.139
0.60	0.575	0.222	0.073	0.355	0.167	0.091	0.413	0.127
0.80	0.465	0.195	0.066	0.268	0.128	0.062	0.314	0.105
1.00	0.404	0.162	0.058	0.214	0.109	0.054	0.281	0.098
1.50	0.276	0.117	0.048	0.163	0.087	0.044	0.172	0.075
2.00	0.250	0.104	0.039	0.138	0.073	0.035	0.132	0.066

TABLE 7.3

Emission cross sections of He II lines in units of 10^{-20} cm^2/atom

	He II				
	Vacuum monochromator				Leiss monochromator
E_{el} in keV	1640 Å $3 \rightarrow 2$	1215 Å $4 \rightarrow 2$	303 Å $2^2P\text{-}1^2S$	256 Å $3^2P\text{-}1^2S$	4686 Å $4 \rightarrow 3$
0.08	2.98	—	13.6	0.83	—
0.10	5.19	2.22	23.4	1.74	0.316
0.15	7.73	2.87	35.5	3.08	0.480
0.20	8.00	2.69	37.5	3.00	0.485
0.25	7.55	2.50	34.5	2.48	0.459
0.30	6.85	2.18	30.7	2.68	0.419
0.35	6.55	2.02	27.0	2.36	0.376
0.40	5.89	1.84	26.0	2.13	0.352
0.50	4.98	1.55	21.0	1.66	0.297
0.60	4.31	1.31	18.4	1.45	0.262
0.80	3.24	1.02	13.7	1.06	0.198
1.0	2.63	0.810	11.7	0.881	0.161
1.5	1.80	0.540	7.85	0.625	0.116
2.0	1.31	0.448	5.87	0.450	0.087
2.5	1.10	—	4.78	0.357	0.069
3.0	—	—	3.98	0.287	0.059

7.1.2. General behaviour

In this chapter we shall mainly confine our discussion to results of the He I excitation. A comparison with theory, partly discussed in chapter 2, is given in chapter 8.

In Figures 7.1 to 7.6 it is shown that the cross sections for levels of a term series have the same energy dependence (see also section 1.5). This energy dependence is different for singlet and triplet levels (see also chapter 2) and is dependent on the azimuthal quantum number l, as we see in Fig. 7.8 for singlet transitions.
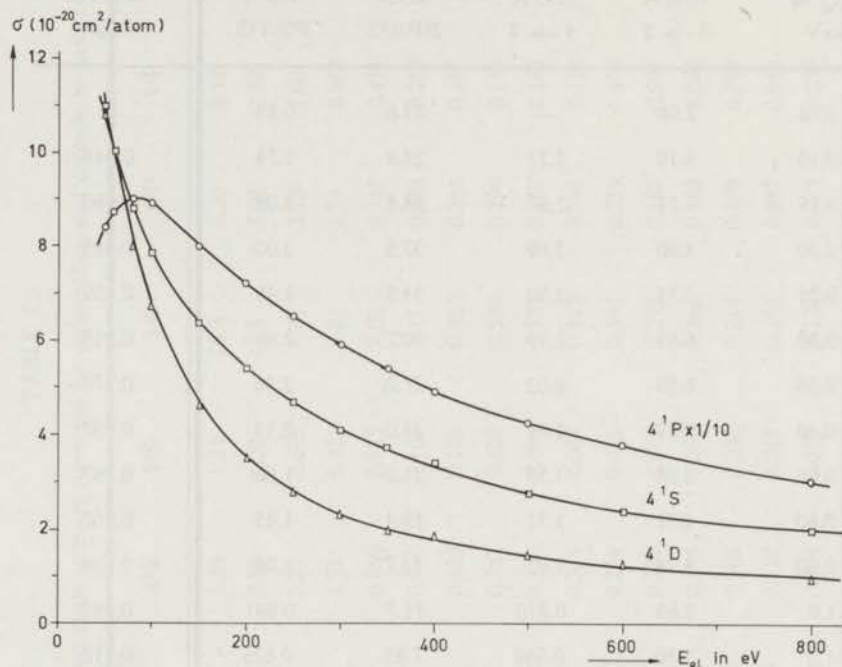
Fig. 7.8 Absolute excitation cross sections of 4^1S, 4^1P and 4^1D levels.

For a term series it appears that σ is approximately proportional to n^{-3}, where n is the principal quantum number. This n^{-3} dependence can be explained with a classical model (O c h k u r and P e t r u n k i n, 1963). To bring the electron into level n, an excitation energy is needed which lies between E_n and E_{n+1}. If we represent the cross section for excitation to level n by $\sigma(n)$ and for excitation with excitation energy between ε and $d\varepsilon$ by $\sigma(\varepsilon)$,

76

it follows that

$$\sigma(n) = \int_{E_n}^{E_{n+1}} \sigma(\varepsilon) \, d\varepsilon \approx \sigma(\varepsilon) \, (E_{n+1} - E_n) \tag{7.1.1}$$

For sufficiently large n, $\sigma(\varepsilon)$ does not change much in the energy interval and the field of the remaining electron can be approximated by a Coulomb field. Here we have

$$E_{n+1} - E_n \simeq \text{constant} \left(\frac{1}{n^2} - \frac{1}{(n+1)^2} \right) \approx n^{-3} \tag{7.1.2}$$

Quantum mechanically, the same dependence can be derived by using Born approximation (O c h k u r and P e t r u n k e n, 1963).

In order to study the reliability of the experimental data it is useful to make a table in which at different electron impact energies the excitation cross section of one series (constant l) are compared at different n values. The cross section may then be expressed in terms of n proportional to n^{-x}. The power x is calculated from the observed excitation cross sections by taking each time the ratio of the cross sections of the neighbouring levels of the spectral series; for example:

$$\frac{\sigma_{exc}(4^1S)}{\sigma_{exc}(5^1S)} = \left(\frac{4}{5} \right)^{-x} \rightarrow x = \frac{\log \sigma(4^1S)/\sigma(5^1S)}{\log 1.25}$$

The ratios are determined for different electron impact energies and given in Table 7.4 for singlet and triplet He I levels.

From Table 7.4, one can see the following:

a) The ratios are almost constant (mostly within about 5% different from the average) at electron impact energies higher than 200 eV.

b) We see that the $n = 4/n = 5$ ratios are more or less the same for different series, except for ^3S. This holds also for $n = 5/n = 6$ ratios only measured for two series. There is some difference in the ratios of $n = 3/n = 4$.

c) Table 7.4 shows also the power x which has been defined before. If this power were exactly equal to 3, then we should have:

$$\frac{\sigma(n=3)}{\sigma(n=4)} = 2.37 : \frac{\sigma(n=4)}{\sigma(n=5)} = 1.95; \text{ and } \frac{\sigma(n=5)}{\sigma(n=6)} = 1.73.$$

77

TABLE 7.4

The ratio's of the cross sections in the case of excitation of helium by electrons. Power x is explained in the text.

E_{el} in keV	$\left(\dfrac{3^1S}{4^1S}\right)$	$\left(\dfrac{4^1S}{5^1S}\right)$	$\left(\dfrac{5^1S}{6^1S}\right)$	$\left(\dfrac{3^1P}{4^1P}\right)$	$\left(\dfrac{4^1P}{5^1P}\right)$	$\left(\dfrac{3^1D}{4^1D}\right)$	$\left(\dfrac{4^1D}{5^1D}\right)$	$\left(\dfrac{5^1D}{6^1D}\right)$	$\left(\dfrac{3^3S}{4^3S}\right)$	$\left(\dfrac{4^3S}{5^3S}\right)$	$\left(\dfrac{3^3P}{4^3P}\right)$	$\left(\dfrac{4^3P}{5^3P}\right)$	$\left(\dfrac{3^3D}{4^3D}\right)$
0.06	3.20	2.29	1.72	2.60	1.94	2.10	1.89	1.80	1.94	3.80	2.50	1.95	2.60
0.08	2.96	2.17	1.79	2.74	1.94	2.10	1.82	1.87	2.05	3.62	2.46	1.97	3.05
0.10	2.90	2.11	1.84	2.91	1.97	2.10	1.78	1.90	2.14	3.35	2.87	1.77	3.41
0.20	2.81	2.04	1.84	2.93	2.00	2.26	1.77	1.88	2.65	3.42	2.71	1.70	3.78
0.30	2.87	1.95	1.87	2.88	2.01	2.25	1.68	2.02	2.57	3.59	2.00	1.99	3.76
0.40	2.76	1.86	1.85	2.86	2.02	2.20	1.73	2.08	2.38	3.69	1.68	1.98	3.55
0.50	2.95	1.76	1.81	2.86	1.99	2.28	1.65	2.09	2.53	3.48	1.78	2.12	3.40
0.60	2.98	1.75	1.82	2.84	1.97	2.31	1.71	2.06	2.58	3.05	2.12	1.84	3.27
0.80	2.70	1.85	1.93	2.90	2.06	2.44	1.65	2.00	2.39	2.95	2.09	2.06	3.00
1.00	2.86	1.67	1.91	2.78	2.06	2.19	1.79	1.95	2.49	2.80	1.97	2.02	2.88
1.50	2.92	1.64	1.93	2.59	2.08	2.11	1.70	2.00	2.36	2.44	1.88	1.98	2.30
2.00	2.86	1.75	1.92	2.66	2.01	2.06	1.74	2.09	2.40	2.67	1.89	2.08	2.00
3.00	2.92	1.76	1.78	2.88	1.95	2.14	1.74	1.88					
4.00	2.51	1.66	1.85	3.09	1.95	2.06	1.67	2.07					
5.00	2.52	1.74	1.83	2.88	2.02	2.05	—	2.20					
mean value	2.85	1.87	1.84	2.83	2.00	2.19	1.74	1.99	2.37	3.24	2.16	1.97	3.09
x	3.63	2.80	3.32	3.61	3.09	2.73	2.48	3.74	3.02	5.20	2.70	3.01	3.95

We see that our experimental mean values scatter around these numbers, except for $4^3S/5^3S$ and $3^3D/4^3D$, which give much higher numbers. These high numbers are not well understood.

Comparing the excitation cross sections of levels with the same principal quantum-number n and different azimuthal quantum numbers l, one can see from Fig. 7.8 that $\sigma(n^1P) > \sigma(n^1S) > \sigma(n^1D)$, $n = 4$, where ^1S and ^1D arise from optically forbidden transitions ($\triangle\, l \neq 1$) and ^1P arises from a collision induced dipole transition (optically allowed transitions, $\triangle\, l = 1$).

In the case of triplet excitation we found (see Fig. 7.9) that for
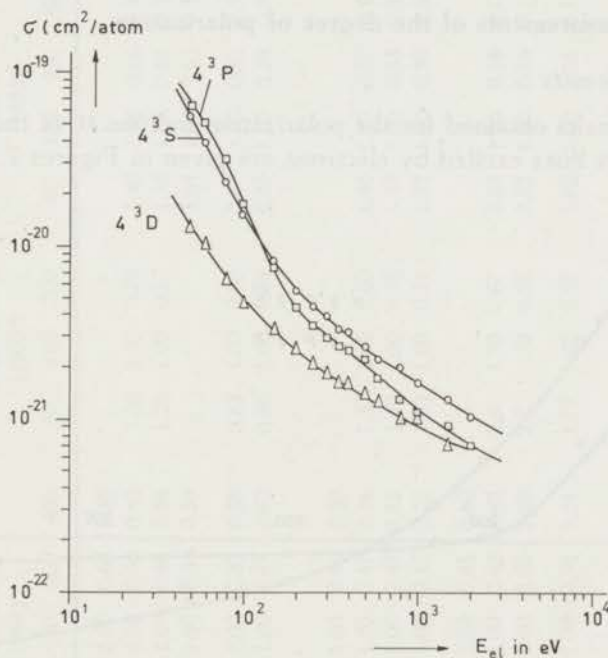
Fig. 7.9 Absolute excitation cross sections of 4^3S, 4^3P and 4^3D levels.

energies larger than 100 eV $\sigma(4^3S) > \sigma(4^3P) > \sigma(4^3D)$, while the shape of the ^3P curve decreases steeper as a function of increasing electron energy than ^3S and ^3D as is shown in Figure 7.9. However, following the Ochkur theory (see chapter 2), they should all have the same energy dependence at high impact energies.

79

7.1.3 The shapes of the excitation functions compared with other investigators

Table 7.5 shows a comparison between the shapes of our apparent excitation functions as a function of the electron impact energy with those of other authors. Each excitation function has been normalized to unity for an electron energy of 100 eV. The same comparison has also been done by S t. J o h n et al. (1964). From the table, one sees that the shapes often differ between the different authors. In the next chapter we shall see that at sufficiently high impact energies the shape can be compared with theory.

7.2. Measurements of the degree of polarization

7.2.1. Results

The results obtained for the polarization fraction Π of the singlet and triplet lines excited by electrons are given in Figures 7.10, 7.11

Fig. 7.10 The polarization fraction of $n^1P\text{-}2^1S$ ($n = 3, 4$) transitions versus electron energy.

TABLE 7.5

Shape comparison of experimental apparent excitation functions of helium

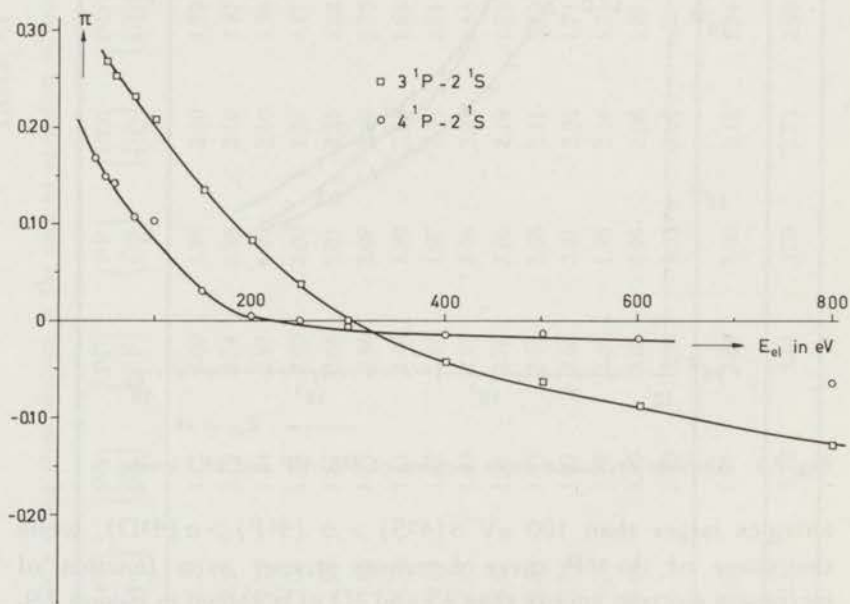| Level	This work 60	100	200	400	St. John et al. (1964) 60	100	200	400	Yakhontova (1959) 60	100	200	Thieme (1933) 60	100	200	400	Heddle and Lucas (1962) 60	100	200	McFarland and Soltysik (1962) 60	100	200
3^1S	1.35	1.00	0.69	0.43	1.28	1.00	0.68	0.49													
4^1S	1.25	1.00	0.69	0.43	1.26	1.00	0.66	0.42	1.08	1.00	0.79	1.40	1.00	0.66	0.41	1.20	1.00	0.77			
5^1S	1.18	1.00	0.70	0.48	1.25	1.00	0.68	0.38	1.23	1.00	0.77	1.35	1.00	0.61	0.35						
6^1S	1.26	1.00	0.71	0.48	1.31	1.00	0.66	0.39				1.61	1.00	0.51	0.35						
3^1P	0.92	1.00	0.71	0.49	0.83	1.00	0.85	0.58	0.88	1.00	0.85	0.87	1.00	0.82	0.53	1.1	1.00	0.84	0.98	1.00	0.59
4^1P	0.98	1.00	0.78	0.53	0.76	1.00	0.87	0.60	0.86	1.00	0.84	0.85	1.00	0.79	0.42						
5^1P	0.97	1.00	0.77	0.52																	
3^1D	1.51	1.00	0.53	0.26	1.50	1.00	0.51	0.30											1.06	1.00	0.63
4^1D	1.47	1.00	0.47	0.24	1.32	1.00	0.47	0.28	1.37	1.00	0.60	1.40	1.00	0.57	0.55	1.48	1.00	0.56	1.35	1.00	0.44
5^1D	1.41	1.00	0.51	0.27	1.32	1.00	0.47	0.28	1.40	1.00	0.56	1.30	1.00	0.53	0.31				1.39	1.00	0.47
6^1D	1.45	1.00	0.52	0.25	1.32	1.00	0.47	0.28	1.43	1.00	0.51	1.42	1.00	0.59	0.34						
3^3S	2.40	1.00	0.40	0.20	2.90	1.00	0.48	0.40													
4^3S	2.60	1.00	0.35	0.20	2.90	1.00	0.48	0.40	2.6	1.00	0.67	2.62	1.00	0.18	0.14	2.0	1.00	0.77	3.6	1.00	0.29
5^3S	2.30	1.00	0.35	0.18	2.90	1.00	0.48	0.40	2.7	1.00	0.58	2.82	1.00	0.24	0.14						
3^3P	2.50	1.00	0.26	0.11	3.1	1.00	0.34	0.24	1.75	1.00	0.50	3.00	1.00	0.28	0.12	3.9	1.00	0.38	2.8	1.00	0.33
4^3P	2.80	1.00	0.26	0.15																	
5^3P	2.60	1.00	0.26	0.13																	
3^3D	1.80	1.00	0.54	0.37	2.7	1.00	0.65	0.48	1.46	1.00	0.63	1.95	1.00	0.52	0.38				1.33	1.00	0.76
4^3D	2.20	1.00	0.48	0.29	2.7	1.00	0.65	0.48	1.85	1.00	0.69	1.78	1.00	0.50	0.28	2.75	1.00	0.47	1.50	1.00	0.55
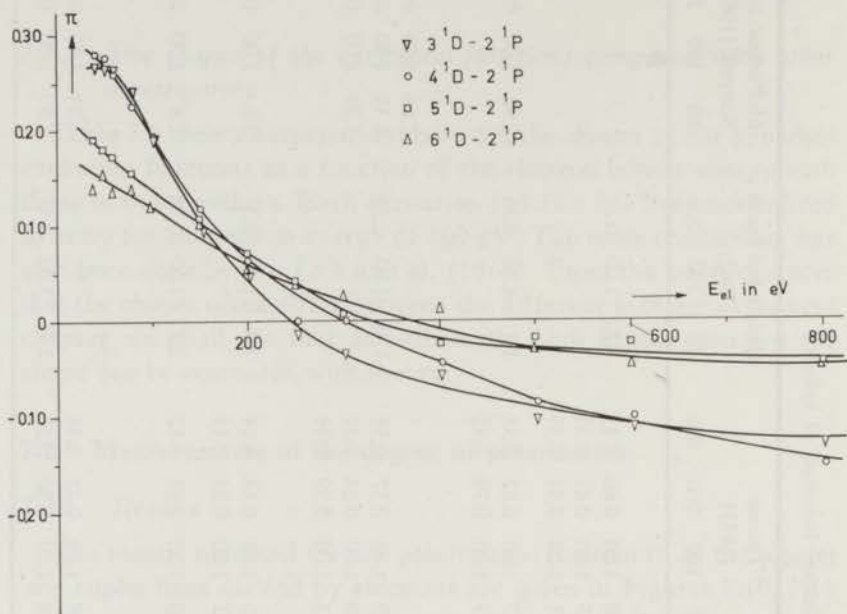
Fig. 7.11 The polarization fraction of $n^1D\text{-}2^1P$ ($n = 3, 4, 5$ and 6) transitions versus electron energy.
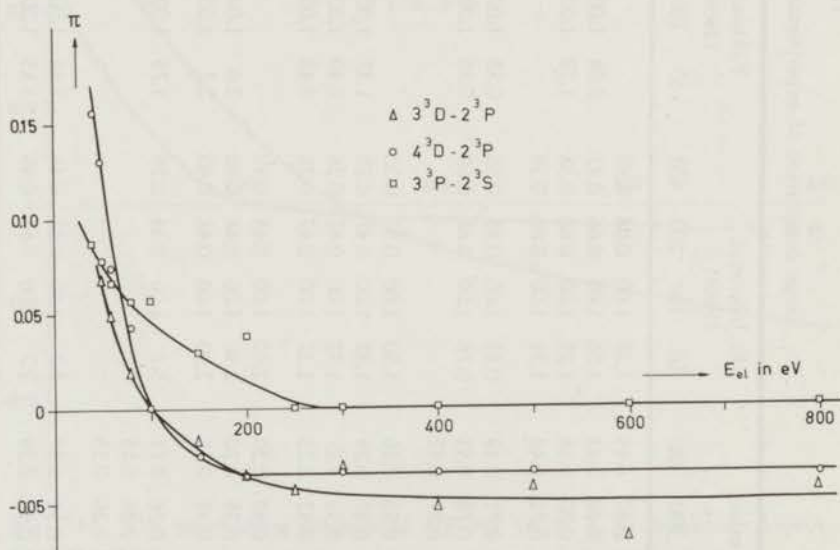

Fig. 7.12 The polarization fraction of $3^3D\text{-}2^3P$ ($\lambda = 5876\,\text{Å}$), $4^3D\text{-}2^3P$ ($\lambda = 4472\,\text{Å}$) and $3^3P\text{-}2^3S$ ($\lambda = 3889\,\text{Å}$) transitions versus electron energy.

and 7.12 and summarized in Table 7.6. No polarization measurements on He II were done. The random errors in the polarization measurements are important only in determining $I_{//}$ and $I_{\perp}$ (see section 5.2a). The random error in the ratio $I_{//} / I_{\perp}$ is about 5% which implies that the random error in the polarization degree may amount to about 10%. These errors are somewhat higher in lower Π values and also for the measurements at high electron impact energies, where the light signals become weak.

7.2.2. *General behaviour*

Just as with the excitation cross sections (see section 7.1.2.) there is a large conformity in the energy dependent behaviour of Π for lines of a spectral series. Approximately Π should be equal for all lines of such a series at every impact energy (see section 2.5). However, experimentally a decrease in Π is present with increasing the principal quantum number n. At lower impact energies < 200 eV) we found positive Π values while at high impact energies negative Π values have been obtained in most cases. The same behaviour can be predicted theoretically (see section 2.5).

7.2.3. n^1S-2^1P lines

The polarization degree of 4^1S-2^1P (5047 Å) transition has been measured. We found that the polarization degree always is close to zero at all energies. This is because of the spherical symmetry of the S-states.

7.2.4. n^1P-2^1S lines

The results of 3^1P-2^1S (5016 Å) and 4^1P-2^1S (3965 Å) are given in Fig. 7.10. At low electron impact energies (< 200 eV), the polarization degree of 3^1P-2^1S and 4^1P-2^1S are both positive. However, in the case of 5^1P-2^1S almost no polarization has been found (see Table 7.6). At electron energies higher than 200 eV a negative degree of polarization is found. Comparing our measurements with the other authors (see Table 7.7), we can see that our results are in agreement with those of M c F a r l a n d and S o l t y s i k

TABLE 7.6

Polarization fraction Π

E_{el} in keV	3^1P-2^1S 5016 Å	4^1P-2^1S 3965 Å	5^1P-2^1S 3614 Å	3^1D-2^1P 6678 Å	4^1D-2^1P 4922 Å	5^1D-2^1P 4388 Å	6^1D-2^1P 4144 Å	3^3D-2^3P 5875 Å	4^3D-2^3P 4472 Å	3^3P-2^3S 3889 Å
0.04	—	0.168	0.043	0.265	0.280	0.190	0.138	—	0.156	0.087
0.05	0.267	0.149	0.040	0.265	0.278	0.180	0.153	0.067	0.130	0.078
0.06	0.252	0.142	0.005	0.264	0.259	0.173	0.134	0.048	0.074	0.066
0.08	0.230	0.107	0.005	0.241	0.227	0.156	0.138	0.017	0.043	0.057
0.10	0.206	0.103	— 0.015	0.190	0.196	0.139	0.119	0.000	0.000	0.057
0.15	0.134	0.029	0.000	0.095	0.119	0.107	0.099	— 0.018	— 0.025	0.029
0.20	0.082	0.005	0.000	0.047	0.063	0.070	0.052	— 0.036	— 0.036	0.038
0.25	0.036	0.000	0.000	— 0.013	0.000	0.040	0.038	— 0.044	—	0.000
0.30	0.000	— 0.007	0.000	— 0.036	0.000	0.005	0.024	— 0.032	— 0.034	0.000
0.40	— 0.045	— 0.015	— 0.027	— 0.058	— 0.045	— 0.025	— 0.011	— 0.053	— 0.034	0.000
0.50	— 0.064	— 0.017	— 0.044	— 0.102	— 0.087	— 0.020	— 0.031	— 0.042	— 0.034	0.000
0.60	— 0.090	— 0.019	— 0.058	— 0.111	— 0.102	— 0.025	— 0.047	— 0.069	—	—
0.80	— 0.132	— 0.066	— 0.058	— 0.130	— 0.153	— 0.047	— 0.050	— 0.042	— 0.036	0.000
1.0	— 0.143	— 0.075	— 0.058	— 0.143	— 0.163	— 0.031	— 0.034	— 0.050	— 0.052	—
1.5	— 0.190	— 0.075	—	— 0.169	— 0.176	— 0.047	— 0.046	—	—	—
2.0	— 0.197	— 0.095	— 0.058	— 0.163	— 0.194	— 0.065	— 0.058	—	—	—
2.5	— 0.219	— 0.124	—	— 0.176	— 0.203	— 0.045	— 0.048	—	—	—
3.0	— 0.250	— 0.143	—	— 0.159	— 0.192	— 0.025	— 0.039	—	—	—
4.0	— 0.250	— 0.148	—	—	— 0.187	— 0.041	— 0.036	—	—	—
5.0	—	— 0.143	—	—	— 0.194	— 0.069	—	—	—	—

(1962), which have measured at slightly higher pressure. H e d d l e and L u c a s (1962) obtain the highest Π values.

7.2.5. n^1D-2^1P lines

The polarization degrees of these lines ($n = 3, 4, 5$ and 6) are given in Fig. 7.11.

We can see also from Table 7.7 that our Π results of this series are much lower than of the other authors. M c F a r l a n d and S o l t y s i k (1962b) published that the polarization degree of this series is dependent on the axial magnetic field. We did not find any effect of the axial magnetic field on the polarization degree (see chapter 6). In recent work of S o l t y s i k et al. (1967) the independence of the polarization on the magnetic field has been affirmed.

7.2.6. 3^3D-2^3P (5876 Å), 4^3D-2^3P (4472 Å) and
3^3P-2^3S (3889 Å) transitions

The results are given in Fig. 7.12. For n^3D-2^3P ($n = 3$ and 4) the polarization degree falls off rapidly with increasing electron impact energy. We found zero at 100 eV. Above 100 eV we found a small constant negative value. Also in this case our data differ much from those of H e d d l e and L u c a s (1962).

For the 3^3P-2^3S line we found a small positive polarization degree below 250 eV. Above that energy no polarization was found.

TABLE 7.7

Comparison of the experimental polarization fractions Π

Line	E_{el} in eV	Polarization fraction *)							
		This work	Heideman (1962)	Heddle and Lucas (1962)		McFarland and Soltysik (1962)		Hughes et al. (1961)	
		0.34 μ**)	5.3 μ	0.35 μ	5 μ	0.5 μ	5 μ	5 μ	
3¹P-2¹S	25		0.155						
	30		0.190				between	0.210	
	35		0.195	0.53	0.17	0.210	0.06-0.10	0.210	
	40			0.52		0.210		0.205	
	50	0.267		0.50		0.215		0.200	
	100	0.206		0.32		0.136		0.135	
	150	0.134		0.16		0.080		0.040	
	175	—		0.07		0.060		0.010	
	200	0.082		0.00		0.040		—0.010	
	250	0.036		—		0.014		—0.022	
	300	0.000		—		—		—	
		1.00 μ	5.3 μ	1.3 μ	0.5 μ	0.5 μ	10.0 μ	0.5 μ	5 μ
4¹D-2¹P	35		0.41						
	40	0.280		0.60	0.60	0.530	0.332	0.500	0.500
	50	0.278		0.56		0.470	0.314	0.460	0.433
	60	0.259		0.53		0.443	0.284	0.440	0.420
	80	0.227		0.48		0.379	0.221	0.375	0.345
	100	0.196		0.42		0.328	0.171	0.320	0.292
	150	0.119		0.28		0.229	0.092	0.205	0.180
	200	0.063		0.16		0.158	0.028	0.130	0.095
	250	0.000		0.068		0.095	0.000	0.077	0.045
	300						—0.014	0.045	0.000
		1.04 μ	5.3 μ			5 μ	10 μ	3.5 μ	
5¹D-2¹P	35		0.41						
	40	0.190				0.410	0.295	0.475	
	50	0.180				0.373	0.259	0.432	
	60	0.173				0.343	0.235	0.400	
	80	0.156				0.295	0.175	0.331	
	100	0.139				0.240	0.127	0.256	
	150	0.107				0.168	0.054	0.150	
	200	0.070				0.102	0.018	0.075	
	250	0.040				0.072	0.000		
	300	0.000				0.060	0.000		
		1.05 μ	5.3 μ	0.5 μ		0.5 μ	2.5 μ	0.4 μ	5 μ
3³P-2³S	40	0.087	0.44						
	50	0.078		0.219		0.140	0.128	0.137	0.125
	60	0.066		—		0.154	0.135	0.148	0.132
	100	0.057		0.185		0.135	0.108	0.118	0.095
	150	0.029		0.139		0.092	0.058	0.060	0.040
	200	0.038		0.093		0.055	0.026	0.020	0.000
	250	0.000		0.040		0.034	0.010	—	0.000
		1.04 μ	5.3 μ	1 μ	5 μ	1 μ	10 μ	5 μ	
4³D-2³P	35		0.125	0.230	0.10			0.150	
	40	0.156				0.140	0.070		
	50	0.130		0.200				0.100	
	60	0.074		0.149			0.050	0.070	
	70	—		0.107				0.048	
	80	0.043		0.057			0.008	0.028	
	90			0.012			0.000	0.009	
	100	0.000		—				0.000	
	120			—				—0.028	
	150	0.025		—					
	200	0.036		—				—0.041	

*) All these reported results have been taken from the graphs related to the mentioned authors.

**) The experimental gas pressures are given in μ.

CHAPTER 8

COMPARISON WITH THEORY

8.1. Excitation cross section

As has been derived before, equations (2.3.4) and (2.4.5) show that at high electron energies the cross section for the optically allowed transition is proportional to $E_{el}^{-1} \ln E_{el}$, while the cross section of the optically forbidden transition is proportional to E_{el}^{-1}. In the case of triplet excitation, where exchange of electrons with antiparallel spin occurs, the excitation cross section should decrease with E_{el}^{-3} (O c h k u r, 1964). Then the best way to compare our data with theory is to plot them in graphs of σE_{el} versus $\ln E_{el}$ for optically allowed transitions and graphs of σE_{el} versus $\ln E_{el}$ or E_{el} for optically forbidden transitions.

8.1.1. *He I excitation*

A) *Singlet excitation*

Figs. 8.1, 8.2, and 8.3 present $\sigma E_{el}/4\pi a_0^2 R$ versus $\ln E_{el}$ and σE_{el} versus E_{el} for n^1P levels ($n = 3, 4$ and 5), n^1D levels ($n = 3, 4, 5$ and 6) and n^1S levels ($n = 3, 4, 5$ and 6) respectively. From Fig. 8.1 one can see that at electron energies above 100 eV our data are in excellent agreement with the Bethe-Born relation for optically allowed transitions. The slope of this graph gives the value of M_n^2 in eq. (2.4.3) which is equal to $f_n R/E_n$, i.e. we can find the value of the optical oscillator strength, f_n, for every level. Table 8.1 gives a comparison between the theoretical and experimental values of the optical oscillator strengths. The theoretical f_n values of M o t t and M a s s e y, O c h k u r and
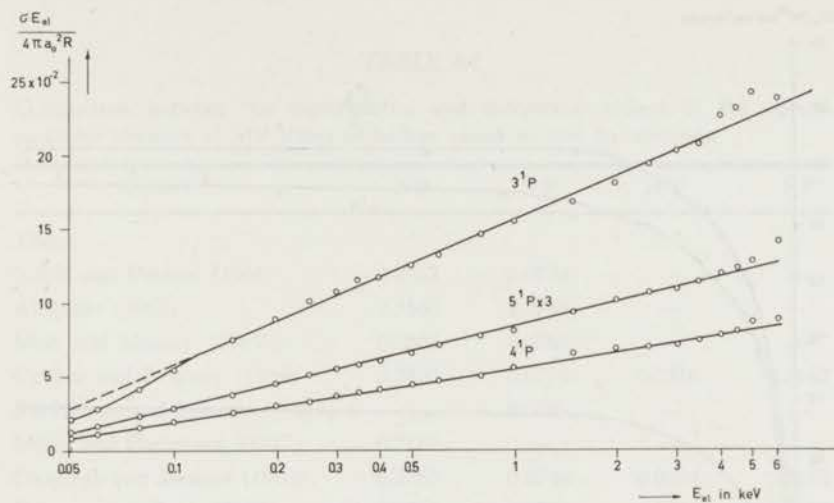
Fig. 8.1 Plot of $\sigma E_{el}/4\pi a_0^2 R$ versus ln E_{el} for the absolute excitation cross sections of n^1P levels.
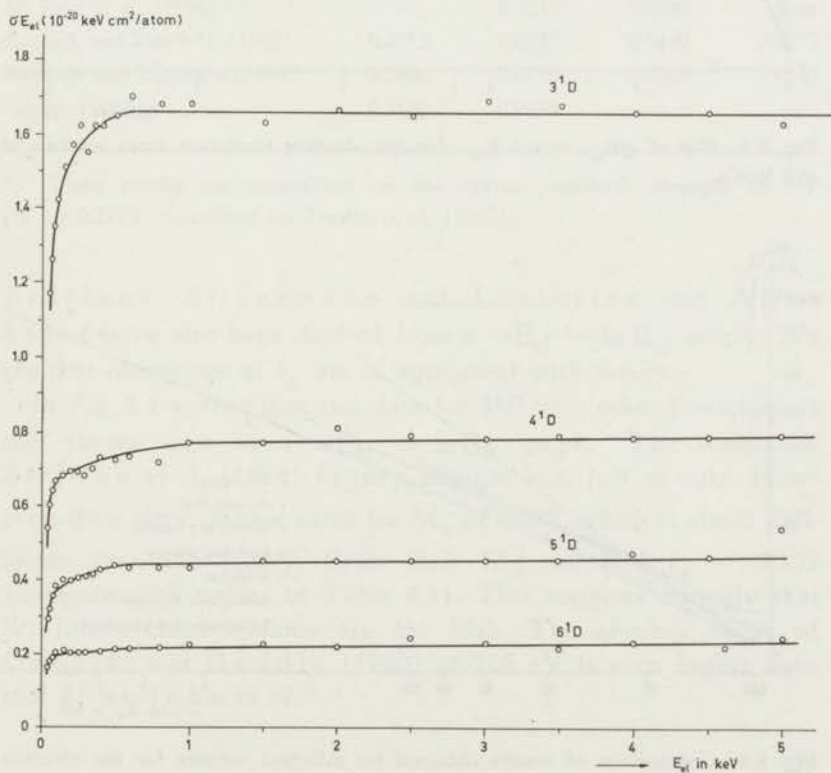

Fig. 8.2 Plot of σE_{el} versus E_{el} for the absolute excitation cross sections of n^1D levels.
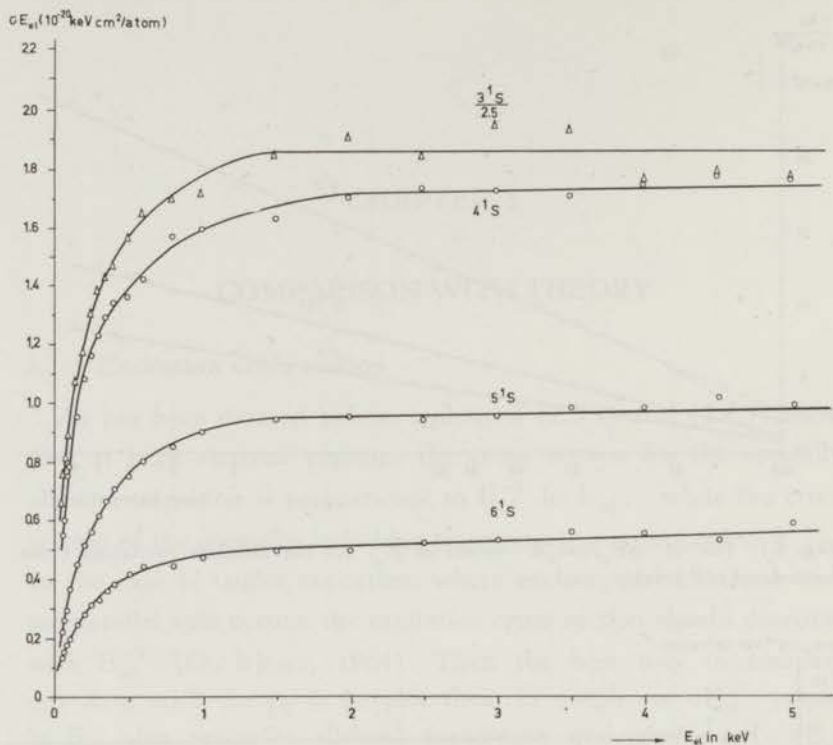
Fig. 8.3 Plot of σE_{el} versus E_{el} for the absolute excitation cross sections of n^1S levels.
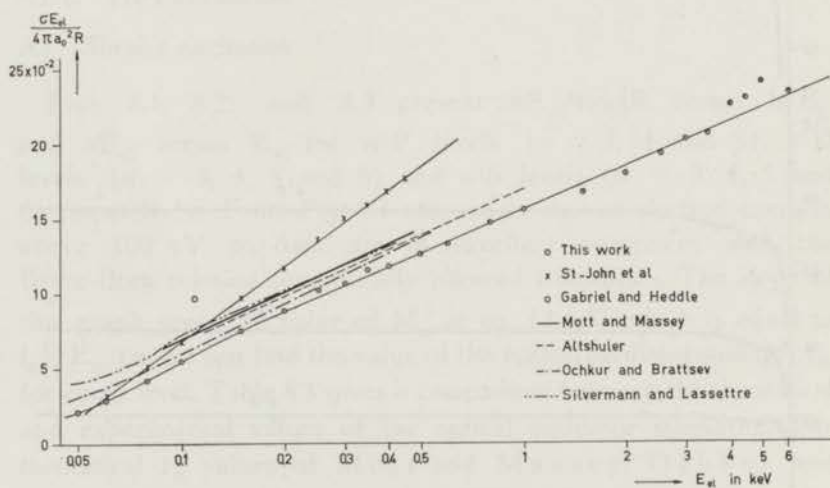

Fig. 8.4 Comparison of results obtained by different authors for the absolute excitation cross sections of the 3^1P level, plotted as $\sigma E_{el} / 4\pi a_0^2 R$ versus $\ln E_{el}$.

TABLE 8.1

Comparison between the experimental and theoretical values of the optical oscillator strength of n^1P states of helium atoms excited by electrons

Autors	2^1P	3^1P	4^1P	5^1P
Theor.				
Schiff and Pekeris (1964)	0.2762	0.0734	—	—
Altshuler (1952)	0.2860	0.0755	—	—
Mott and Massey (1965b)	0.2800	0.0768	—	—
Ochkur and Brattsev (1965)	0.2800	0.0774	0.0316	0.0162
Silvermann and Lassettre (1965)	—	0.0726	—	—
Miller and Platzmann (1957)	0.2770	—	—	—
Dalgarno and Stewart (1960)	0.2750	0.0746	0.0304	0.0153
Salpeter and Zaidi (1962)	0.2717	0.0706	0.0329	0.0177
Exp.				
This work	—	0.0730	0.0280	0.0141
St. John et al. (1964)	—	0.1218	0.0640	—
Boersch and Reich *) (1965)	0.2719	0.0787	0.0489	0.0272
Skerbele and Lassettre (1964)	0.2680	0.0730	0.0300	0.0145
Geiger (1963)	0.3120	0.0898	—	—

*) Their results are normalized on the optical oscillator strength of 2^1P $(f_n = 0.2719)$ calculated by Trefftz et al. (1957).

Brattsev, Silvermann and Lassettre and Altshuler have also been derived from a $\sigma E_{el} - \ln E_{el}$ graph. We see that our values of f_n are in agreement with theory.

In Fig. 8.4 we compare our data for 3^1P with other investigators and theory, also in a $\sigma E_{el} - \ln E_{el}$ graph. The results of St. John et al. (1964) fit on a straight line, just as ours. However, their slope gives a value for M_n^2 of 0.072, which is about 70% larger than the theory. From their M_n^2 we find $f_n = 0.122$ (compare with values in Table 8.1). This suggests strongly that St. John's cross sections are too high. The absolute value of Gabriel and Heddle (1960) at 108 eV is even higher than that of St. John et al.

91

Fig. 8.4 shows also that our results are in very good agreement with the theoretical calculations done by Altshuler's Method II (1952), M o t t and M a s s e y (1965b), O c h k u r and B r a t t - s e v (1965) and the semi-empirical calculations of S i l v e r m a n n and L a s s e t t r e (1965).

The theoretical and experimentical results of 3^1P are also given in Table 8.2. One can see that below 200 eV the calculations by

TABLE 8.2

Comparison of the experimental excitation cross sections of the 3^1P level with the theoretical calculations in units of 10^{-20} cm²/atom.

	experiment			theory		
E (eV)	This work	St. John et al. (1964)	Mott and Massey (1965b)	Altshuler (1953)	Silvermann and Lassettre (1965)	Ochkur and Prattsev (1965)
60	228	255			400	300
80	247	305			380	300
100	260	325	338	—	345	291
150	238	307	—	278	285	256
200	211	287	242	239	246	220
300	170	240	—	186	191	176
400	140	200	159	154	157	150
500	121	187	—	132	—	132

Born approximation (M o t t and M a s s e y and A l t s h u l e r) and also the semi-empirical calculations of S i l v e r m a n n and L a s s e t t r e give higher cross sections than our experiments. O c h k u r's calculation is more closer to our results.

In Figs. 8.2 and 8.3 we made $\sigma E_{el} - E_{el}$ plots for n^1D and n^1S respectively. One can see that σE_{el} for n^1D levels becomes almost constant above 200 eV. For n^1S states σE_{el} becomes almost constant at rather high electron energies (> 1000 eV).

In Figs. 8.5 and 8.6 we compare our 3^1D and 4^1D results with S t. J o h n et al., G a b r i e l and H e d d l e (1960) and theory.
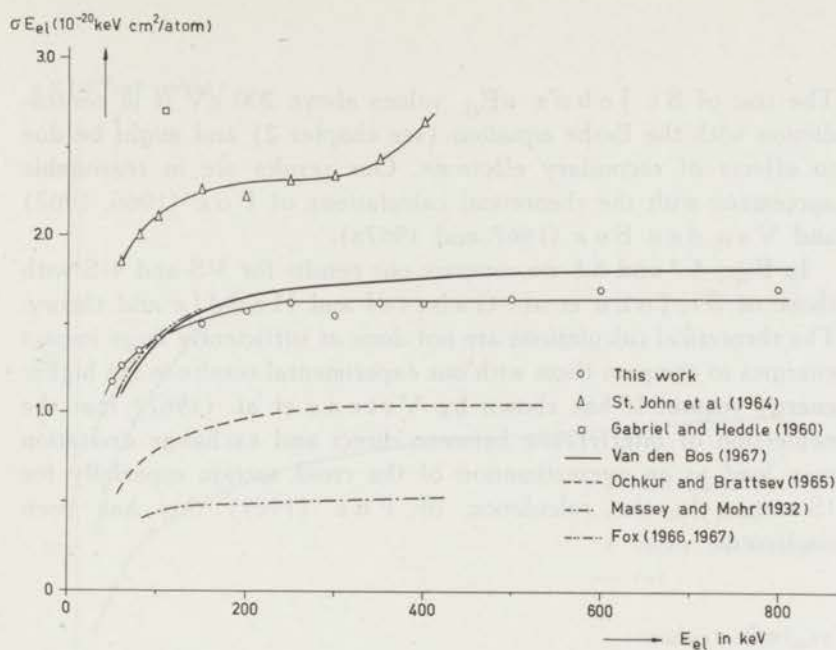
Fig. 8.5 Comparison of results obtained by different authors for the absolute excitation cross section of the 3^1D level, plotted as σE_{el} versus E_{el}.
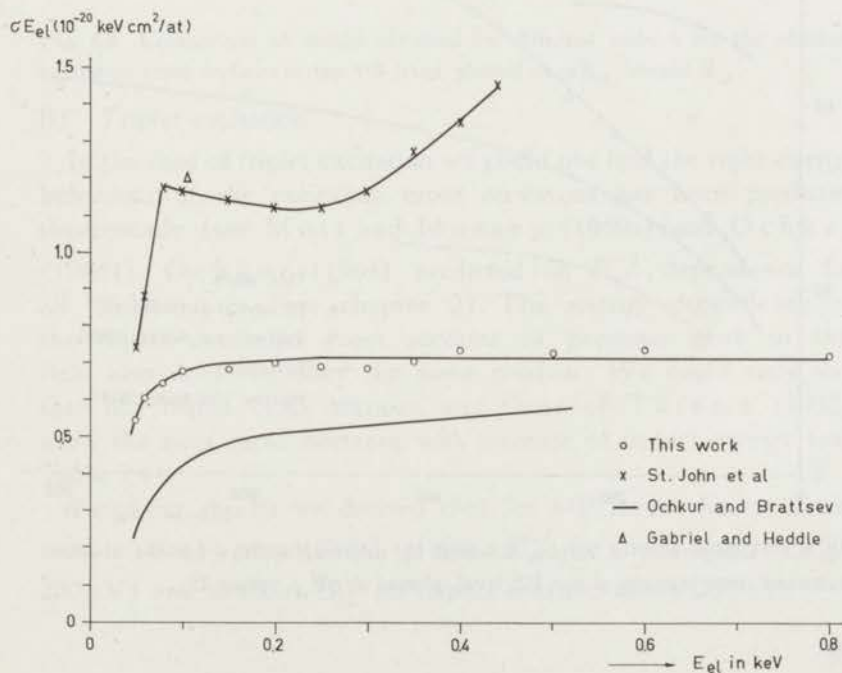

Fig. 8.6 Comparison of results obtained by different authors for the absolute excitation cross section of the 4^1D level, plotted as σE_{el} versus E_{el}.

The rise of St. John's σE_{el} values above 200 eV is in contradiction with the Bethe equation (see chapter 2) and might be due to effects of secondary electrons. Our results are in reasonable agreement with the theoretical calculations of Fox (1966, 1967) and Van den Bos (1967 and 1967a).

In Figs. 8.7 and 8.8 we compare our results for 3^1S and 4^1S with those of St. John et al., Gabriel and Heddle and theory. The theoretical calculations are not done at sufficiently large impact energies to compare them with our experimental results in the higher energy region. It has shown by Vriens et al. (1967) that the neglection of interference between direct and exchange excitation may lead to an overestimation of the cross section especially for ^1S-states. In the calculation of Fox (1965) this has been neglected.
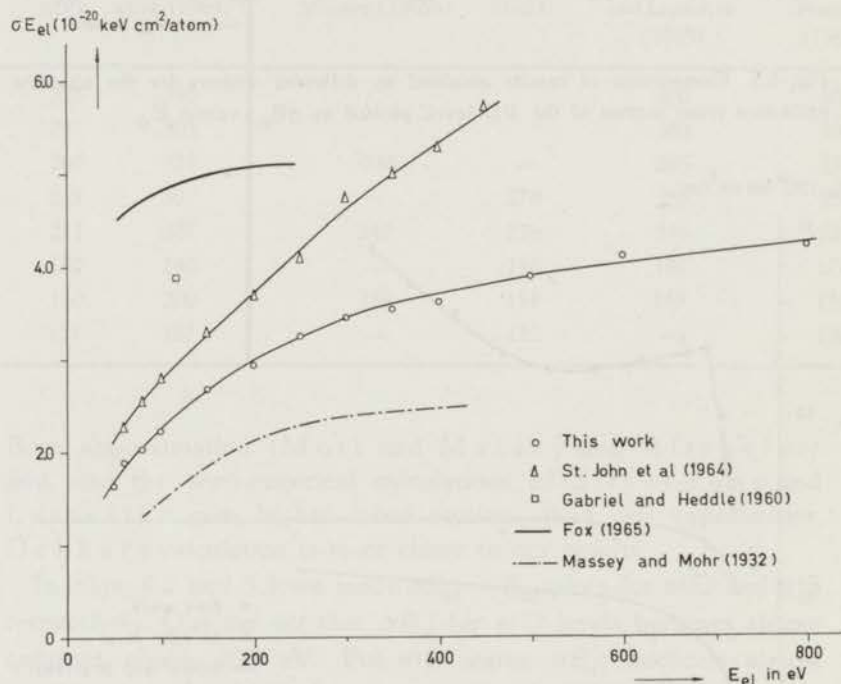

Fig. 8.7 Comparison of results obtained by different authors for the absolute excitation cross sections of the 3^1S level, plotted as σE_{el} versus E_{el}.
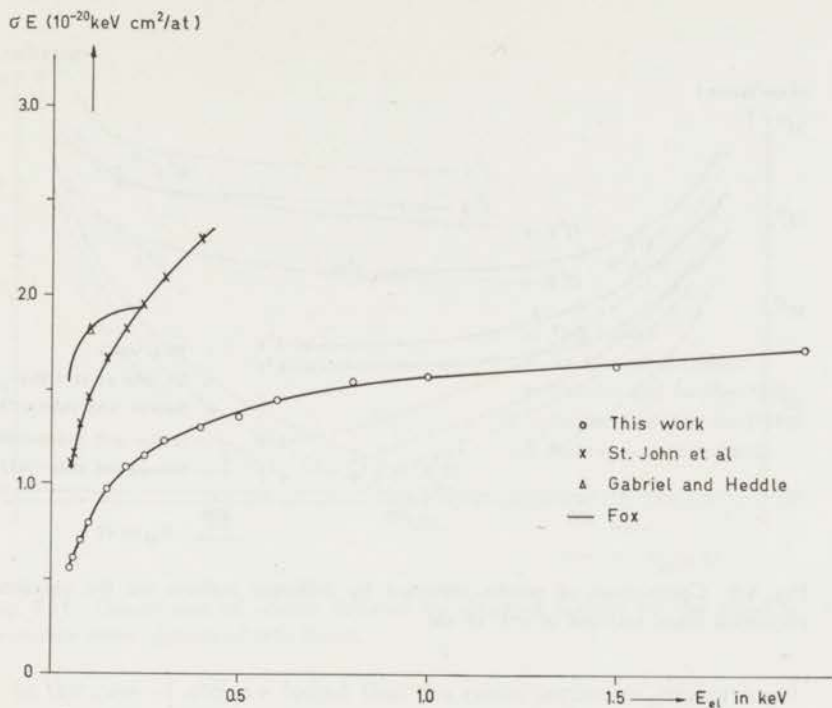
94

σE (10⁻²⁰keV cm²/at)

$\sigma E\ (10^{-20}\text{keV cm}^2/\text{at})$

3.0

2.0

1.0

0

o   This work
x   St. John et al
▲   Gabriel and Heddle
—   Fox

0.5   1.0   1.5 ——→ E_{el} in keV

Fig. 8.8 Comparison of results obtained by different authors for the absolute excitation cross sections of the 4^1S level, plotted as σE_{el} versus E_{el}.

B)   *Triplet excitation*

In the case of triplet excitation we could not find the right energy behaviour of the excitation cross secion as has been predicted theoretically (see M o t t and M a s s e y (1949a) and O c h k u r (1964)). O c h k u r (1964) predicted an E_{el}^{-3} dependence for all triplet states (see chapter 2). The energy dependence of the triplet excitation cross sections of previous work in this field also does not obey the same relation. We could only say that our triplet cross sections and those of T h i e m e (1933) show the most rapid decrease with increase of impact energy (see Table 7.4).

From our results we derived that for n^3P levels the excitation cross section is proportional to about E_{el}^{-2} for lower energies (50-200 eV) and to about E_{el}^{-1} for impact energies above 200 eV.
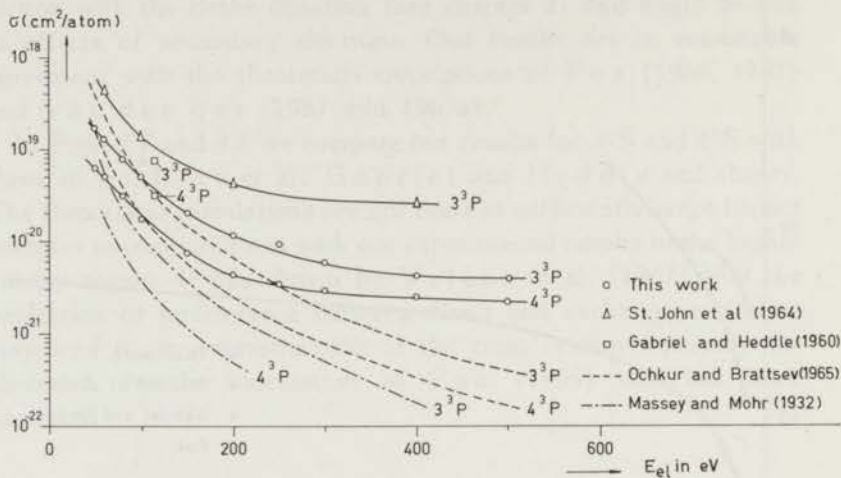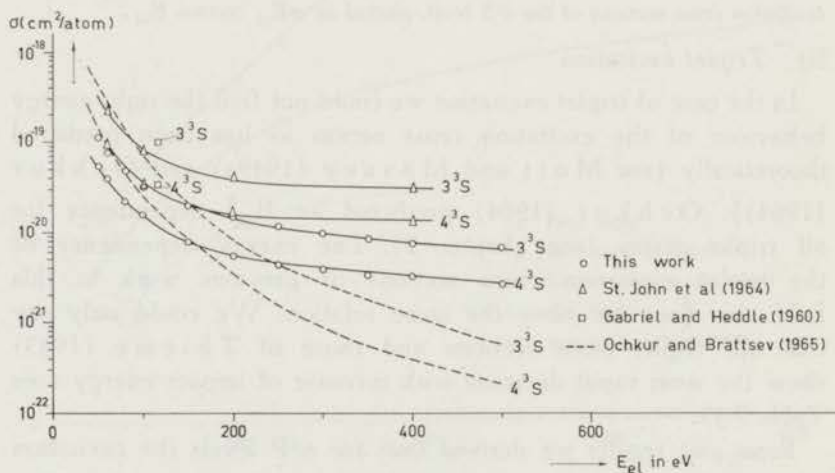
95

Fig. 8.9 Comparison of results obtained by different authors for the absolute excitation cross sections of n^3P levels.

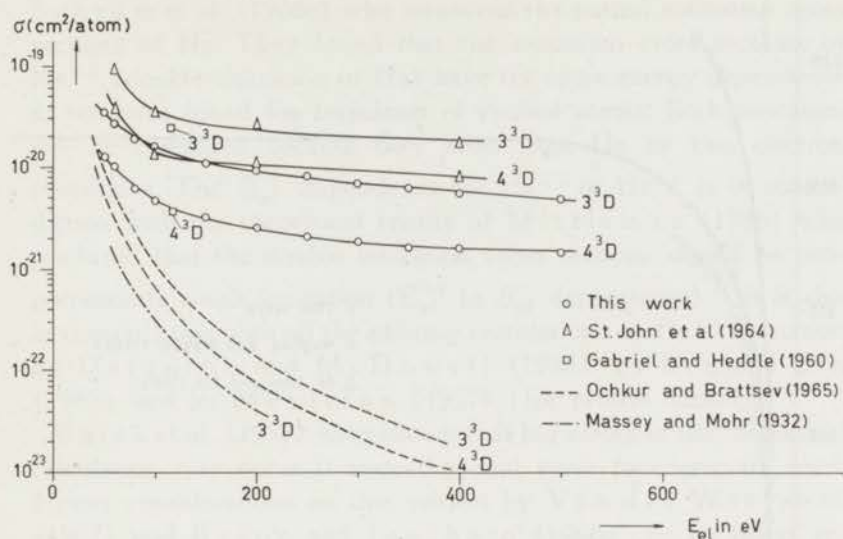Fig. 8.10 Comparison of results obtained by different authors for the absolute excitation cross sections of n^3S levels.

96

Fig. 8.11 Comparison of results obtained by different authors for the absolute excitation cross sections of n^3D levels.

In the case of n^3S we found that the cross section is proportional to about $E_{el}^{-0.7}$ at high electron impact energies (> 200 eV).

For n^3D the energy power is even less in absolute value than for n^3S. We found about -0.5.

Experimental and theoretical results are presented in Figures 8.9, 8.10 and 8.11.

More effort is going on into a critical examination in order to solve the discrepancy between experiment and theory.

8.1.2. *He II excitation*

In the case of helium ion excited lines (see Table 6.1), we found that all the emission cross sections behave as an optically forbidden transition (i.e. the cross section $\sigma \sim E_{el}^{-1}$). Figs. 8.12 and 8.13 show the energy dependence of all He II lines which have been measured. The results of H u g h e s and W e a v e r (1963) and also of S t. J o h n and L i n (1964) of 4686 Å are demonstrated. From the graph one can see that σE_{el} becomes constant for all transitions at electron energy higher than 500 eV. This is in agreement with
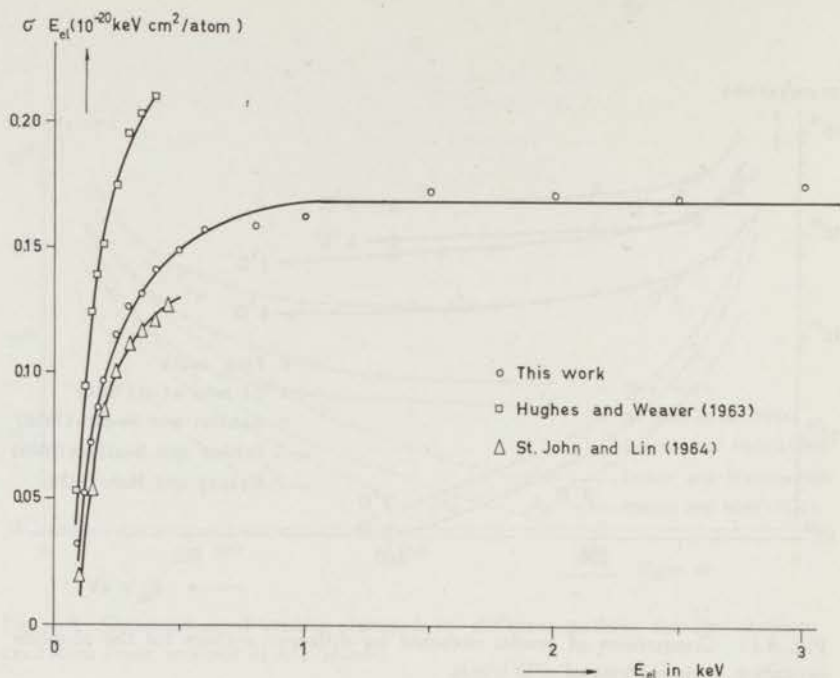
97

Fig. 8.12 Comparison of results obtained by different authors for the emission cross sections of $\lambda = 4686$ Å $(4 \rightarrow 3)$.
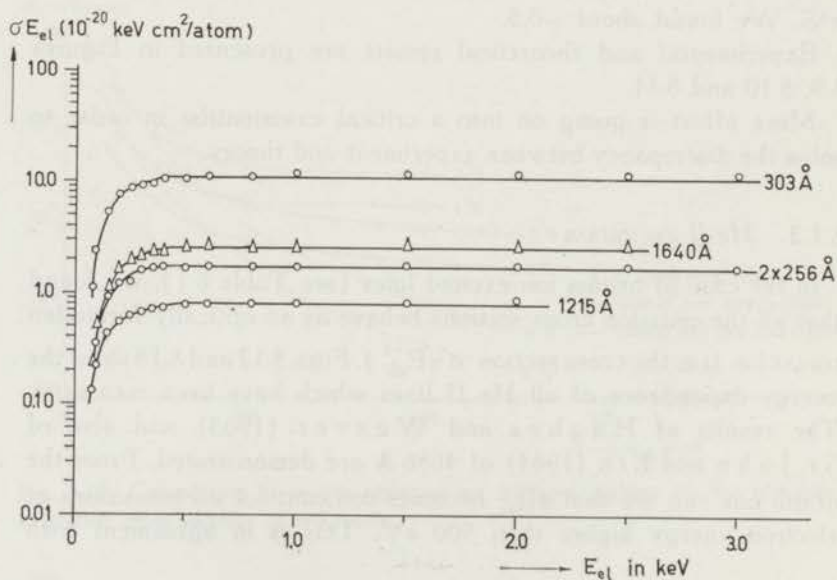

Fig. 8.13 Plot of σE_{el} versus E_{el} for the emission cross sections of He II lines $\lambda = 1215$ Å $(4 \rightarrow 2)$, $\lambda = 1640$ Å $(3 \rightarrow 2)$, $\lambda = 303$ Å $(2^2P\text{-}1^2S)$, $\lambda = 256$ Å $(3^2P\text{-}1^2S)$.

S c h r a m et al. (1966c) who measured the partial ionization cross sections of He. They found that the ionization cross sections of He^{++} (double ionization of He) have the same energy dependence as we have found for formation of excited atoms. Both processes can be compared because they arise from He by two electron transitions. The E_{el}^{-1} dependence for He^{++} or He^{+*} is in contradiction with the theoretical results of M i t t l e m a n (1966) who predicted that the double ionization cross sections should be proportional to single ionization (E_{el}^{-1} ln E_{el} dependence). It is also in contradiction with all the existing calculations on He^{+*} excitation by D a l g a r n o and M c D o w e l l (1956), by L e e and L i n (1965) and by M a p l e t o n (1957) (for proton impact).

B a t e s et al. (1950) have shown that big errors in the theoretical calculation may occur if nonorthogonal wave functions are used. Newer considerations on this subject by V a n d e r W i e l et al. (1967) and B y r o n and J o a c h a i n (1966) can be better reconciled with experiments. It appears to be necessary to carry out calculations which explain the dominance of the E_{el}^{-1} contribution in the process of double ionization or simultaneous ionization and excitation.

If we consider the absolute values of the different emission cross sections, we see that our values of $\sigma(3^2P \rightarrow 1^2S)$ are smaller than those of $\sigma(3 \rightarrow 2)$. This would mean that the excitation to the He^{+*} 3^2P state is relatively small. Such a conclusion can however not be definite, because of the uncertainty in the intensity calibration, especially for 256 Å (see section 4.2).

Because of the unreliability of the theory, we think that we cannot yet attribute much significance to the relative population of S, P, D and F states as found by D a l g a r n o and M c D o w e l l (1956), by L e e and L i n (1965) and by M a p l e t o n (1957) (for proton impact). Also discrepancies in the theoretical excitation cross sections are present in the calculations of D a l g a r n o and M c D o w e l l and of M a p l e t o n, when compared at equal projectile velocities. The cross sections differ one order of magnitude. M a p l e t o n's results and those of L e e and L i n give almost the same value for the 4S excitation at high impact velocities.

8.2 The degree of polarization

Eqs. 2.5.10 and 2.5.11 show that $I_\perp/I_{//}$ of the spectral lines $(n^1P\text{-}2^1S)$ is proportional to $\ln c\, E_{el}$ and $I_\perp/I_{//}$ of the spectral lines $(n^1D\text{-}2^1P)$ is a constant at high impact energies. Therefore, it is useful to check our experimental results on the degree of polarization (see Table 7.6) in view of these asymptotic behaviours. In Fig. 8.14 we plotted simply $I_\perp/I_{//}$ of $3^1P\text{-}2^1S$ (5016 Å) as a function of $\ln E_{el}$. From the figure one can see that our experimental results show the asymptotically predicted energy dependence. In Fig. 8.15 we plotted again $I_\perp/I_{//}$ of $4^1D\text{-}2^1P$ (4922 Å) as a function of $\ln E_{el}$. We see that at sufficiently high electron energies (> 1.5 keV) the polarization degree is in qualitative agreement with the predicted behaviour.
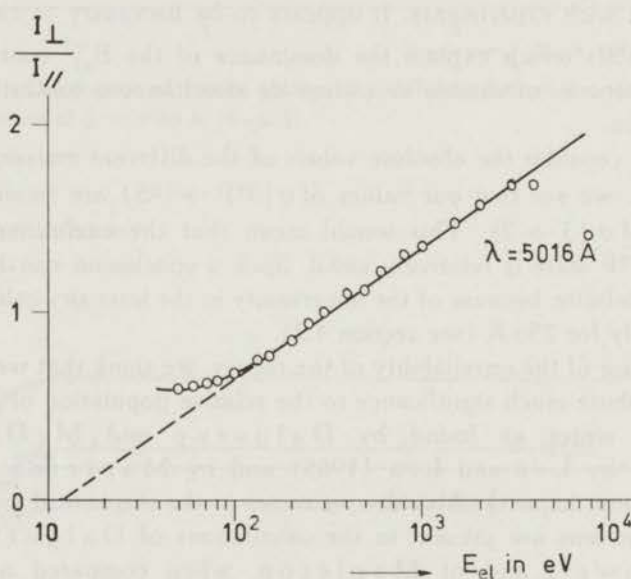

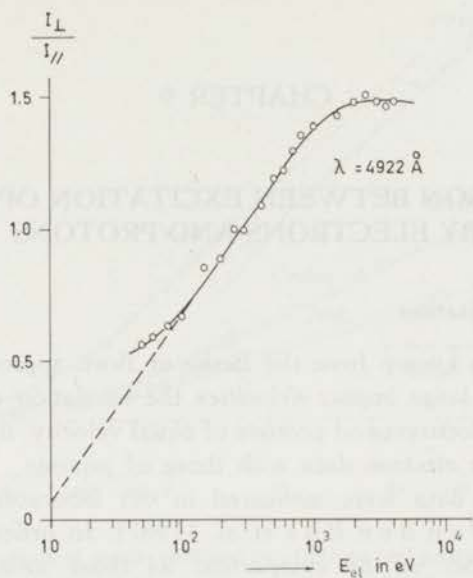Fig. 8.14 Plot of $I_\perp/I_{//}$ of the $3^1P\text{-}2^1S$ transition ($\lambda = 5016$ Å) versus $\ln E_{el}$.

100

Fig. 8.15   Plot of $I_\perp/I_{//}$ of the 4^1D-2^1P transition ($\lambda = 4922$ Å) versus $\ln E_{el}$

CHAPTER 9

COMPARISON BETWEEN EXCITATION OF HELIUM BY ELECTRONS AND PROTONS

9.1. He I excitation

Because it is known from the Bethe or Born approximation that at sufficiently large impact velocities the excitation cross sections are equal for electrons and protons of equal velocity, it is interesting to compare our electron data with those of protons.

The proton data were measured in our laboratory from 1 to 150 keV by Van den Bos et al. (1967). In order to eliminate systematic errors in the comparison as those arising from the absolute intensity calibration and McLeod pressure reading, proton excitation measurements have also been carried out with the apparatus used for electron excitation. For that purpose the electron gun was removed and the apparatus was put behind a proton accelerator, operating between 30 and 150 keV.

In Fig. 9.1 we plot the excitation cross sections of the optically allowed transitions (1^1S-n^1P) in a σE_{el} versus $\ln E_{el}$ plot both for electron and proton impact. The proton energies are transformed into electron energies by putting them equal to $\frac{1}{2} m_e v_p^2$, where m_e is the electron mass and v_p is the proton velocity. From the figure we see that there is reasonable agreement between our electron and proton data at high velocities. The proton cross sections are mostly somewhat higher, but the difference may decrease at higher velocities. We must remark that the proton data of 3^1P have been normalized on the correct optical oscillator strength by decreasing the cross sections of Van den Bos et al. by about 9%.

In Fig. 9.2 we compare in the same way our excitation cross sections for n^1D levels ($n = 4$, 5 and 6) with the proton results of Van den Bos et al. in a σE_{el} versus $\ln E_{el}$ plot. According to

102

Fig. 9.1 Comparison of results obtained by electrons and protons for the absolute excitation cross sections of n^1P levels plotted as $\sigma E_{el} / 4\pi a_0^2 R$ versus $\ln E_{el}$.
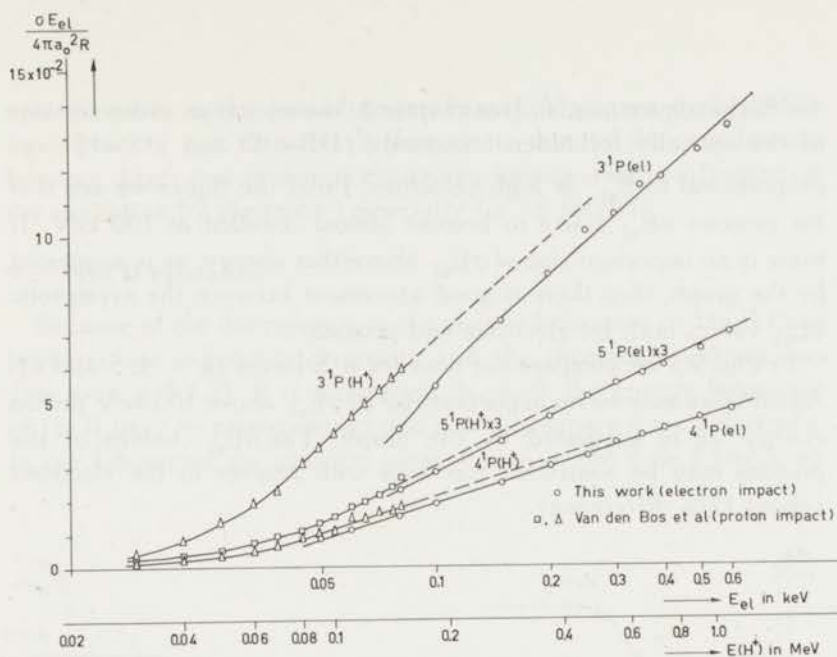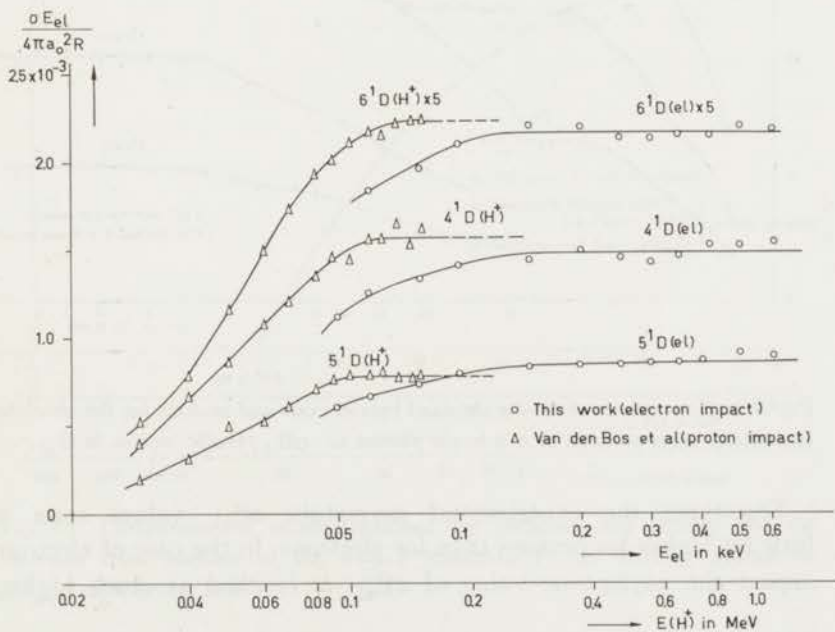

Fig. 9.2 Comparison of results obtained by electrons and protons for the absolute excitation cross sections of n^1D levels plotted as $\sigma E_{el} / 4\pi a_0^2 R$ versus $\ln E_{el}$.

the Bethe approximation (see chapter 2) the excitation cross sections of the optically forbidden transitions (1^1S-n^1D and 1^1S-n^1S) are proportional to E_{el}^{-1} at high velocities. From the figure we see that for protons σE_{el} starts to become almost constant at 100 keV. If there is no important rise of σE_{el} above that energy, as is suggested by the graph, then there is good agreement between the asymptotic σE_{el} values both for electrons and protons.

In Fig. 9.3 we compare the data for n^1S levels ($n = 4, 5$ and 6). Again there may be no important rise of σE_{el} above 100 keV proton energy, as is suggested by the graph. The σE_{el} values of the protons may be somewhat too high with respect to the electrons (about 12% difference).
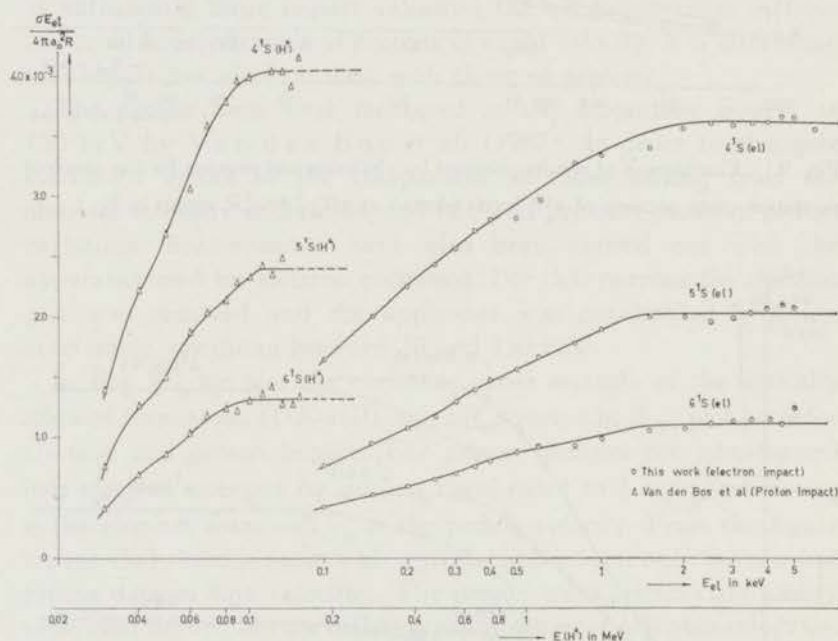

Fig. 9.3 Comparison of results obtained by electrons and protons for the absolute excitations cross sections of n^1S levels plotted as $\sigma E_{el}/4\pi a_0^2 R$ versus ln E_{el}.

Sometimes the experimental asymptotic σE_{el} values seem a little bit higher for protons than for electrons. In the case of electron impact the asymptotic value of σE_{el} is reached at much higher

104

velocities than in the case of proton impact. V r i e n s et al. (1967) have pointed out that this difference is due to the interference between direct and exchange excitation, having a large influence on the excitation by electrons (especially for ^1S levels).

9.2. He II excitation

Because of the discrepancy in the energy behaviour of He II lines between our experimental results and the theoretical calculations (see section 8.1.2), it is interesting to check the energy behaviour of He II lines by proton impact and also to compare it with electrons. In our laboratory the emission cross section of the $4 \rightarrow 3$ transition
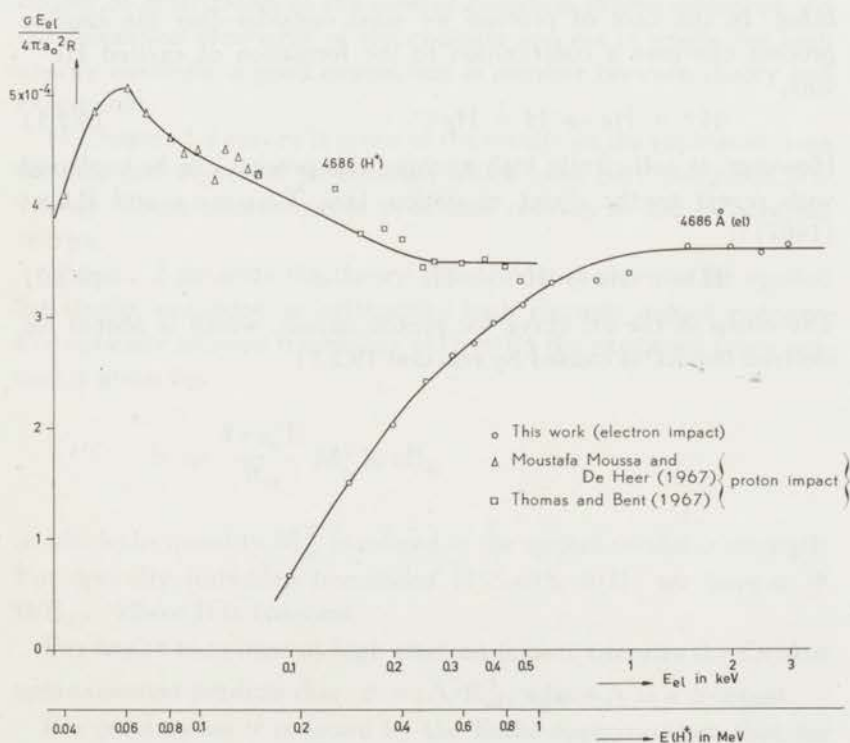

Fig. 9.4 Comparison of results obtained by electrons and protons for the emission cross sections of the $4 \rightarrow 3$ transition ($\lambda = 4686$ Å) plotted as $\sigma E_{el} / 4\pi a_0^2 R$ versus $\ln E_{el}$.

(4686 Å) by proton impact has been measured between 30 and 150 keV (see Moustafa Moussa and De Heer (1967)). The same transition has also been measured by proton impact from 150 to 900 keV by Thomas and Bent (1967). Comparing the emission cross section results for protons obtained by Moustafa Moussa and by Thomas, we found that Moustafa's results are a factor 2.3 higher. Therefore, we normalized the results of Thomas and Bent on those of Moustafa Moussa and De Heer at 150 keV in order to follow the energy behaviour up to rather high velocities. The results are presented in Fig. 9.4. We see from the figure that at proton energies higher than 400 keV the emission cross section is proportional to E_{el}^{-1}. The asymptotic σE_{el} values of electrons and protons are in good agreement with each other. In the case of protons we must consider that the capture process can give a contribution to the formation of excited He^{+*} ions:

$$H^+ + He \rightarrow H + He^{+*} \tag{9.2.1}$$
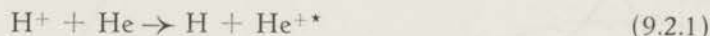
However, at sufficiently high energies this process can be neglected with repect to the direct excitation (see Thomas and Bent (1967)):

$$H^+ + He \rightarrow H^+ + He^{+*} + e \tag{9.2.2}$$

The bump in the σE curve for proton impact, which is absent for electron impact, is caused by reaction (9.2.1).

SUMMARY

The investigation described in this thesis concerns the experimental determination of the absolute excitation cross sections for high energy electrons (0.05-6 keV) incident on helium. The cross sections are determined from intensity measurements of the emitted radiation created by a transition of the excited level to a lower lying level. The degree of polarization of the emitted radiation is also measured. As the theoretical treatment of the collision process is simple for high energy electrons, a good comparison is possible between theory and experiment.

In Chapter 1 a survey is given of the results on the excitation cross sections and degree of polarization which have been published previously. These measurements were done only up to 450 eV electron energy.

Chapter 2 presents the theory. The Bethe theory can be applied for singlet excitation at sufficiently high electron impact energies. For optically allowed transitions (1^1S-n^1P) the excitation cross section is given by:

$$\sigma = \frac{4 \pi a_0^2 R}{E_{el}} M_n^2 \ln c E_{el}$$

in which the quantity M_n^2 is related to the optical oscillator strength. For optically forbidden transitions (1^1S-n^1S, n^1D) we have $\sigma = B/E_{el}$, where B is constant.

For triplet excitation at high electron impact energies the Ochkur approximation predicts that $\sigma = A/E_{el}^3$, where A is a constant.

For polarization it is found by the Bethe approximation that for n^1P-2^1S lines $I_\perp/I_{//} \sim \ln c E_{el}$ where c is a constant and for n^1D-2^1P lines that $I_{//}/I_\perp$ approaches a constant value at high impact energies. Here $I_\perp$ and $I_{//}$ are the light intensities observed

107

perpendicular to the electron beam with electric vectors respectively perpendicular and parallel to the beam direction.

In Chapter 3 a description of the apparatus used for the excitation measurements is given. It is the same apparatus as used for measuring gross ionization cross sections for high energy electrons incident on noble and diatomic gases. Some modifications were however necessary in order to create the possibility of observation of photons by means of a monochromator. The light intensities were measured with two different monochromators in different wavelength regions between 200 and 7300 Å. Interference filters with bandwidths varying from 6 Å to 60 Å have also been used for relative intensity measurements of some spectral lines. In this way weak signals at low gas pressures and high energies could be obtained more accurately, gaining a factor of about 30 with respect to the monochromator sensitivity.

In Chapter 4 we discuss the determination of the quantum yield (that is the output signal per incoming photon) of the monochromators used in our experiment.

In Chapter 5 the experimental procedure and the calculation of the excitation cross sections from the measured light intensity signals are given.

Chapter 6 is concerned with the pressure dependence of the light emission and the polarization degree. A critical study has especially been made of n^1P-2^1S transitions. For the 3^1P-2^1S line an interference filter of 6Å bandwidth has been used, so that measurements could be done at very low gas pressures. A considerable signal due to the background gas has been found in the case of 4^3S-2^3P (4713Å) and 3^3P-2^3S (3889Å) transitions. The effect of the background gas increases relatively strongly with increasing electron impact energy. Also in this chapter the influence of the axial magnetic field was studied on the intensity and the polarization of the light. No effect due to the axial magnetic field has been found.

In Chapter 7 experimental results are given on the excitation cross sections and the polarization degree as a function of electron energy, for both He I and He II.

In Chapter 8 the experimental results are compared with theory. The energy dependence of the excitation cross sections of the optically allowed transitions as well as the forbidden transitions is in

108

very good agreement with the Bethe approximation. Our values of the optical oscillator strengths of n^1P levels are generally in good agreement with the theoretical values. In the case of triplet excitation the decrease of the experimental excitation cross sections with increase of impact energy is much smaller than predicted by the Ochkur theory.

The energy dependence of the emission cross sections of He II lines is found as E_{el}^{-1} (i.e. as an optically forbidden transition) which is in contradiction with existing theoretical calculations which give the $E_{el}^{-1} \ln c E_{el}$ relation (i.e. as optically allowed transitions). The discrepancy is probably caused by the choice of nonorthogonal wave functions in the theoretical calculations. Our results of the polarization degree are in good agreement with the theoretically predicted energy behaviour.

In Chapter 9 the results of excitation of helium by electrons and protons (measured with the same apparatus) have been compared at equal velocities. Generally, there is good agreement at high velocities and almost equal excitation cross sections for electrons and protons are found, for both He I and He II excitation. At low velocities the electrons are less effective in excitation than the protons.

SAMENVATTING

Het in dit proefschrift beschreven onderzoek heeft betrekking op metingen van de werkzame doorsnede voor excitatie van heliumgas door electronen met energie variërend tussen 0.05 en 6 keV. De excitatie doorsneden worden bepaald met behulp van metingen van de intensiteit van de uitgezonden straling, welke ontstaat door een overgang van het aangeslagen niveau naar een lager gelegen niveau. De polarisatiegraad van de straling wordt ook gemeten. Daar de theoretische behandeling van het botsingsproces eenvoudig is voor electronen van hoge snelheid, is een goede vergelijking tussen theorie en experiment mogelijk.

Hoofdstuk 1 geeft een overzicht van de literatuur aangaande de experimenten van excitatie van helium door electronen en over de polarisatie van de uitgezonden straling. Deze metingen werden uitgevoerd voor electronen met een lagere energie dan 400 eV.

Hoofdstuk 2 behandelt de theorie. De theorie van Bethe kan worden toegepast voor de singulet aanslag van helium bij voldoende grote botsingsenergieën van de primaire electronen. Voor optisch toegestane overgangen (1^1S-n^1P) wordt de excitatiedoorsnede gegeven door

$$\sigma = \frac{4\pi a_0^2 R}{E_{el}} M_n^2 \ln c E_{el}$$

waarin de grootheid M_n^2 verband houdt met de optische oscillatorsterkte. Voor optisch verboden overgangen (1^1S-n^1S, n^1D) geldt $\sigma = B/E_{el}$, waarbij B een constante is. Voor triplet aanslag voorspelt de benadering van Ochkur dat $\sigma = A/E_{el}^3$ bij grote botsingsenergieën, waarbij A een constante is.

Met behulp van de Bethe benadering vinden we voor de polarisatie van n^1P-2^1S lijnen dat $I_\perp/I_{//} \sim \ln c E_{el}$ (c = constante) en voor de polarisatie van n^1D-2^1P lijnen dat $I_{//}/I_\perp$ tot een constante waarde nadert bij grote botsingsenergieën. $I_\perp$ en $I_{//}$ zijn de intensiteiten

110

van de componenten van het licht dat loodrecht ten opzichte van de electronen bundel wordt uitgezonden, met electrische vectoren respectievelijk loodrecht en parallel aan de richting van de bundel.

Hoofdstuk 3 geeft een beschrijving van het apparaat dat wordt gebruikt voor de excitatiemetingen. Het is hetzelfde apparaat als dat gebruikt werd voor het meten van totale ionisatiedoorsneden bij bombardement van edelgassen en twee-atomige gassen door electronen. Enkele wijzigingen waren noodzakelijk om de mogelijkheid te scheppen dat het uitgezonden licht met een monochromator kon worden waargenomen. Hiertoe werden twee monochromatoren gebruikt voor het golflengtegebied van 2800 Å-7300 Å en van 200 Å-2000 Å. Voor sommige spectraallijnen werden ook interferentiefilters gebruikt met een bandbreedte van 6 Å tot 60 Å. Op deze manier konden zwakke lichtsignalen, verkregen bij lage gasdruk en grote botsingsenergie, nauwkeuriger gedetecteerd worden. Met betrekking tot de monochromator wonnen we met de filters ongeveer een factor dertig in gevoeligheid.

Hoofdstuk 4 behandelt de bepaling van de quantumopbrengst (dat is het uitgangssignaal per invallend foton) van de monochromatoren, die voor het experiment gebruikt werden.

Hoofdstuk 5 geeft een beschrijving van de experimentele werkwijze en de berekening van de excitatiedoorsneden uit de gemeten lichtintensiteit.

Hoofdstuk 6 gaat over de drukafhankelijkheid van de lichtemissie en de polarisatiegraad. Een kritische studie is speciaal uitgevoerd voor de n^1P-2^1S overgangen. Bij de 3^1P-2^1S lijn is gebruik gemaakt van een interferentiefilter van 6 Å bandbreedte, zodat bij zeer lage gasdrukken gemeten kon worden. Een belangrijk achtergrondsignaal is gevonden voor 4^3S-2^3P (4713 Å) en 3^3P-2^3S (3889 Å). Dit signaal neemt relatief sterk toe bij grotere botsingsenergie. In dit hoofdstuk is ook de invloed nagegaan van het axiale magneetveld op de emissie en de polarisatie van het uitgezonden licht. Er bleek geen effect van dit veld aanwezig te zijn.

Hoofdstuk 7 geeft experimentele resultaten van de excitatiedoorsnede en de polarisatiegraad, zowel voor He I en He II.

Hoofdstuk 8 geeft een vergelijking tussen experiment en theorie. Het energiegedrag van de excitatiedoorsneden, zowel voor optisch toegestane als wel voor optisch verboden overgangen, is in zeer

111

goede overeenstemming met de theorie van Bethe. Bovendien zijn de experimentele waarden van de optische oscillatorsterkten van de n^1P niveaux in goede overeenstemming met de theoretische waarden.

Voor triplet aanslag is de afname van de doorsnede met toename van de botsingsenergie veel kleiner dan door de theorie van Ochkur voorspeld wordt.

Voor He II aanslag wordt een E_{el}^{-1} afhankelijkheid gevonden bij grote botsings energieën, dat wil zeggen een gedrag van de emissiedoorsnede welke overeenkomt met een door botsing geïnduceerde optisch verboden overgang. Dat is in tegenstelling tot bestaande theoretische berekeningen welke een $E_{el}^{-1} \ln E_{el}$ afhankelijkheid geven (overeenkomstig optisch toegestane overgangen. De discrepantie wordt waarschijnlijk veroorzaakt door de keuze van niet orthogonale golffuncties in de theoretische berekeningen. Het energiegedrag van de polarisatiegraad van 3^1P-2^1S en 4^1D-2^1P is in overeenstemming met de theorie van Bethe.

Hoofdstuk 9 vergelijkt de aanslag van helium door electronen en protonen bij gelijke snelheden. Excitatiedoorsneden voor protonen werden in hetzelfde apparaat gemeten. In het algemeen is er een goede overeenstemming bij hoge snelheden waar electronen en protonen nagenoeg even grote excitatiedoorsneden vertonen, zowel voor He I als voor He II aanslag. Bij kleine snelheden exciteren de electronen in mindere mate vergeleken met protonen.

112

REFERENCES

Altshuler, S., Phys. Rev. **87**, 992, (1952).

Bates, D. R., Fundaminsky, A. and Massey, H. S. W., Trans. Roy. Soc. (London) **A243**, 93, (1950).

Bethe, H. A., Ann. der Phys. **5**, 325, (1930).

Boersch, H., and Reich, H. J., Optik, **22**, 289, (1965).

Byron, F. W., and Joachain, C. J., Phys. Rev. Letters **16**, 1139, (1966).

Čermák, V., J. Chem. Phys. **44**, 3774, (1966).

Chamberlain, G. E., Heideman, H. G. M., Simpson, J. A., and Kuyatt, C. E., IV Intern. Conf. on the Physics of Electronic and Atomic collisions, Quebec, Canada, (1965).

Crothers, D. S. F. and Holt, A. R., Proc. Phys. Soc. **88**, 75, (1966).

Dalgarno, A., and McDowell, M. R. C., The Airglow and the Aurorae, Pergamon Press, New York, 340, (1956).

Dalgarno, A., and Stewart, A. L., Proc. Phys. Soc. (London), **76**, 49, (1960): see also Dalgarno, A., and Lynn, W., Proc. Phys. Soc. (London), **A70**, 802, (1957).

De Heer, F. J., Advances in Atomic and Molecular Physics, Vol. **2**, edited by D. R. Bates and Immanual Eastermann (1966).

De Vos, J. C., The emissivity of tungsten ribbon, thesis, Amsterdam (1953).

De Vries, A. E., and Rol, P. K., Vacuum **15**, 135, (1965).

Dugan, J. L. G., Richards, H. L., and Muschlitz, E. E., J. Chem. Phys. **46**, 346, (1967).

Elenbaas, W., Z. f. Physik, **59**, 289, (1929).

Fedorov, V. L., and Golovanevskaya, L. E., Optics and Spectroscopy (U.S.A.), **20**, 219, (1966.

Fite, W. L., and Brackmann, R. T., Phys. Rev., **112**, 1151, (1958).

Fleming, R. J., and Higginson, G. S., Proc. Phys. Soc. (London), **84**, 531, (1964).

Fox, M. A., Proc. Phys. Soc., **86**, 789, (1965).

Fox, M. A., Proc. Phys. Soc., **88**, 65, (1966).

Fox, M. A., Proc. Phys. Soc., **90**, 585, (1967).

Frost, L. S., and Phelps, A. V., Res. Rep. Westinghouse Res. Lab. 6-94439-6-R3.

Gabriel, A. H., and Heddle, D. W. O., Proc. Roy. Soc. (London), **A258**, 124, (1960).

Geiger, J., Z. Physik **175**, 530 (1963); **177**, 138, (1964) and **181**, 413, (1964).

Hass, G., and Tousey, R., J. Opt. Soc. Amer., **49**, 593, (1959).

Haidt, D., and Kleinpoppen, H., Z. f. Physik, **196**, 72, (1966).

Hanle, W., Z. f. Physik, **56**, 94, (1929).

Heddle, D. W. O., and Lucas, G. B., Proc. Roy. Soc. **A271**, 129, (1962).

Hughes, R. H., Waring, R. C., and Fan, C. Y., Phys. Rev. **122**, 525, (1961).

Hughes, R. H., and Weaver, L. D., Phys. Rev., **132**, 710, (1963).

Ishii, H., and Nakayama, K., Vacuum Symposium transactions 8-I, 519, (1961).

Johnson, F. S., Watanabe, K., and Tousey, R., J. Opt. Soc. Amer., **41**, 702, (1951).

Kuppermann, A., and Raff, L. M., Disc. Far. Soc. **35**, 30, (1963).

Kuyatt, C. E., and Simpson, J. A., Proc. 3rd Intern. Conf. Electronic and Atomic Collisions, North Holland, Amsterdam, 191, (1964).

Lassettre, E. N., and Co-workers, 10 papers, J. Chem. Phys. **40**, 1208-1275, (1964).

Lee, E. T. P., and Lin, C. C., Phys. Rev., **138**, A 301, (1965).

Lees, J. H., Procc. Roy. Soc., **A137**, 173, (1932).

Maier, H., and Leibnitz, Z. Physik, **95**, 499, (1935).

Mapleton, R. A., Phys. Rev., **109**, 1166, (1957).

Massey, H. S. W., and Mohr, C. B. O., Proc. Roy. Soc. (London), **A140**, 613, (1932).

McFarland, R. H., Phys. Rev., **133**, A 986, (1964).

McFarland, R. H., and Soltysik, E. A., Phys. Rev., **127**, 2091, (1962).

McFarland, R. H., and Soltysik, E. A., Report UCRL, 6749, University of California, Livermore, 1962 a).

McFarland, R. H., and Soltysik, E. A., Phys. Rev., **128**, 2222, (1962 b).

Meinke, C., and Reich, G., Vacuum Technik, **12**, 79, (1963).

Miller, W. F., and Platzman, R. L., Proc. Phys. Soc. **70**, 299, (1957).

Mittleman, M. H., Phys. Rev. Letters, **16**, 489, (1966).

Mott, N. F., and Massey, H. S. W., The theory of Atomic Collisions, 2nd ed. p. 261 (1949 a).

Mott, N. F., and Massey, H. S. W., ibid, p. 367, (1949 b).

Mott, N. F., and Massey, H. S. W., The Theory of Atomic Collisions, 3rd ed. p. 328, Oxford University Press (1965 a).

Mott, N. F., and Massey, H. S. W., ibid, p. 498, (1965 b).

Moustafa Moussa, H. R., and De Heer, F. J., to be published in Physica (1967).

Ochkur, V. I., J. E. T. P., **18**, 503, (1964).

Ochkur, V. I., and Petrun'kin, A. M., Optics and Spectr. (U.S.A.), **14**, 245, (1963).

Ochkur, V. I., and Brattsev, V. F., Optics and Spectr. (U.S.A.), **19**, 274, (1965).

Pendleton, W. R., and Hughes, R. H., Phys. Rev. **138**, A 683, (1965).

Phelps, A. V., Phys. Rev. **110**, 1362, (1958).

Perel, V. I., and Fedorov, V. L., Optics and Spectr. (U.S.A.), **20**, 412, (1966).

Percival, I. C., and Seaton, M. I., Phil. Trans. Roy. Soc. (London), 113, (1958).

Reich, H. I., IV Intern. Conf. on the physics of Electronic and Atomic Collisions, Quebec, Canada, (1965).

Salpeter, E. E., and Zaidi, M. H., Phys. Rev., **125**, 248, (1962).

Schiff, B., and Pekeris, C. L., Phys. Rev., **134**, A 640, (1964).

Schram, B. L., Thesis University of Amsterdam (1966 a).

Schram, B. L., and Vriens, L., Physica, **31**, 1431, (1965).
Schram, B. L., De Heer, F. J., Van der Wiel, M. J. and Kistemaker, J., Physica
    31, 94, (1965).
Schram, B. L., Moustafa, H. R., Schutten, J., and De Heer F. J., Physica, **32**,
    734, (1966 b).
Schram, B. L., Boerboom, A. J. H., and Kistemaker, J., Physica, **32**, 185, (1966 c).
Shreider, E. Ya., Soviet. Tech. Phys., **9**, 1609, (1965).
Schutten, J., Van Deenen, P. J., De Haas, E., and De Heer, F. J., J. Scientific
    Instruments, **44**, 153, (1967).
Schulz, G. J., and Fox, R. E., Phys. Rev., **106**, 1179, (1957).
Schulz, G. J. Phys. Rev., **116**, 1141, (1959).
Silvermann, S. M., and Lassettre, E. N., J. Chem. Phys. (U.S.A.), **44**,
    2219, (1966).
Skerbele, A. M., and Lassettre, E. N., J. Chem. Phys. (U.S.A.), **40**, 1271, (1964).
Sluyters, T. J. M., Thesis University of Amsterdam, (1959).
Smit, C., Thesis University of Utrecht, (1961).
Smit, J. A., Physica, **2**, 104, (1965).
Soltysik, E. A., Fournier, A. Y., and Gray, R. L., Phys. Rev. **153**, No. 1, 152,
    (1967).
St. John, R. M., Miller, F. L., and Lin, C. C., Phys. Rev., **134**, A 888, (1964).
St. John, R. M., Bronco, C. J., and Fowler, R. G., J. Opt. Soc. Amer., **50**, 28,
    (1960).
St. John, R. M., and Fowler, R. G., Phys. Rev., **122**, 1813, (1961).
St. John, R. M., and TSU-Wei Nee, J. Opt. Soc. Amer. **55**, 426, (1965).
St. John, R. M., and Lin, C. C., J. Chem. Phys., **41**, 195, (1964).
Steiner, K., Z. f. Physik, **52**, 516, (1928).
Thieme, O., Z. f. Physik, **86**, 646, (1933).
Teter, M. P., and Robertson, W. W., J. Chem. Phys. **45**, 2167, (1966).
Thomas, E. W., and Bent, G. D., to be published in Phys. Rev. (1967).
Tousey, R., Johnson, F. S., Richardson, J., and Toran, N., J. Opt. Soc. Amer.,
    41, 696, (1951).
Trefftz, E., Schlüter, A., Dettmar, K. H., and Jörgens, K., Z. Astrophys., **44**, 1,
    (1957).
Van Eck, J., De Heer, F. J., and Kistemaker, J., Physica, **30**, 1171, (1964 a).
Van Eck, J., Thesis University of Amsterdam (1964 b).
Van Eck, J., and De Heer, F. J., Proc. 6th Intern. Conf. Ionization Phenomena
    in Gases, Paris, Vol. IV, pp 11.13 Centre de Documentations Universi-
    taires, Paris, (1963).
Van den Bos, J., Thesis University of Amsterdam (1967).
Van den Bos, J., and De Heer, F. J., Physica, **33**, 234, (1967).
Van den Bos, J., to be published in Physica (1967 a).
Van den Bos, J., Winter, G., and De Heer, F. J., to be published in Physica,
    (1967).
Van der Wiel, M. J., De Heer, F. J., and Wiebes, G., Phys. Letters 24A, 423,
    (1967).
Vriens, L., Phys. Rev., **141**, 88, (1966).

Vriens, L., De Heer, F. J., Van den Bos, J., and Moustafa Moussa, H. R., to be published in Inter. Conf. on the Physics of Electronic and Atomic Collisions, Leningrad, U.S.S.R., (July 1967).

Watanabe, K., and Edward, C. J., J. Opt. Soc. Amer., **41,** 702, (1953).

Wolf, R., and Maurer, W., Z. f. Physik, **115,** 410, (1940).

Yakhontova, V. E., Westnik. Leningr. Univers. ser. Phys. Chim. **10,** 27 (AERE-Trans. 951), (1959).

Zapesochnyi, I. P., and Feltsan, P. V., Optics and Spectr. (U.S.A.), **18,** 514, (1965).

Zinsmeister, G., Advances in vacuum Science and Technology, Vol. I., p. 335, Pergamon Press, London, (1958).